1991

Effect of the coefficient of thermal expansion of a coating on waterwalls in a super-critical coal fired utility boiler

Charles Patrick Erksine
Lehigh University

Effect of

The Coefficient of Thermal Expansion of a Coating

on Waterwalls

in a Super-Critical Coal Fired

Utility Boiler

by

Charles Patrick Erskine

A Thesis

Presented to the Graduate Committee

of Lehigh University

in Candidacy for the Degree of

Master of Science

in

Mechanical Engineering

Lehigh University

1991

Certificate of Approval

This thesis is accepted and approved in partial fulfillment of the requirements for the degree of Master of science in Mechanical Engineering.

May 9, 1991

(date)

Ronald J. Hartranft

Ronald J. Hartranft

Professor in Charge

Robert G. Sarrubi

Robert G. Sarrubi

Assistant Chairman

of Department

Acknowledgements

I would like to thank my advisor, Professor Ronald J. Hartranft, for his guidance throughout the many facets of this research project and specifically for suggestions directly relating to the production of this thesis.

I would also like to acknowledge the support of this research by the participating companies, Potomic Electric Power Company (PEPCO), Virginia Power, Ohio Edison, Pennsylvania Power and Light (PP&L)/Pennsylvania Electric Energy Research Council (PEERC) and Public Service Electric and Gas (PSE&G).

This thesis is dedicated to Lynn for all of her patience.

Table of Contents

List of Tables

List of Figures

List of Symbols

A = cross sectional area of modeled portion of waterwall

A_m = cross sectional area of membrane

c = center to center waterwall tube spacing

$c_{p,b}$ = bulk specific heat of cooling water

$c_{p,c}$, $c_{p,b}$ = specific heat of coating and base materials

C_0, C_1, C_2, C_3 = coefficients for temperature dependent radiation coeffecient

d = inner diameter of waterwall tube

$D_{h,b}$ = thermal diffusivity of base material

E_c, E_b = elastic moduli of coating and base materials

G = shear modulus

h_b = bulk convection coefficient for waterside

h_f = convection coefficient for free convection on ambientside

h_r = radiation coefficient for fireside

i_b = bulk enthalpy of cooling water

i_w = enthalpy of cooling water adjacent to inside of waterwall

k_b = bulk coefficient of heat conduction for cooling water

k_c, k_b = coefficient of heat conduction for coating and base materials

Nu_b = bulk Nusselt number

p = internal pressure

Pr_b = bulk Prandtl number

q_x, q_z, q_r = components of heat flux

q_n = component of heat flux normal to waterwall surface

r = radial coordinate

r_i, r_o = inner and outer radius of waterwall tube

Re_b = bulk Reynolds number

T = temperature

t = elapsed time (seconds) after slag fall

T_{ba} = bulk temperature of fluid adjacent to ambientside

T_{bf} = bulk temperature of fire ball in furnace

T_{bi} = bulk temperature of cooling water

T_0 = 460 °R

u, v, w = displacements in x, y, and z directions

u_m = mean cooling water flow velocity

w_t = wall thickness of waterwall tube

x = coordinate in plane of waterwall perpendicular to axis of tubes

y = coordinate perpendicular to waterwall

z = coordinate parallel to axis of waterwall tubes

α_c, α_b = coefficients of thermal expansion for coating and base materials

$\epsilon_x, \epsilon_y, \epsilon_z$ = components of normal strain

$\gamma_{xy}, \gamma_{yz}, \gamma_{xz}$ = components of shear strain

ν_c, ν_b = Poisson's ratio for coating and base material

μ_b = bulk dynamic viscosity for cooling water

ρ_b = bulk density of cooling water

ρ_c, ρ_b = density of coating and base materials

ρ_w = density of cooling water adjacent to inside of waterwall

σ = Stefan Boltzman constant

$\sigma_1, \sigma_2, \sigma_3$ = principal stresses

σ_n = stress component normal to surface of waterwall

σ_{vM} = von Mises stress

$\sigma_x, \sigma_y, \sigma_z$ = normal stress components

$\sigma_{ys,b}$ = yield stress for base material

$\sigma_{ys,c}$ = yield stress for coating material

τ_{nz}, τ_{ns} = shear stress components on surface of waterwall

τ_{rz}, $\tau_{r\theta}$ = radial shear stress components

τ_{xy}, τ_{yz}, τ_{xz} = cartesian shear stress components

ABSTRACT

Elastic-plastic thermal stresses in a coated waterwall of a coal fired utility boiler are calculated using the finite element method. The finite element analysis uses a three dimensional model of a section in the waterwall. There is radiant heat transfer on the fireside, and convection on the backside. The waterside is subjected to a forced convection condition at supercritical pressure .

Both steady-state stresses and transient stresses resulting from slag falls or soot blowing operations are examined. Various material properties of both the base and the coating are analyzed in an attempt to find combinations better able to survive in a boiler environment. It is found that some systems of base material and coating combine to enhance the performance of the tube. Specifically, a laser clad cast stainless steel coating with a coefficient of thermal expansion five percent less than that of the base steel (2.25Cr-1Mo) appears to offer lower values of residual stress in the coating than both a control case in which there is no coating and a case with an actual stainless steel coating whose coefficient of thermal expansion is twenty percent less than that of the base material.

It is found that at the apex the coating does not yield following a slag fall, but the base does. After the temperatures return to the steady conditions existing before the slag fall, the residual tensile stress in the base places the fireside of the coating in compression in the axial direction and leaves a tensile stress of 9,000 psi in the tangential direction. This would be an ideal situation in a corrosive environment because the lack of large residual tensile stresses reduces the harmful effects from thermal fatigue cycles associated with subsequent slag falls and make the coating less susceptible to intergranular corrosion. Thermal fatigue and intergranular corrosion are considered to be important factors in the initiation and propagation of circumferential cracks [1].

However, at the fireside fillet, the coating yields in compression following the slag fall. This results in residual tensile stresses of 17,000 psi in the tangential direction and 3,500 psi in the axial direction. Therefore the coating would endure a harmful thermal fatigue cycle with each subsequent slag fall or soot blowing operation. This could result in cracks forming perpindicular to the tangential stress direction (vertical) in the fillet region.

1. INTRODUCTION

Waterwall tube failure is a significant problem in fossil fueled power plants. A typical section from a waterwall is shown if Figure 1.1. Corrosion, erosion, creep, and thermal fatigue which lead to circumferential cracking and rupture are typical failure scenarios. Research has been conducted to characterize the corrosion mechanisms [1] as well as the corrosion/thermal fatigue mechanism leading to circumferential cracking [1,2]. A laboratory corrosion/thermal fatigue simulation was in fact developed to improve the understanding of the corrosion/thermal fatigue mechanism leading to circumferential cracking [3]. This simulation demonstrated that intergranular corrosion in combination with a thermal fatigue cycle (rapid heating followed by gradual cooling) could in fact produce cracks in a tube sample similar to those cracks found in actual boiler waterwalls. Therefore it is widely believed that a coating should be applied to the waterwall in order to combat the mechanisms associated with waterwall failure. As a result, much attention has been directed to the various protective coatings available for use in utility boilers.

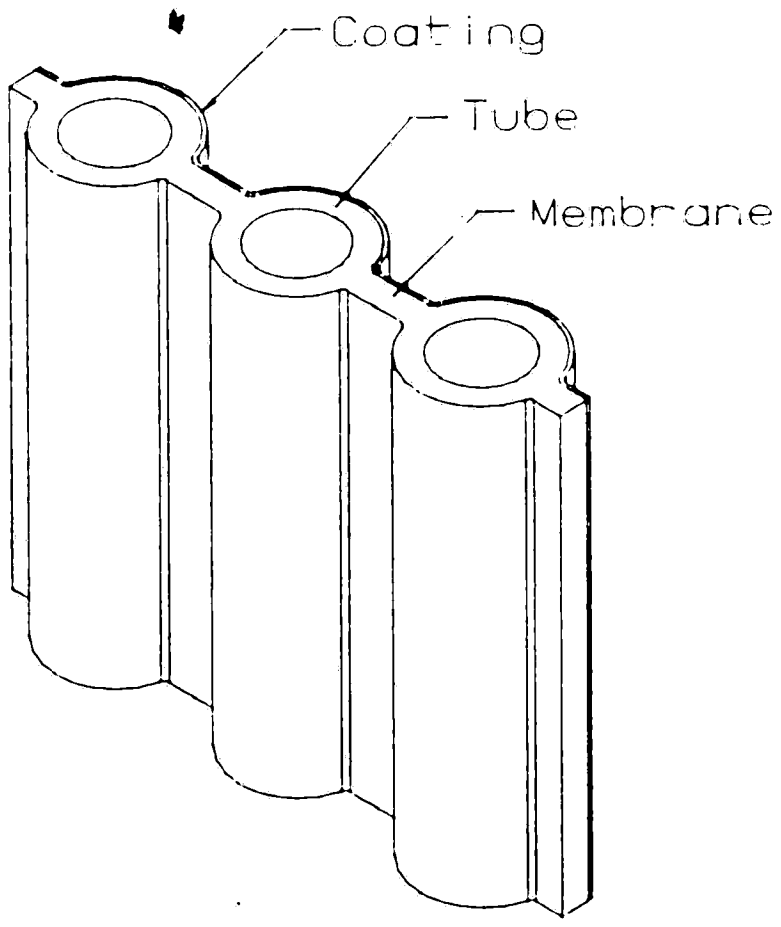

Figure 1.1: Section of a typical waterwall.

Some of the parameters deemed important to the selection of coatings are: corrosion, erosion, spalling and cracking resistance within the boiler environment, as well as cost effectiveness, and method of application [4]. Corrosion, due to the chemical constituents of the furnace environment, erosion, due to high velocity ash particles in the combustion products, and spallation, in which the coating falls off the base material primarily because of a weak bond should all be avoided because they remove the protective coating. Cracking of the coating, which may be caused by the combined interaction of the coating with the base material and the boiler environment should also be avoided because crack growth can lead to waterwall failure with or without a coating in place. Cost effectiveness of the coating is important because it would be impractical to apply a coating if the application and material costs outweigh the long-term costs associated with waterwall failure. Finally, method of application should also be considered in determining the overall quality and repairability of the coating.

Many coating processes and materials are available for use in coal fired utility boilers. Some coatings currently under investigation at Lehigh University are: diffusion (chromized), thermal spray (plazma, d-gun etc.), and laser clad. There are advantages and disadvantages to each coating process and material. For instance, diffusion coatings appear to be extremely resistant to spalling. However, these coatings are typically extremely thin and susceptible to scratches and offer little erosion resistance [5]. Thermal spray coatings may offer good corrosion and erosion resistance, but they are mechanically bonded to the base and hence likely to spall [4]. Finally, laser clad coatings, in which a powdered material covering the base is subsequently melted in place by a traversing laser beam, offer good resistance to spalling because they are metallurgicaly bonded to the base. They can also be made quite thick (.062 in.) and homogeneous. Many different materials could be applied with such a process. High strength, nickel based super alloys are currently being used for laser clad coatings in boilers, at considerable material cost.

Corrosion/thermal fatigue testing in the lab on a tube coated with a nickel based super-alloy, known by its trade name as INCONEL 625, has shown it to be extremely resistant to corrosion, spalling and cracking [6].

Because of their material and geometric flexibility as well as their homogeneity and good bond strength, laser clad coatings appear to be the best initial choice to study in this analysis. However, cast stainless steels, less expensive than INCONEL 625, will be considered as possible coating materials. Furthermore, for good corrosion resistance the stainless steel should have at least twenty percent chromium by weight. Metallurgically it should have a single phase structure because multiphase alloys have a somewhat unstable structure at elevated temperatures. Cast alloy properties are used because laser cladding is in fact a casting process.

First, a model which consists of a single material, but has the same geometry as the coated waterwall will be be evaluated to provide a basis on which to judge the effects of the material properties of the coating on the tube/coating system. Then, a coating material which satisfies the requirements stated in the previous paragraph will be selected and its material properties will be used so as to provide a realistic starting point for initial calculations with a coating. A subsequent analysis will be conducted using a coating material which has a different value of the coefficient of thermal expansion. Note, however, that a material with exactly these other properties may not be available. The alternate analyses are intended to determine what changes in properties would produce a tube/coating structure which is more resistant to cracking.

Waterwalls are presently made of SA213-T2, T11 and T22 (1.0Cr-.5Mo, 1.25Cr-.5Mo and 2.25Cr-1.0Mo) high strength, low alloy seamless tube steel, typically 1.25 in. outside diameter and 0.22 in. wall thickness. The tubes are welded into panels 1.84 in. apart on center joined by .275 in. thick membranes (Figure 1.2). Material

properties of T22, which is widely used in boilers because of its high corrosion resistance, will be used for the base material in the analysis. The coating thickness will be taken to be 0.04 in. (1 mm). It is important to remember that the quantitative results of the analysis apply only to this particular combination of base, coating material, and geometry. The qualitative effect of the various changes in material properties, however, may be helpful in material selection.

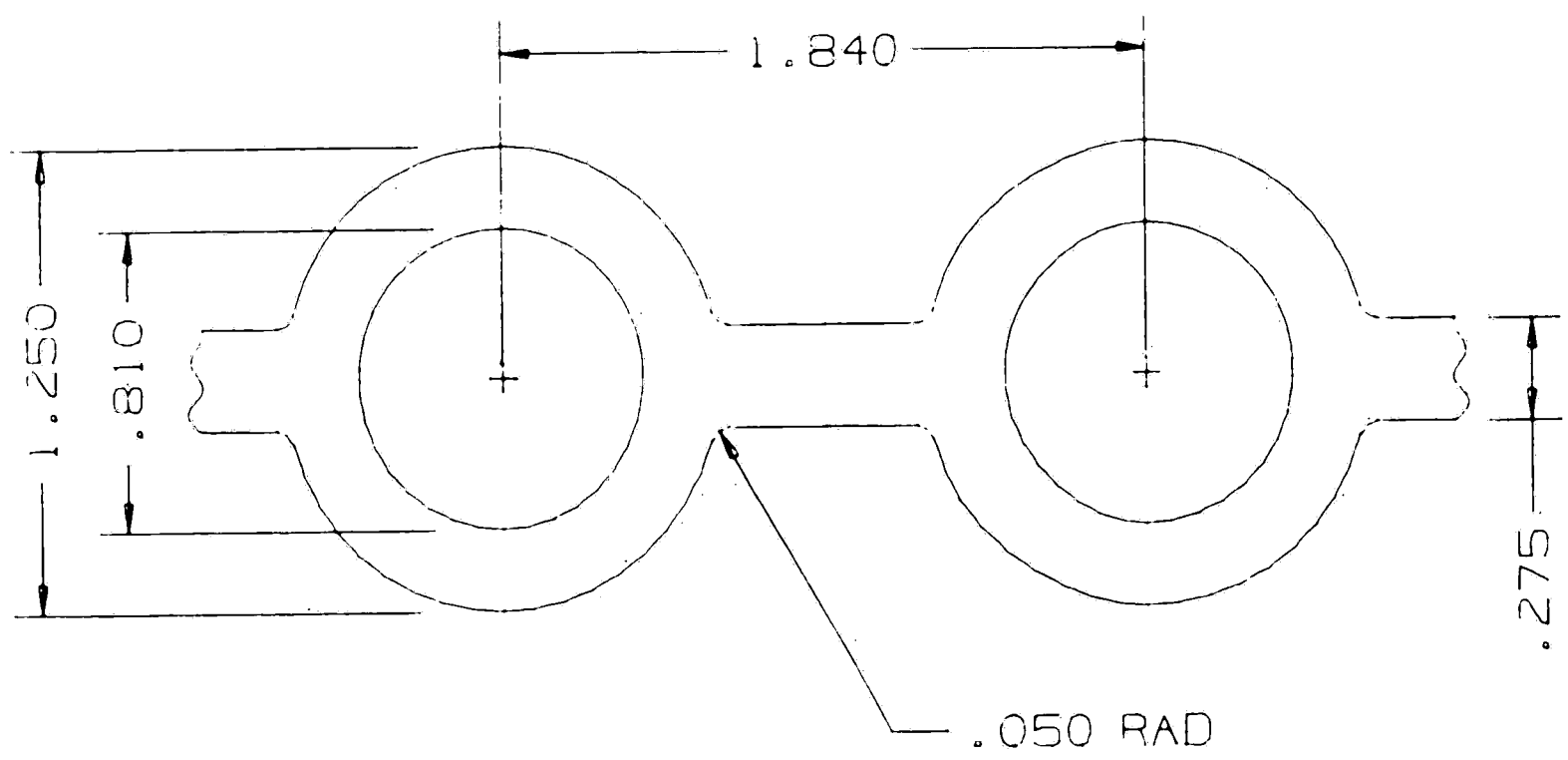

Figure 1.2: Typical dimensions (in inches) of uncoated waterwall tubes [7].

This analysis will focus on thermal stresses that develop in the waterwall during normal operation of a coal fired supercritical pressure boiler. Typically these waterwalls are exposed on one side to a fireball temperature between 2500 °F and 3100 °F and seasonal ambient temperatures on the backside [2]. They are cooled on the inside by water near the pseudo-critical (maximum specific heat) region, around 700 °F and 3500 psia. to 4300 psia. [8]. Furthermore, soot blowing operations or slag falls can cause temperature excursions on the fireside of 50 °F to 300 °F above steady state or nominal

temperatures [9]. Steady and transient elastic–plastic thermal stresses will be calculated using ANSYS finite element software [10]. ANSYS allows the use of temperature dependent material properties in both the thermal and structural analyses as well as the modeling of non–linear irreversible plastic deformation during the structural analysis.

A brief summary of the results from three analyses is presented in Table 1.1. The residual stresses, after a slag fall and subsequent slag buildup, in the axial and tangential directions are reported at the fireside surface of the apex and the fillet for three combinations of T22 base and coating. In case 1, when there is no coating, the residual stresses are all tensile. In case 2 the addition of a coating (CC50) whose yield stress is twice that of T22 and whose coeffecient of thermal expansion is twenty percent less produces residual stresses that are significantly higher. In this case the coating did not yield, but the mismatch in thermal expansion produces highly tensile stresses in the coating. In case 3 (modified) the yield stress of the coating is still twice that of T22, but the coefficient of thermal expansion is increased so that it is only five percent less than that of T22. This results in residual stresses that are significantly lower than the previous cases. However, in the fillet region the yielding of the coating in compression results in a tensile residual stress in the tangential direction that could still be considered quite large.

		Residual Stress (psi)			
		Apex		Fillet	
Case	Coating	Axial	Tangential	Axial	Tangential
1	None	21,000	12,500	20,000	35,500
2	CC50	37,000	44,000	47,000	80,000
3	Modified	-1,000	9,000	3,500	17,000

Table 1.1 Residual stresses at the fireside surface of the apex and fillet for the three combinations of coating and T22 base.

2. Material Properties

Base material

The finite element analysis uses the material properties of SA213-T22 (2.25Cr-1Mo) for the base material of the waterwall. T22 is a high strength, low allow seamless boiler tube steel widely used in utility boiler applications. Figures 2.1, 2.2 and 2.3 show thermal conductivity, thermal diffusivity, and thermal expansion as functions of temperature for 2.25Cr-1Mo (T22) steel.

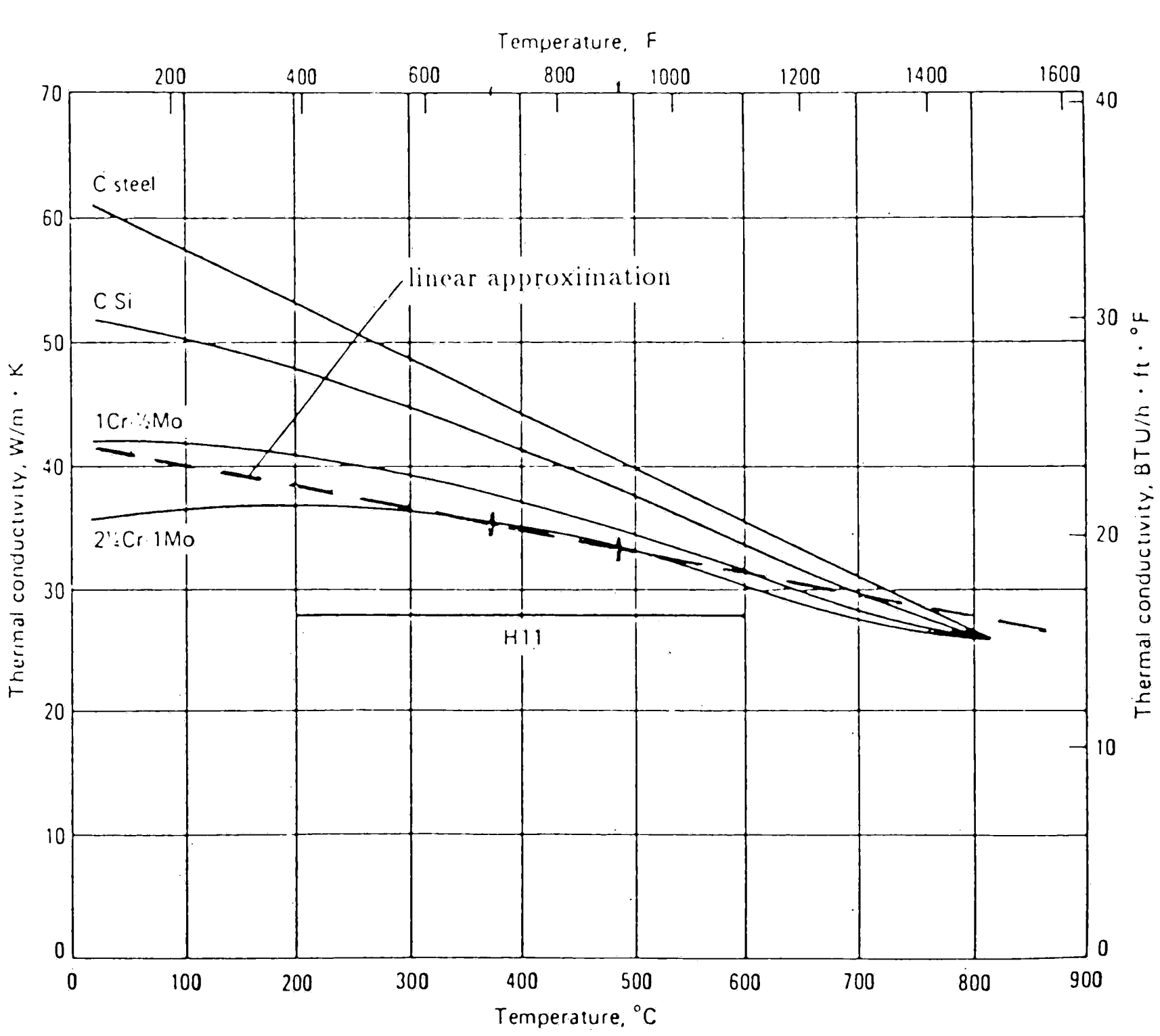

Figure 2.1: Thermal conductivity as a function of temperature for 2.25Cr-1Mo steel [11, pg. 652].

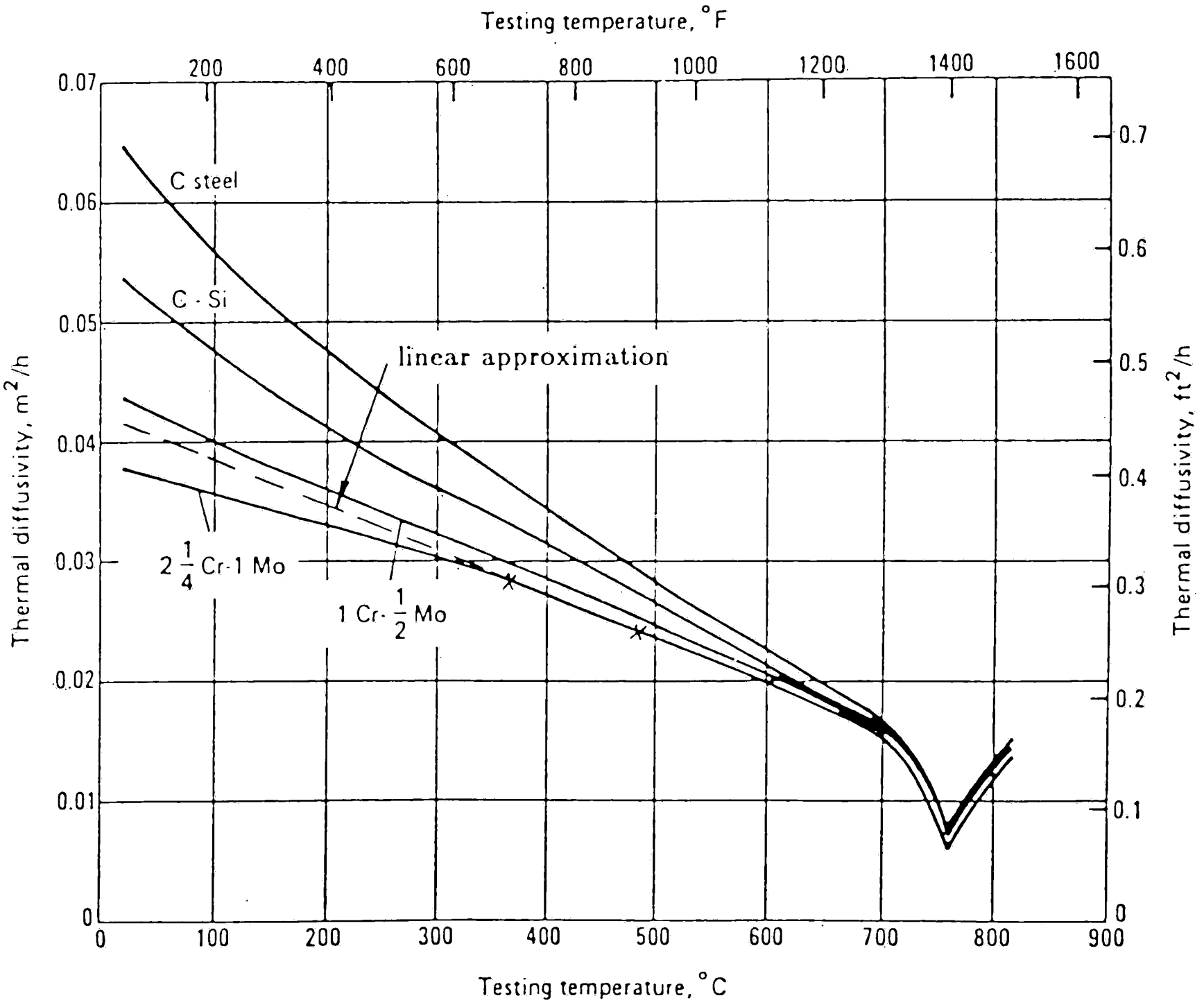

Figure 2.2: Thermal Diffusivity as a function of temperature for 2.25-1Mo steel [11, pg. 652].

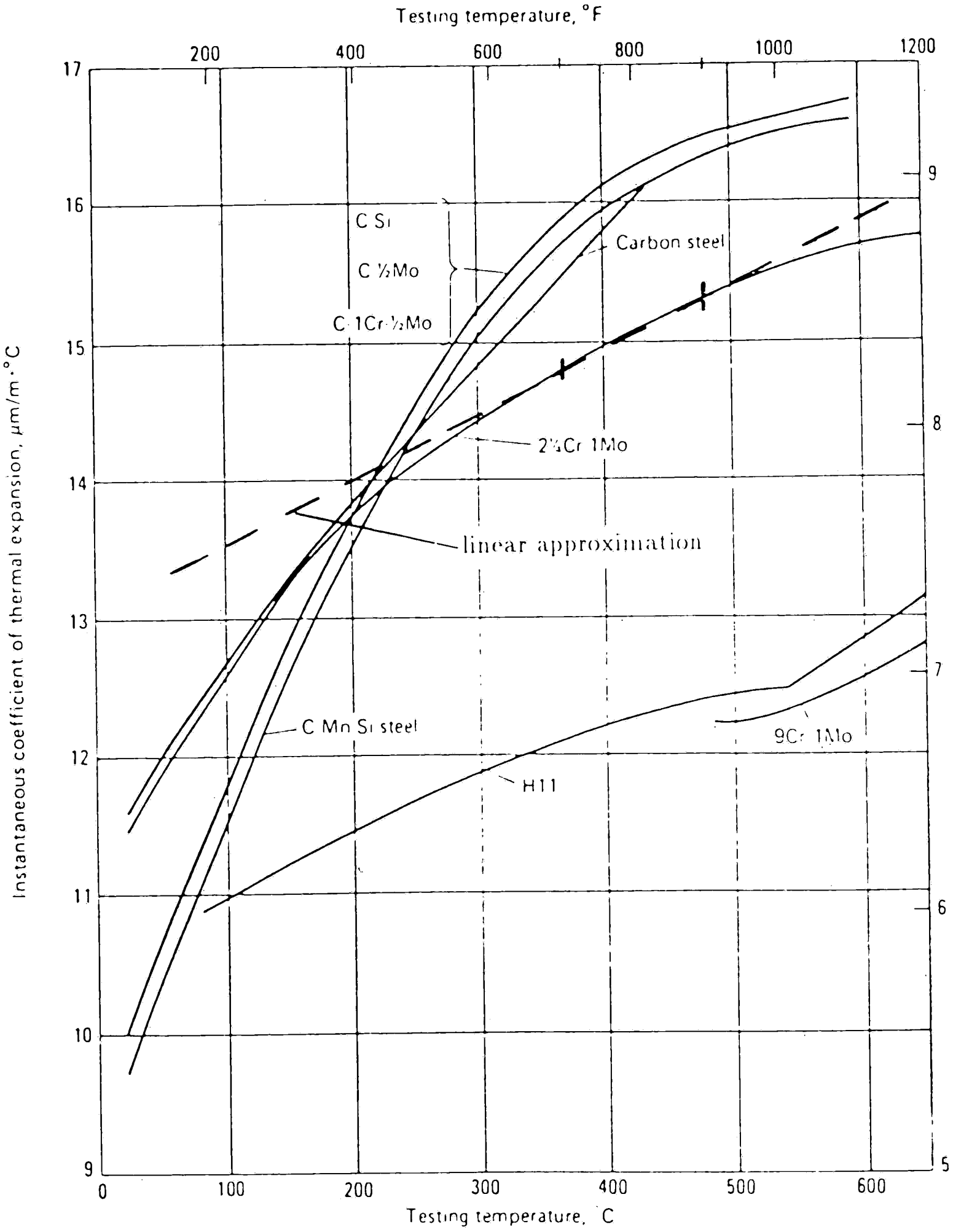

Figure 2.3: Thermal expansion as a function of temperature for 2.25–1Mo steel [11, pg. 653].

In the range from 600°F to 1000°F, these curves can be approximated by linear functions of temperature, T,

$$\text{Thermal conductivity: } k_b = [0.547(10)^{-3} - 0.110(10)^{-6}\,\tfrac{T}{^\circ F}]\ \text{BTU/(sec·in·°F)} \tag{2.1}$$

$$\text{Thermal diffusivity: } D_{h,b} = [0.0180 - 8.50(10)^{-6}\,\tfrac{T}{^\circ F}]\ \text{in}^2/\text{sec} \tag{2.2}$$

$$\text{Thermal expansion: } \alpha_b = [7.33(10)^{-6} + 1.30(10)^{-9}\,\tfrac{T}{^\circ F}]\ /^\circ F \tag{2.3}$$

$$\text{Specific heat: } c_{p,b} = [32.86 + 0.029\,\tfrac{T}{^\circ F}]\ \text{BTU·in/(lb·sec}^2\text{·°F)} \tag{2.4}$$

$$\text{Density: } \rho_b = 7.32(10)^{-4}\ \text{lb·sec}^2/\text{in}^4 \tag{2.5}$$

Figures 2.1, 2.2 and 2.3 show equations (2.1), (2.2) and (2.3) as dashed straight lines which are valid over the range of temperatures from 600 °F to 1000 °F to within ±1 % of the actual value. Equations (2.1), (2.3), (2.4) and (2.5) are needed for the thermal stress analysis in ANSYS.

SA 213-T22 steel is linearly elastic before yielding and has some strain hardening after yielding at elevated temperatures. Figure 2.4 shows some stress-strain curves for 2.25Cr-1Mo steel at various temperatures. This material behavior is modeled in ANSYS by a bilinear stress strain curve with similar behavior in both tension and compression. The slope in the linearly elastic portion is the modulus of elasticity of the material. At the yield point, the slope changes to the tangent modulus. The tangent modulus is approximately constant and values for it are taken from Figure 2.4. Calculations are based on the criterion that yielding begins when the von Mises stress, $\sigma_{vM} = \sqrt{\frac{1}{2}[(\sigma_1-\sigma_2)^2+(\sigma_1-\sigma_3)^2+(\sigma_2-\sigma_3)^2]}$ (σ_1, σ_2 and σ_3 are the principal stresses), reaches the yield stress, $\sigma_{ys,b}$, of the base material. In this model, the yield stress, shown in Figure 2.5 for an average 2.25Cr-1Mo steel, and the tangent modulus depend on temperature, but for the temperatures of interest, the elastic modulus ($E_b = 30.0(10)^6$ psi) and Poisson's ratio ($\nu_b = 0.30$) do not. Several values of the yield stress (for T22 explicitly) and tangent modulus are specified in Table 2.1 at different temperatures, and ANSYS interpolates between them.

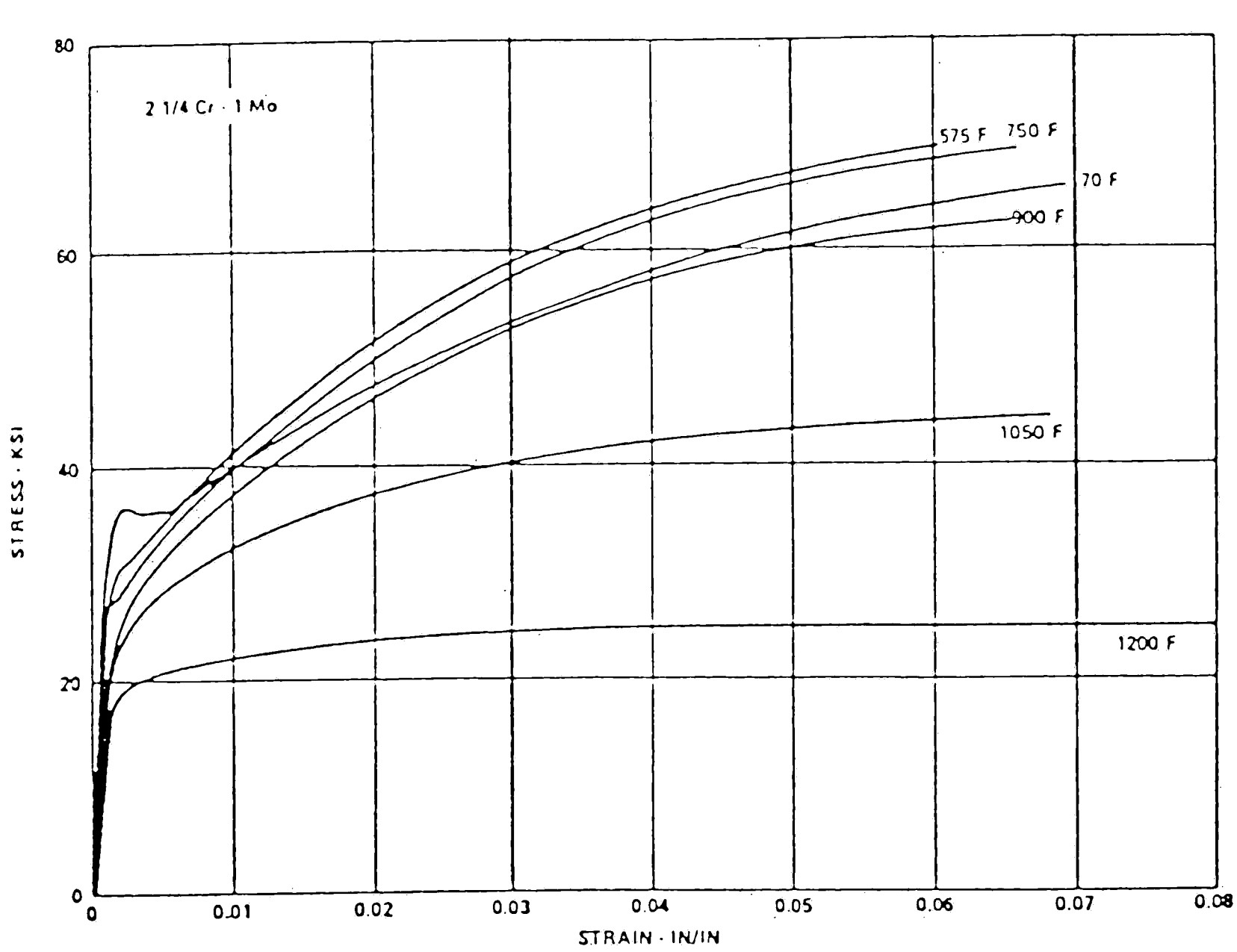

Figure 2.4: Stress–Strain curves for 2.25Cr–1Mo steel at various temperatures [12].

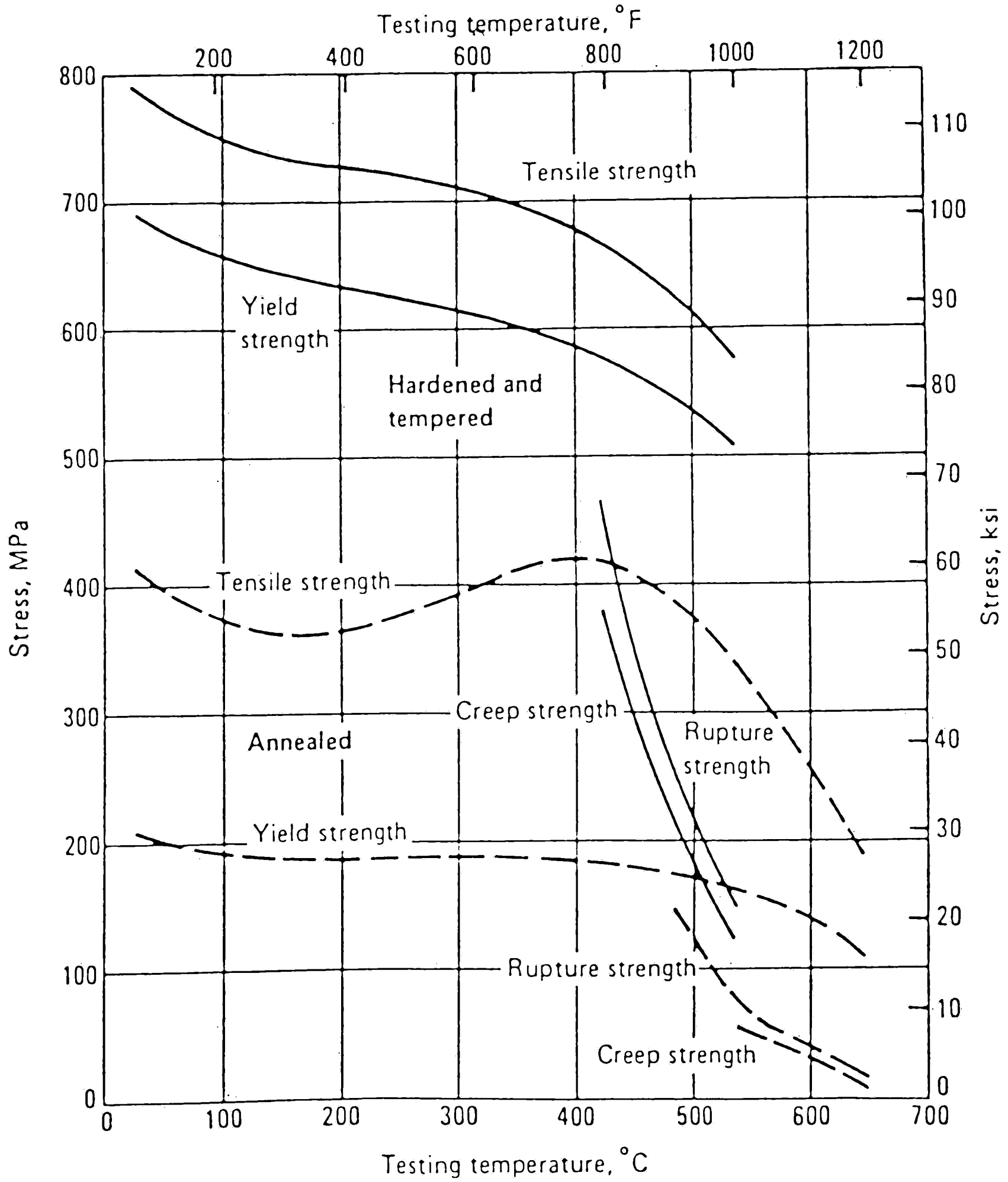

Figure 2.6: Yield stress as a function of temperature for 2.25Cr-1Mo steel [11, pg. 655].

Temperature °F	Yield Stress lb/in^2	Tangent Modulus lb/in^2
575	34,300	$1.15(10)^6$
700	34,000	$1.11(10)^6$
750	32,200	$1.10(10)^6$
900	28,000	$1.00(10)^6$
1100	16,000	$0.48(10)^6$

Table 2.1: Yield stress and tangent modulus of T22 at various temperatures [12,13].

Coating material

The initial finite element analysis, case 1, uses a single material (T22) for both the base and the coating. In this case there really is no coating, however the geometry of the waterwall is the same as if there were a coating. This will ensure that subsequent changes are not due to geometrical effects.

The second analysis uses the material properties of a cast stainless steel alloy, CC50 (ASTM A743) [14], for the coating material on the waterwall. CC50 contains 28 % (by weight) chromium for good corrosion resistance, and has an entirely ferritic structure. Detailed thermal properties as a function of temperature are not available for this alloy. Only the conduction coefficient and thermal expansion coefficient are reported at both 212 °F and 1000°F [14]. They are assumed to vary linearly within that range as a function of temperature, T,

$$\text{Thermal conductivity: } k_c = [2.59(10)^{-4} + 1.56(10)^{-7}\ \frac{T}{^\circ F}]\ \text{BTU}/(\text{sec}\cdot\text{in}\cdot^\circ\text{F}) \tag{2.6}$$

$$\text{Thermal expansion: } \alpha_c = [5.8(10)^{-6} + 6.30(10)^{-10}\ \frac{T}{^\circ F}]\ /^\circ\text{F} \tag{2.7}$$

while the other properties are assumed to remain constant [14],

$$\text{Specific Heat: } c_{p,c} = 46.4\ \text{BTU}\cdot\text{in}/(\text{lb}\cdot\text{sec}^2\cdot^\circ\text{F}) \tag{2.8}$$

$$\text{Density: } \rho_c = 7.04(10)^{-4}\ \text{lb}\cdot\text{sec}^2/\text{in}^4 \tag{2.9}$$

Equations (2.6) through (2.9) are needed for the thermal stress analysis in ANSYS.

CC50 cast stainless steel is assumed to be linearly elastic before yielding with no strain hardening after yielding at elevated temperatures. Again this material behavior is modeled in ANSYS by a bilinear stress strain curve with similar behavior in both tension and compression. The tangent modulus for this analysis is zero because there is no strain hardening. Mechanical properties at elevated temperatures were not available, so the yield stress, the elastic modulus and Poisson's ratio are assumed constant. The values used in the analysis are,

Elastic Modulus: $E_C = 29.0(10)^6$ lb/in^2

Poisson's Ratio: $\nu_C = 0.30$

Yield Stress: $\sigma_{ys,C} = 65.0(10)^3$ lb/in^2

After numerous elastic and elastic-plastic trial analyses, it was determined that the most important material property affecting the thermal stresses in the waterwall was the coefficient of thermal expansion. For the third analysis, or case three, the coefficient of thermal expansion in the coating was therefore made five percent less than the coefficient of thermal expansion of the base. The values used in the analysis are computed from

Thermal expansion: $\alpha_C = [.95(7.33(10)^{-6}) + .95(1.30(10)^{-9})\frac{T}{^\circ F}]$ /$^\circ$F (2.10)

and all other properties are left equal to those of CC50 cast stainless steel. Note that the coefficient of thermal expansion of CC50 is about 20% less than that of the base. Hence, the values obtained from eq. (2.10) represent a 15% increase above those for CC50.

3. Boundary Conditions

The three dimensional waterwall model is subjected primarily to radiation on the fireside, free convection on the ambientside, and forced turbulent convection on the waterside, (Figure 3.1). To model the boiler environment the fireside is first exposed to steady state radiant heat flux corresponding to a slag build up. Then more severe radiant heat flux is imposed on the fireside to model the exposure of the surface after a slag fall. This produces a nonsteady-state situation immediately following the slag fall, however a steady-state is reached rather quickly with the new radiation condition. The fireside radiant heat flux will slowly return to its original state once again as slag builds up.

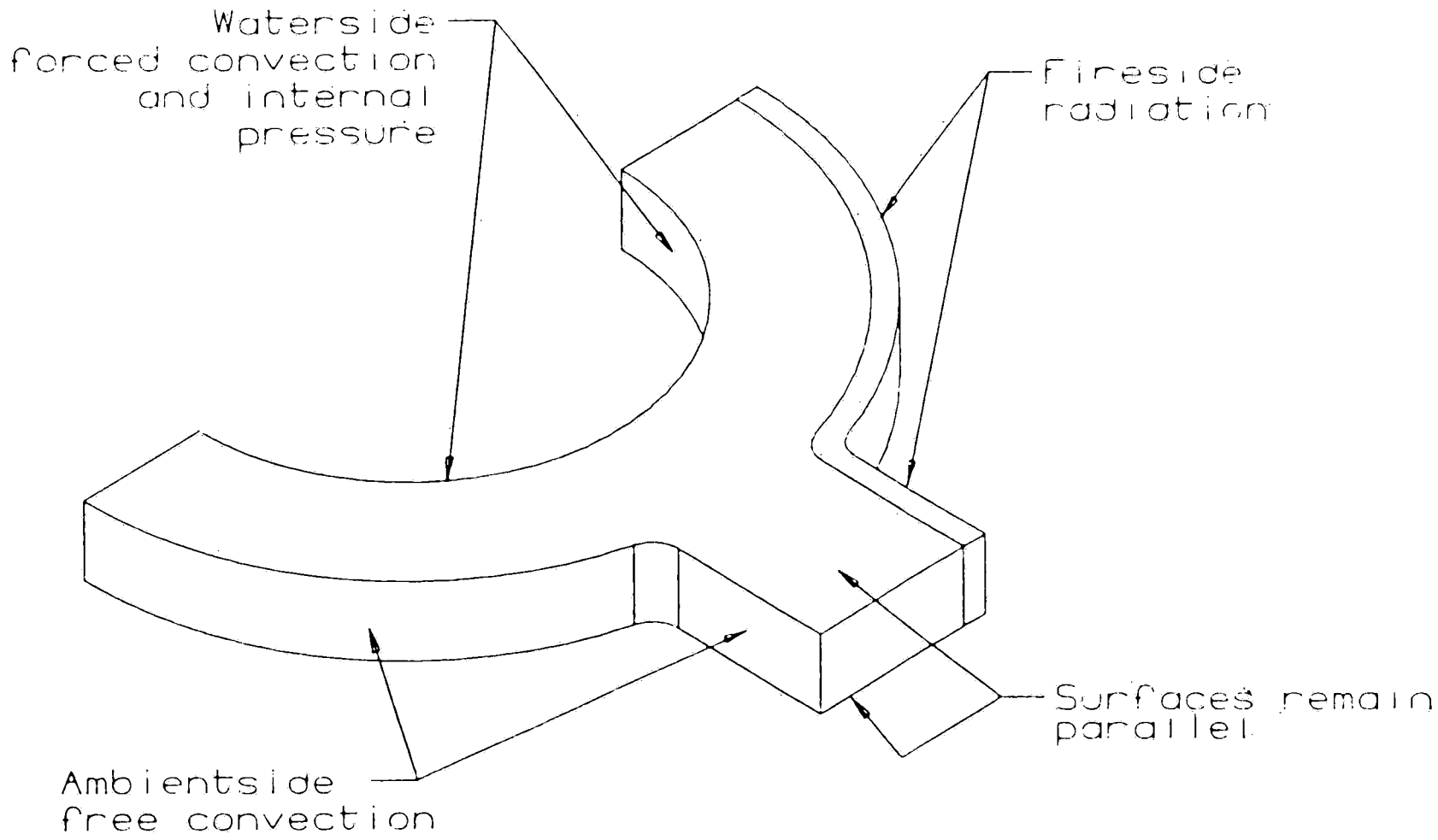

Figure 3.1: Model of coated waterwall section.

In actuality, both radiation and convection occur on the fireside, however radiation accounts for nearly 99 % of the heat flux into the waterwall [2]. Therefore only radiation is considered on the fireside. The radiant heat flux condition can be approximated by a convection condition within ANSYS in the following manner,

$$q = \text{heat flux} = \frac{\text{Energy}}{\text{Area}\cdot\text{time}} = h_r(T_{bf} - T) \tag{3.1}$$

where h_r is a coefficient for radiation heat transfer, T_{bf} is the bulk furnace or fireball temperature and T is wall temperature. To correctly model the fourth power law of radiation, the convection coefficient, h_r, must be

$$h_r = \sigma[(T_b+T_0)^2 + (T+T_0)^2](T_{bf} + T + 2T_0) \tag{3.2}$$

where σ, the Stefan Boltzman constant for black body radiation, equals $3.34(10)^{-15}$ BTU/(sec·in^2·R^4) and $T_0 = 460$ °R. This expression can be simplified for use in ANSYS,

$$h_r = C_0 + C_1T + C_2T^2 + C_3T^3 \tag{3.3}$$

the coefficients ($C_{0,1,2,3}$) are calculated with $T_{bf} = 2500$ °F and the expression is evaluated at various waterwall temperatures to provide for a temperature dependent radiation heat transfer coefficient [2]. To model the reduced heat flux due to slag buildup, T_{bf} in equation (3.1) is simply reduced from 2500 °F to 1125 °F. This reduction in bulk furnace temperature could be replaced by a change in h_r to account for slag buildup, but the end result would still be steady state temperatures similar to those experienced in a real boiler environment [9].

On the backside or ambientside of the waterwall, free convection provides for heat transfer to the surroundings. To model convection, it is necessary to know the film coefficient of convection and the bulk temperature of the fluid adjacent to the convective surface. A typical value for the film coefficient of free convection from steel to air is $h_f = 5$ W/(m^2·°C) $= 1.70(10)^{-6}$ BTU/(sec·in^2·°F) [15]. The bulk temperature was taken to be $T_{ba} = 390$ °F, which is the average of the surrounding seasonal temperature far from the ambientside and the expected tube surface temperature at the ambientside.

The inside or waterside is subject to convection in which a temperature dependent convection coefficient represents the condition found in a supercritical coal fired utility boiler. When the bulk temperature, T_{bi}, of the cooling water is near 700 °F and pressure is about 3600 psia, the water is near the pseudo-critical point, or point of maximum

specific heat. As shown in Figure 3.2, the specific heat varies dramatically as a function of temperature under these operating conditions. This means that the convection coefficient is highly dependent on temperature. The model uses a convection coefficient calculated from a correlation that takes into account temperature dependent fluid properties and is specifically determined for forced internal convection at supercritical pressures in the pseudo-critical region [17].

$$h_b = \frac{Nu_b\ k_b}{d} = \text{convection coefficient} \tag{3.4}$$

$$Nu_b = 0.0183\ Re_b^{0.82}\ Pr_b^{0.5}\ (\frac{\rho_w}{\rho_b})^{0.5}\ (\frac{\bar{c}_p}{c_{p,b}})^{.4} = \text{Nusselt number} \tag{3.5}$$

$$Re_b = \frac{\rho_b\ u_m\ d}{\mu_b} = \text{Reynolds number} \tag{3.6}$$

$$Pr_b = \frac{\mu_b\ c_{p,b}}{k_b} = \text{Prandtl number} \tag{3.7}$$

$$\bar{c}_p = \frac{i_w - i_b}{T_w - T_{bi}} \tag{3.8}$$

$c_{p,b}$ = specific heat

k_b = conduction coefficient

μ_b = dynamic viscosity

i_w, i_b = enthalpy

ρ_w, ρ_b = density

u_m = mean flow velocity

Subscript b refers to bulk properties of the cooling water at T_{bi} = 700 °F, subscript w refers to properties at the inside wall temperature, T_w. The mean flow velocity, u_m, is taken as 72 in./sec. [8] and the flow diameter, d is 0.810 in. The convection coefficient is calculated (see appendix I) at various wall temperatures and used in ANSYS as a temperature dependent parameter.

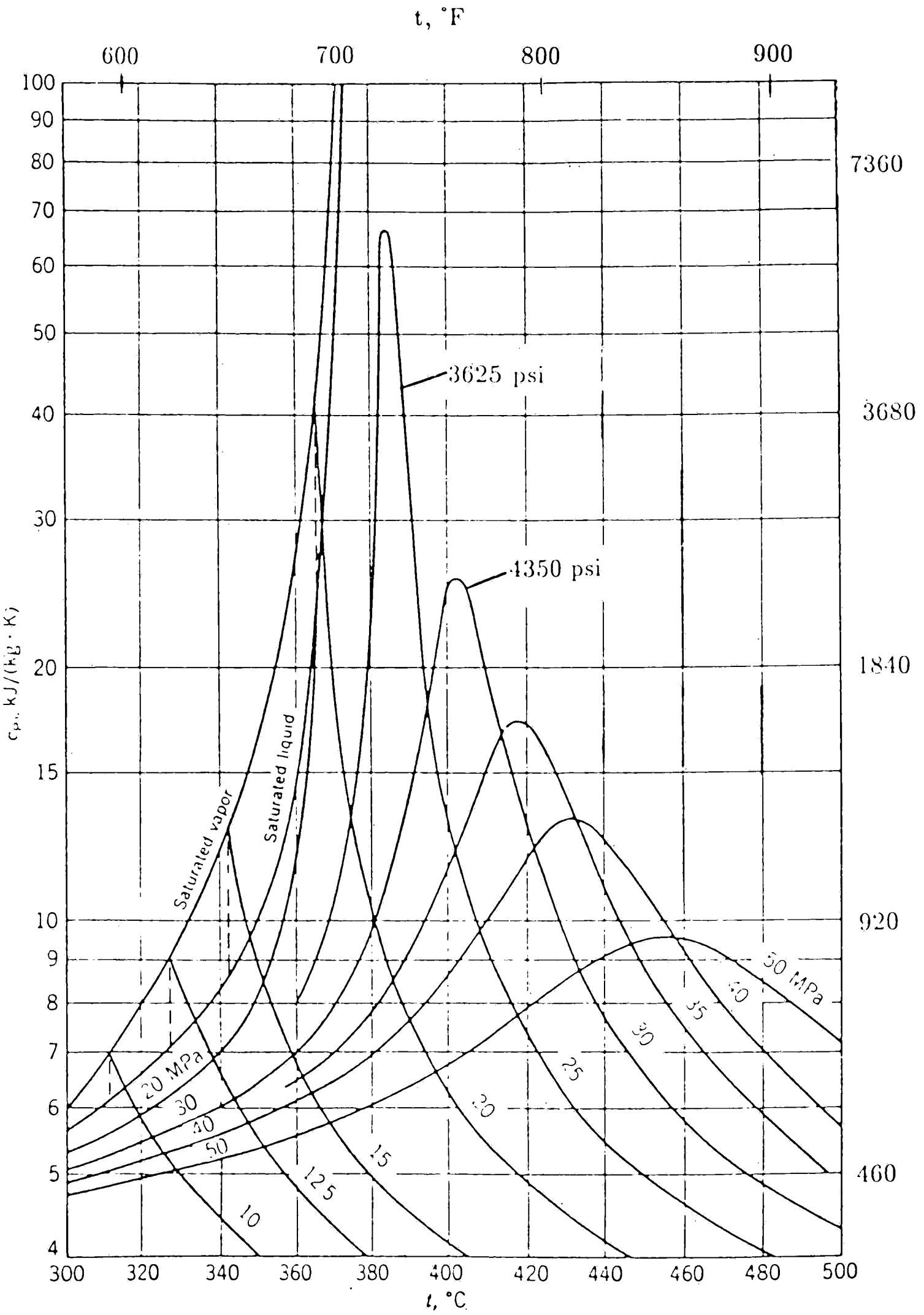

Figure 3.2: Specific heat of water as a function of temperature for various pressures [16].

Therfore, the boundary conditions for the thermal analysis are

Boundary	Before slag fall	Without slag	Slag buildup
	(t=0 sec.)	(0<t≤50.6 sec.)	(50.6<t≤101.2 sec.)
$z = 0$	$q_z = 0$	$q_z = 0$	$q_z = 0$
$z = \frac{w_t}{10}$	$q_z = 0$	$q_z = 0$	$q_z = 0$
$x = 0$	$q_x = 0$	$q_x = 0$	$q_z = 0$
$x = c/2$	$q_x = 0$	$q_x = 0$	$q_z = 0$
Waterside	$q_r = -h_b(T-T_{bi})$	$q_r = -h_b(T-T_{bi})$	$q_r = -h_b(T-T_{bi})$
Fireside	$q_n = h_r(T-.45(T_{bf}))$	$q_n = h_r(T-T_{bf})$	$q_n = h_r(T-.45(T_{bf}))$
Ambientside	$q_n = h_f(T-T_{ba})$	$q_n = h_f(T-T_{ba})$	$q_n = h_f(T-T_{ba})$

where w_t is the tube wall thickness, c is the center to center tube spacing, t is the time measured from the instant of the slag fall, r is the radial coordinate, x is a horizontal coordinate in the plane of the waterwall, y is a horizontal coordinate normal to the plane of the waterwall, z is the vertical, or axial coordinate, q_x, q_z, and q_r are heat fluxes, and T is temperature. The heat flux normal to the surface of the waterwall, q_n, is positive when directed from the wall into the fireball or into the air. The radial heat flux, q_r, on the other hand is positive if directed radially outward from the water into the waterwall tube.

The waterwall is allowed to expand freely, but the centerlines of the waterwall tubes are constrained (by buckstays, etc.) to remain vertical. Thus, the top and bottom surfaces of the portion modeled are horizontal at all times. Because of symmetry, the membrane should have a vertical plane of symmetry at $x = c/2$ which remains flat, and the tube at $x = 0$ should have no displacement in the x direction. The boundary conditions for these surfaces involve, therefore, specifying displacement constraints on the

bottom surface and invoking a generalized plane strain option. The inside and outside surfaces are not constrained. The mechanical boundary conditions for the stress analysis are

$z = 0$	$w = 0$	$\tau_{xz} = \tau_{yz} = 0$	
$z = \frac{w_t}{10}$	$w =$ constant	$\tau_{xz} = \tau_{yz} = 0$	$\int_A \sigma_z dA = 0$
$x = 0$	$u = 0$	$\tau_{xz} = \tau_{xy} = 0$	
$x = c/2$	$u =$ constant	$\tau_{xz} = \tau_{xy} = 0$	$\int_{A_m} \sigma_x dA_m = 0$
Waterside	$\sigma_r = p$	$\tau_{rz} = \tau_{r\theta} = 0$	
Fireside	$\sigma_n = 0$	$\tau_{nz} = \tau_{ns} = 0$	
Ambientside	$\sigma_n = 0$	$\tau_{nz} = \tau_{ns} = 0$	

where u and w are the x and z components of the displacement, σ_n, σ_r, σ_z and τ_{xz}, τ_{yz}, τ_{xy}, τ_{rz}, $\tau_{r\theta}$, τ_{nz}, τ_{ns} are components of stress, p is internal pressure of 3630 psia (25 MPa). A is the cross sectional area of the portion modeled perpendicular to the z axis and A_m is the cross sectional area of the membrane perpendicular to the x axis.

4. Finite Element Analysis Using ANSYS

The finite element thermal analysis of the waterwall section is performed using the isoparametric thermal solid element (STIF70 in ANSYS). It has eight nodal points defining six surfaces, and there is one degree of freedom, temperature, at each node. The element may be used in a three dimensional steady state or transient thermal analysis. The thermal conductivity, specific heat, and density may be functions of temperature.

To compute the stresses in the section, the thermal element is replaced by an equivalent structural element (STIF45 in ANSYS). It has three degrees of freedom, the components of displacement, at each node. The element has the capacity for plastic yielding, and it can be used with a generalized plane strain option. The material properties of this element, the modulus of elasticity, Poisson's ratio, yield stress, tangent modulus, and coefficient of thermal expansion, may depend on temperature.

The temperature distribution is obtained from the numerical solution of the following equation:

$$\rho\, c_p \frac{\partial T}{\partial t} = \frac{\partial}{\partial x}(k \frac{\partial T}{\partial x}) + \frac{\partial}{\partial y}(k \frac{\partial T}{\partial y}) + \frac{\partial}{\partial z}(k \frac{\partial T}{\partial z}) \tag{4.1}$$

where

ρ = density (Mass/Volume)

c_p = specific heat (Energy/(Mass·Deg))

k = Thermal conductivity (Energy/(Length·Time·Deg))

The stresses, strains and displacements in the body can be obtained from the numerical solution of:

(i) Equilibrium equations:

$$\frac{\partial \sigma_x}{\partial x} + \frac{\partial \tau_{xy}}{\partial y} + \frac{\partial \tau_{xz}}{\partial z} = 0 \tag{4.2}$$

$$\frac{\partial \tau_{xy}}{\partial x} + \frac{\partial \sigma_y}{\partial y} + \frac{\partial \tau_{yz}}{\partial z} = 0 \tag{4.3}$$

$$\frac{\partial \tau_{xz}}{\partial x} + \frac{\partial \tau_{yz}}{\partial y} + \frac{\partial \sigma_z}{\partial z} = 0 \tag{4.4}$$

where the normal stresses are σ_x, σ_y, σ_z and the shear stresses are τ_{xy}, τ_{yz}, τ_{xz}.

(ii) Stress-Strain relations (linear elastic, isotropic):

$$\epsilon_x = \frac{1}{E}(\sigma_x - \nu(\sigma_y+\sigma_z)) + \alpha(T-T_{ref}) \tag{4.5}$$

$$\epsilon_y = \frac{1}{E}(\sigma_y - \nu(\sigma_x+\sigma_z)) + \alpha(T-T_{ref}) \tag{4.6}$$

$$\epsilon_z = \frac{1}{E}(\sigma_z - \nu(\sigma_x+\sigma_y)) + \alpha(T-T_{ref}) \tag{4.7}$$

$$\gamma_{xy} = \frac{\tau_{xy}}{G}, \quad \gamma_{yz} = \frac{\tau_{yz}}{G}, \quad \gamma_{xz} = \frac{\tau_{xz}}{G} \tag{4.8), (4.9), (4:10}$$

where the normal strains are ϵ_x, ϵ_y, ϵ_z and the shear strains are γ_{xy}, γ_{yz}, γ_{xz}. T_{ref} is the temperature at which there are no thermal strains. In any plastic zones that may develop, the appropriate elactic-plastic relations between stresses and strains are used.

α = coefficient of thermal expansion

E = modulus of elasticity

ν = Poisson's ratio

$G = \frac{E}{2(1+\nu)}$ = shear modulus

(iii) Strain-displacement relations:

$$\epsilon_x = \frac{\partial u}{\partial x}, \quad \epsilon_y = \frac{\partial v}{\partial y}, \quad \epsilon_z = \frac{\partial w}{\partial z} \tag{4.11), (4.12), (4.13}$$

$$\gamma_{xy} = \frac{\partial u}{\partial y} + \frac{\partial v}{\partial x}, \quad \gamma_{yz} = \frac{\partial v}{\partial z} + \frac{\partial w}{\partial y}, \quad \gamma_{xz} = \frac{\partial u}{\partial z} + \frac{\partial w}{\partial x} \tag{4.14), (4.15), (4.16}$$

where the displacements are u, v, w.

Thermal stress solutions are obtained from two ANSYS analyses in sequence. The first analysis determines the temperature distribution within the model for various times. However, since temperature dependent material properties are used along with temperature dependent heating and cooling boundary conditions, several iterations are required for each time step. Then the nodal temperatures from the thermal analysis are directly input to an ANSYS structural analysis to determine the stresses and deformations for each value of time. Again, several iterations are required for each step

in order to determine the extent of the plastic zones and the values of the stresses and strains after the plastic deformations.

5. Temperature Distribution

In this and the following section, references will be made to two regions of the waterwall. These are the apex and fillet regions and their locations are shown in Figure 5.1. Furthermore, values of temperature and stress will be plotted as functions of distance along a path in these regions. These paths are also shown in Figure 5.1, with the path through the apex denoted AA' and the path in the fillet region denoted FF'. It should be noted that at the apex the path starts at the inner radius of the waterwall tube and ends at the fireside while in the fillet region the path begins at the centerline of the membrane and ends normal to the fireside at the midpoint of the fillet arc. Values of temperature and stress at the interface between the coating and the base and at the fireside on AA' and FF' will also be plotted as functions of time following the slag fall .

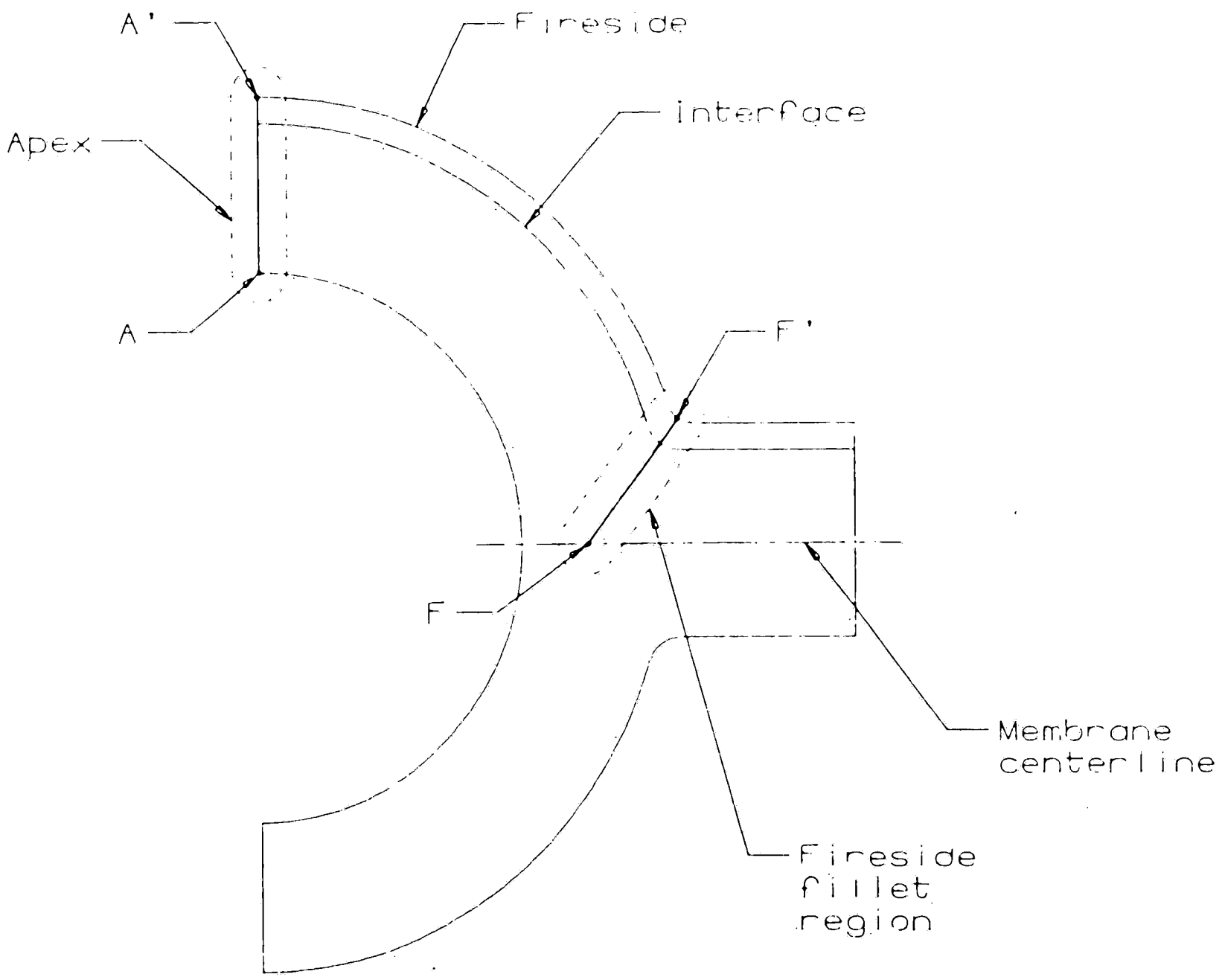

Figure 5.1. Regions of interest in the waterwall model and subsequent paths through the regions.

Varying the thermal properties of the coating has only a small impact on the steady state and transient temperature distributions in the waterwall and virtually no impact on the stresses. In fact, increasing the coeffecient of thermal conductivity of the coating by 20% decreases the stresses in the coating by only about 5%. Therfore only the results of the transient thermal calculations for the combination of T22 base and CC50 coating are presented here. Figure 5.2 shows the temperature distribution on path AA' before the slag fall (0), for several times following the slag fall, and back again to conditions prior to the slag fall (R). Initially there is a nearly bilinear temperature distribution, due to dissimilar thermal properties of the coating and base. Immediately following the slag fall, the fireside surface temperature increases faster than interior points and there is a steeper temperature gradient toward the fireside. After approximately twenty seconds, all of the interior points have reached their respective maximum temperatures, as can be seen by the nearly linear temperature distribution at that time in Figure 5.2. The temperature distribution changes little in the following forty seconds. After a gradual buildup of slag, the temperatures across the apex return to their original levels.

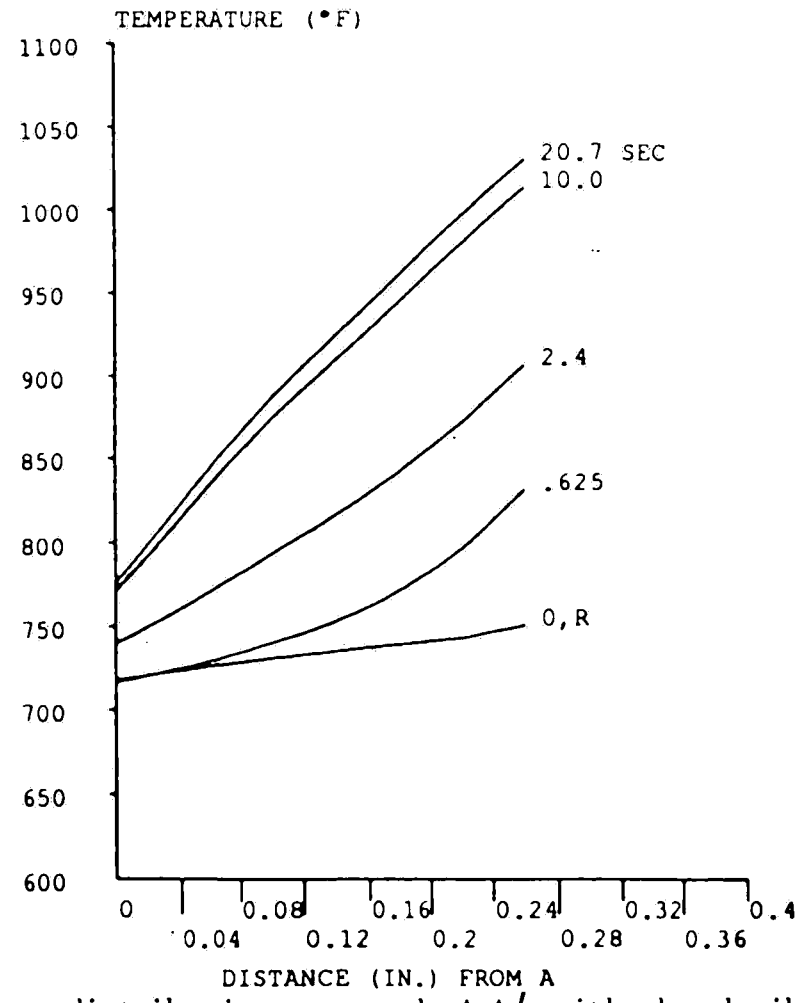

Figure 5.2: Temperature distribution on path AA' with slag buildup (0,R) and at various times after the slag fall.

In Figure 5.3 the temperature at the fireside and interface on path AA' is plotted as a function of time following the slag fall. Notice that the temperature at the fireside increases quickly after the slag fall, and reaches its maximum value in approximately 14 seconds. Notice also that the interface point reaches its peak temperature at about the same time. However, immediately following the slag fall, the temperature at the fireside increases at a slightly faster rate than at the interface.

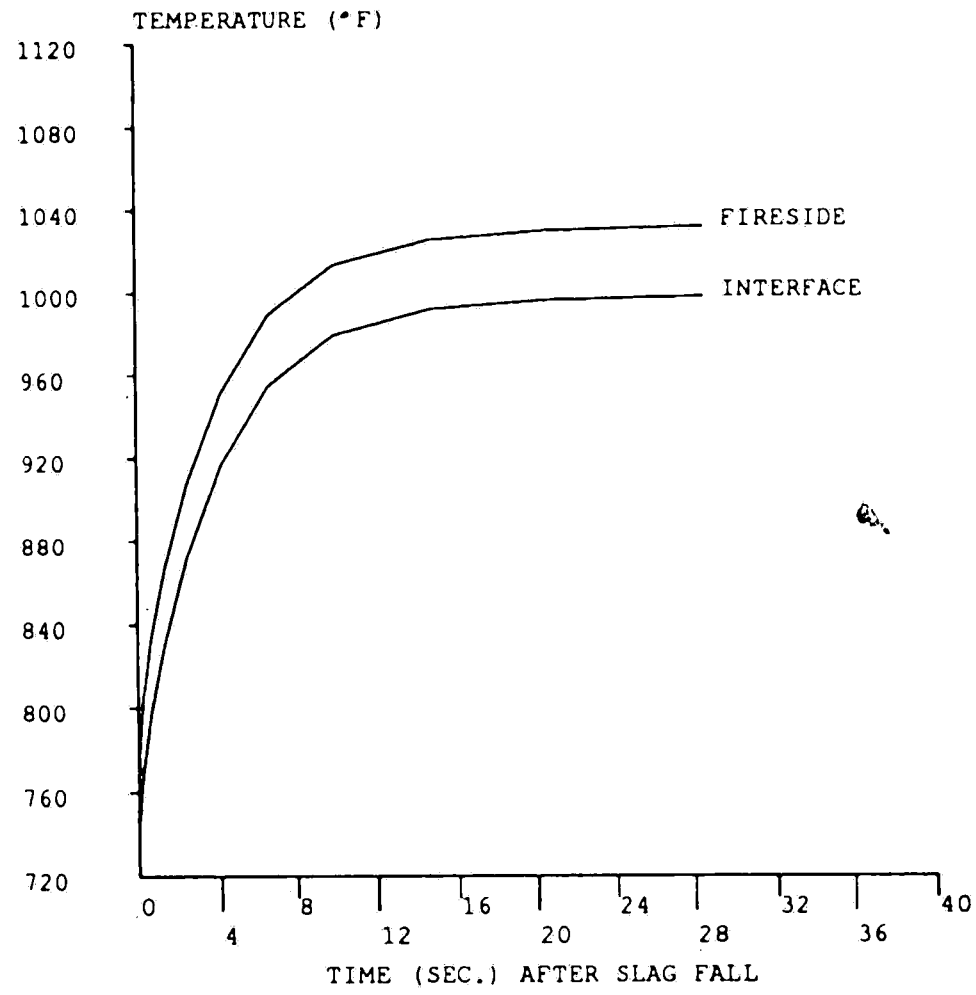

Figure 5.3: Temperature as a function of time following the slag fall for two locations on path AA'.

Figure 5.4 shows the temperature distribution on path FF′ with a slag buildup and for several times after the slag fall. As at the apex there is an initial steady temperature distribution, and following the slag fall the fireside surface temperature increases faster than interior points. However, the thermal gradient is not as severe because the starting point on path FF′ is at the membrane centerline and is not adjacent to the cooling water. After approximately twenty seconds a new steady temperature distribution is achieved as shown in Figure 5.3. After a gradual buildup of slag, the temperatures in the fillet region return to their original levels.

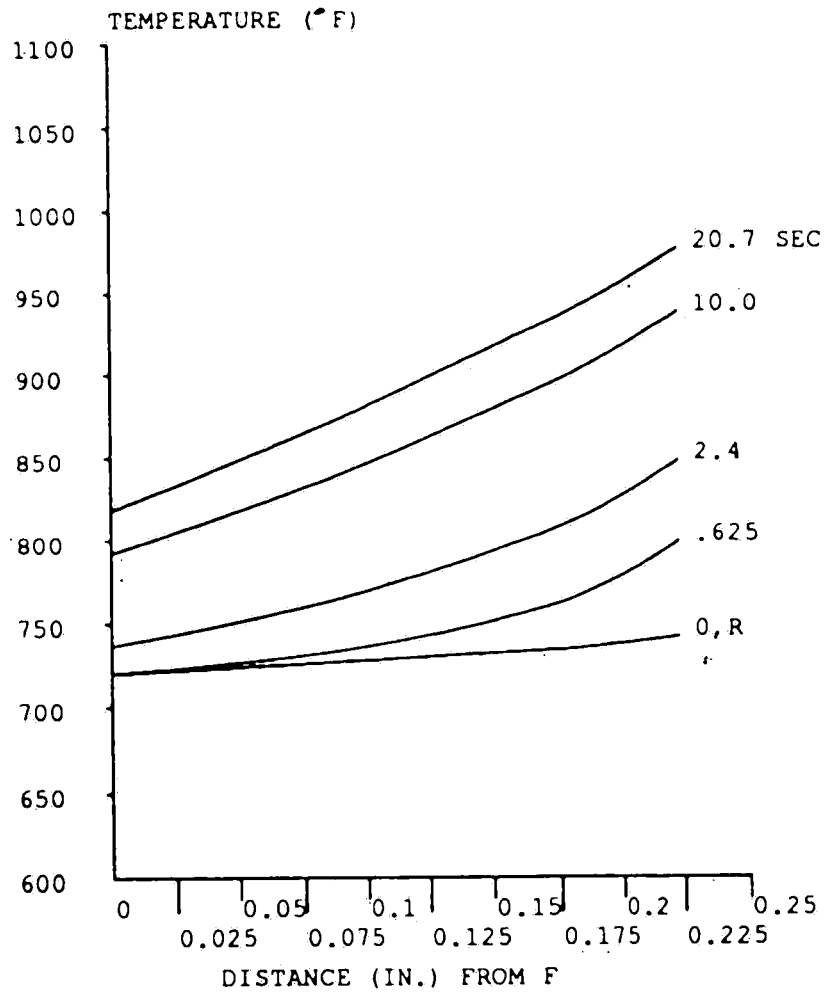

Figure 5.4: Temperature distribution on path FF′ in the fireside fillet region with a slag buildup (0,R) and at various times following the slag fall.

In Figure 5.5 the temperature at the fireside and interface on path FF′ is plotted as a function of time following the slag fall. Notice that the temperatures do not reach their maximum values until at least 28 seconds after the slag fall.

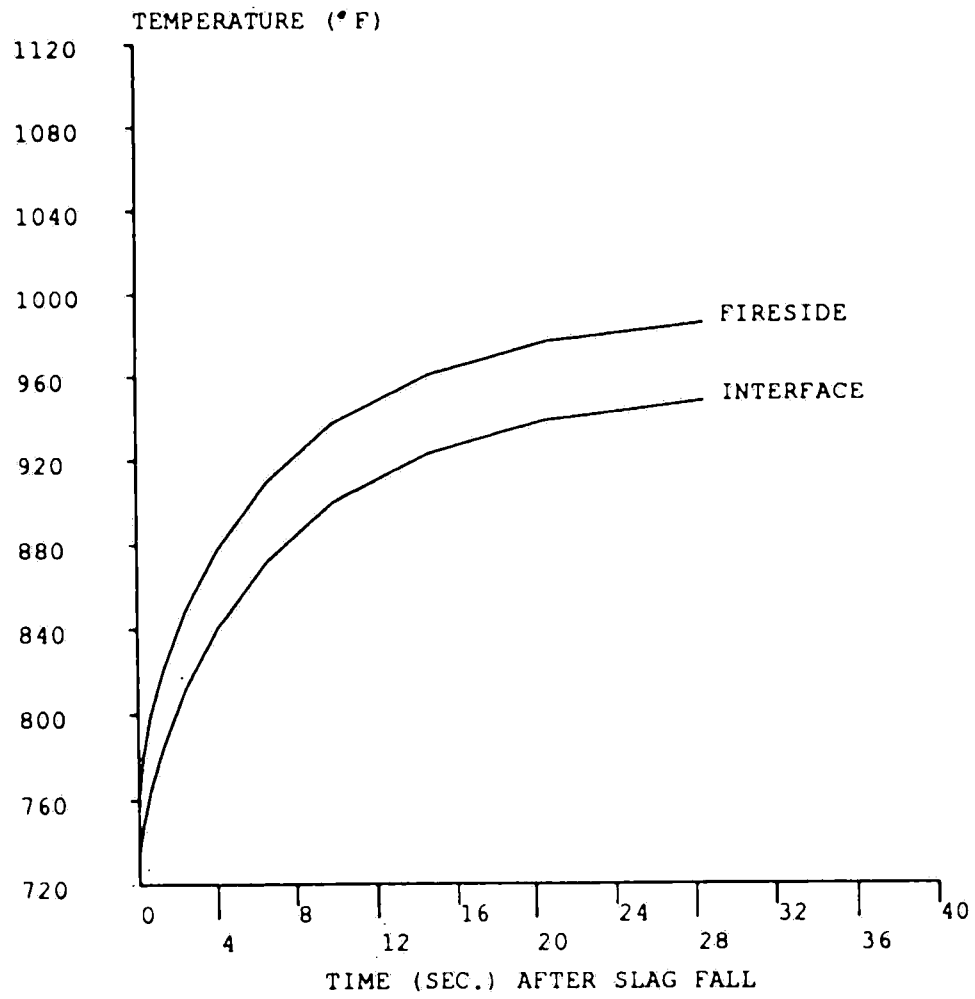

Figure 5.5: Temperature as a function of time following the slag fall at two locations on path FF′.

6. Stress Distribution

Following a slag fall, the material close to the fireside experiences a more rapid and larger temperature increase than interior points. The higher temperatures and temperature gradiants in these regions cause larger thermal stresses. These stresses will decrease to their initial values as the temperature distribution returns to the initial state only if they remain in the elastic range. However, under some conditions, the stresses in the waterwall will be large enough to cause yielding. When yielding takes place, the resulting plastic deformation leads to residual stresses which, depending on their location and sense (compressive or tensile), can either exacerbate or reduce crack initiation and growth. ANSYS was used to analyze the elastic-plastic stress behavior using temperatures computed in the thermal analysis.

Case 1: no coating. Figure 6.1 shows stress distributions on path AA', for the control case in which the waterwall is made entirely of T22. The distributions are shown with slag buildup prior to the slag fall (0), at various times after the slag fall, and again after temperatures return to the values before the slag fall (R). Notice in Figure 6.1(a) that, following the slag fall, there is a residual tensile stress of approximately 21,000 psi in the axial direction, but there is only a residual tensile stress of 12,500 psi in the tangential direction (Figure 6.1(b)). The von Mises stress distributions (Figure 6.1(d)) show the development of the plastic zone, which by twenty seconds after the slag fall is 0.11 in. thick, extending from the fireside to 0.15 in. from the inner radius at A. The radial stresses (Figure 6.1(c)) in the apex region are less than 10 % as large as the other stress components. Furthermore, there is some tensile yielding at the waterside which also affects the residual stresses.

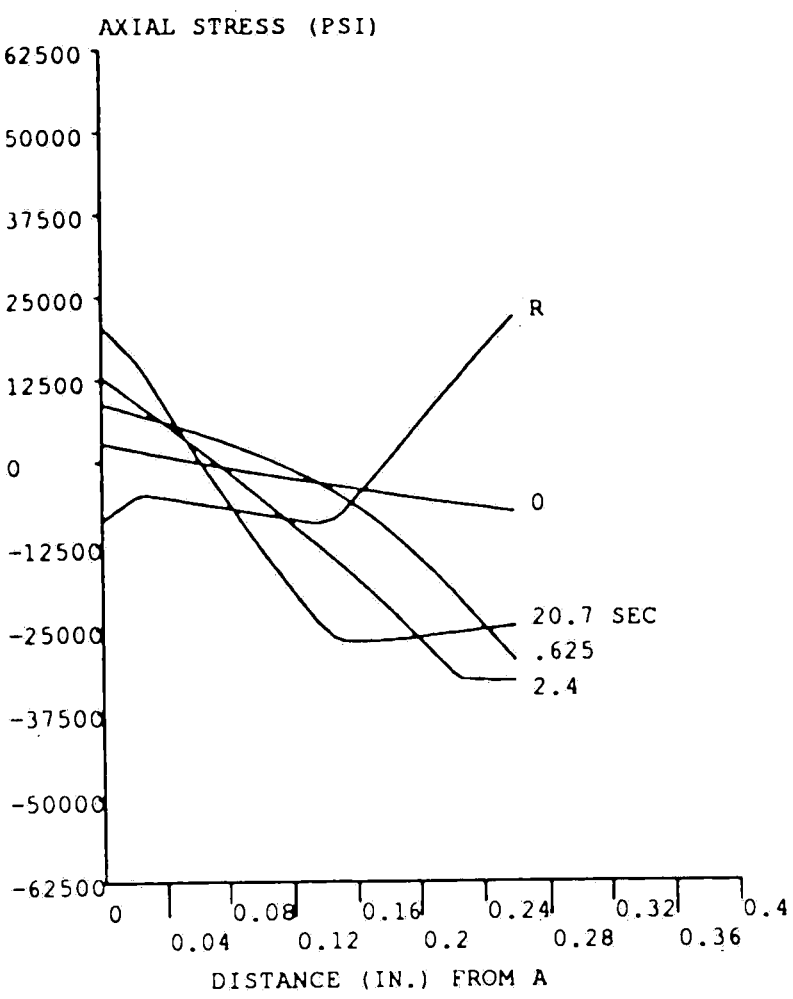

a. Axial stress

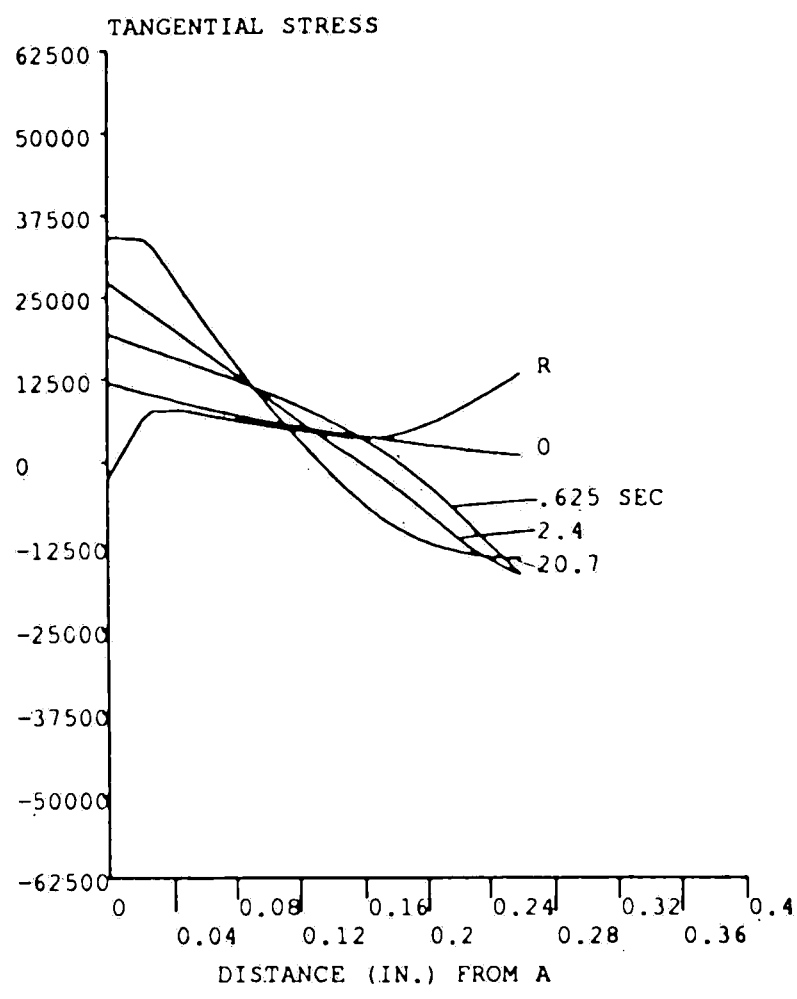

b. Tangential stress

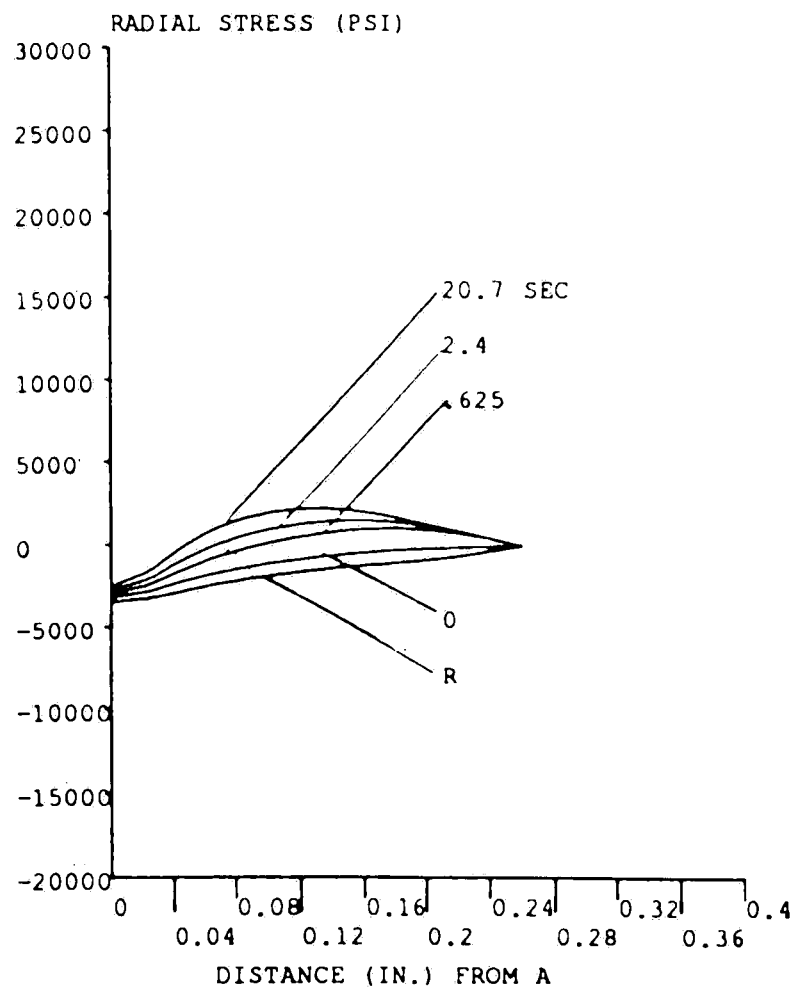

c. Radial stress

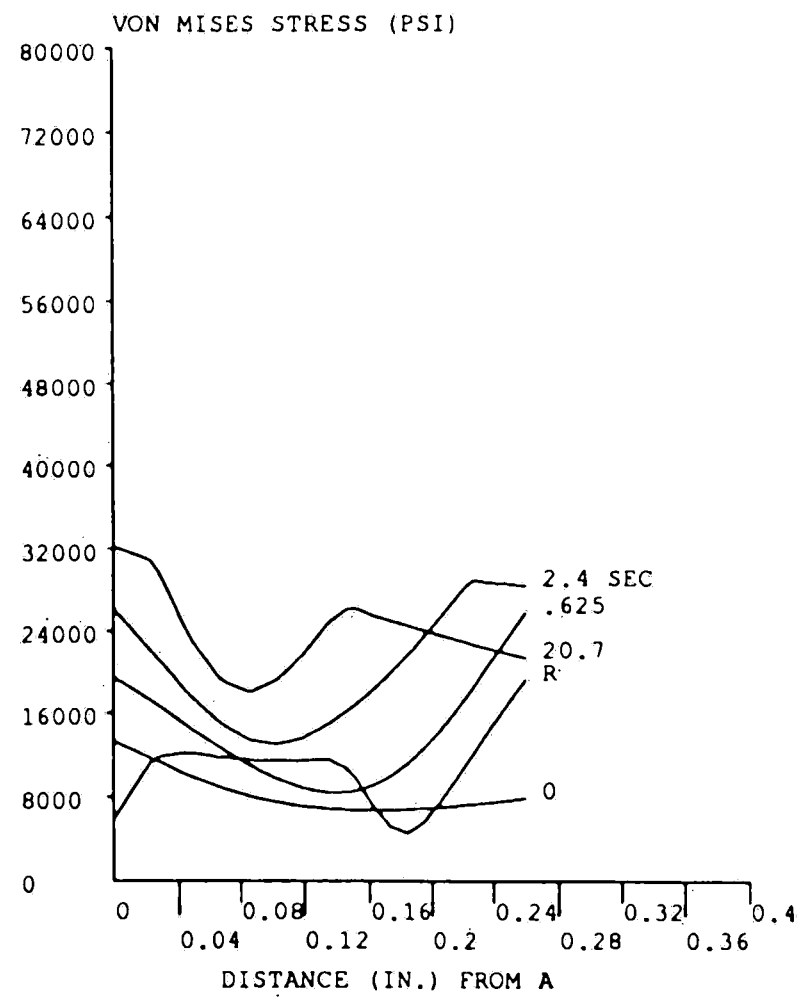

d. Von Mises stress

Figure 6.1: Stress distributions on path AA′ with a slag buildup (0 and R) and at various times after the slag fall for the waterwall made entirely of T22.

Figure 6.2 shows the time dependence of axial and tangential stress following the slag fall, at two locations on path AA' for the waterwall made entirely of T22. Figures 6.2(a) and (b) are similar in that they both show an immediate increase in compressive stress in both the axial and tangential directions at the fireside and at the interface, with the axial stress approaching stress levels equal to the the yield stress for T22. However, the material at the fireside reaches its maximum compressive stress in about 1.5 seconds following the slag fall and the material at the interface reaches its maximum stress at about 2.5 seconds after the slag fall.

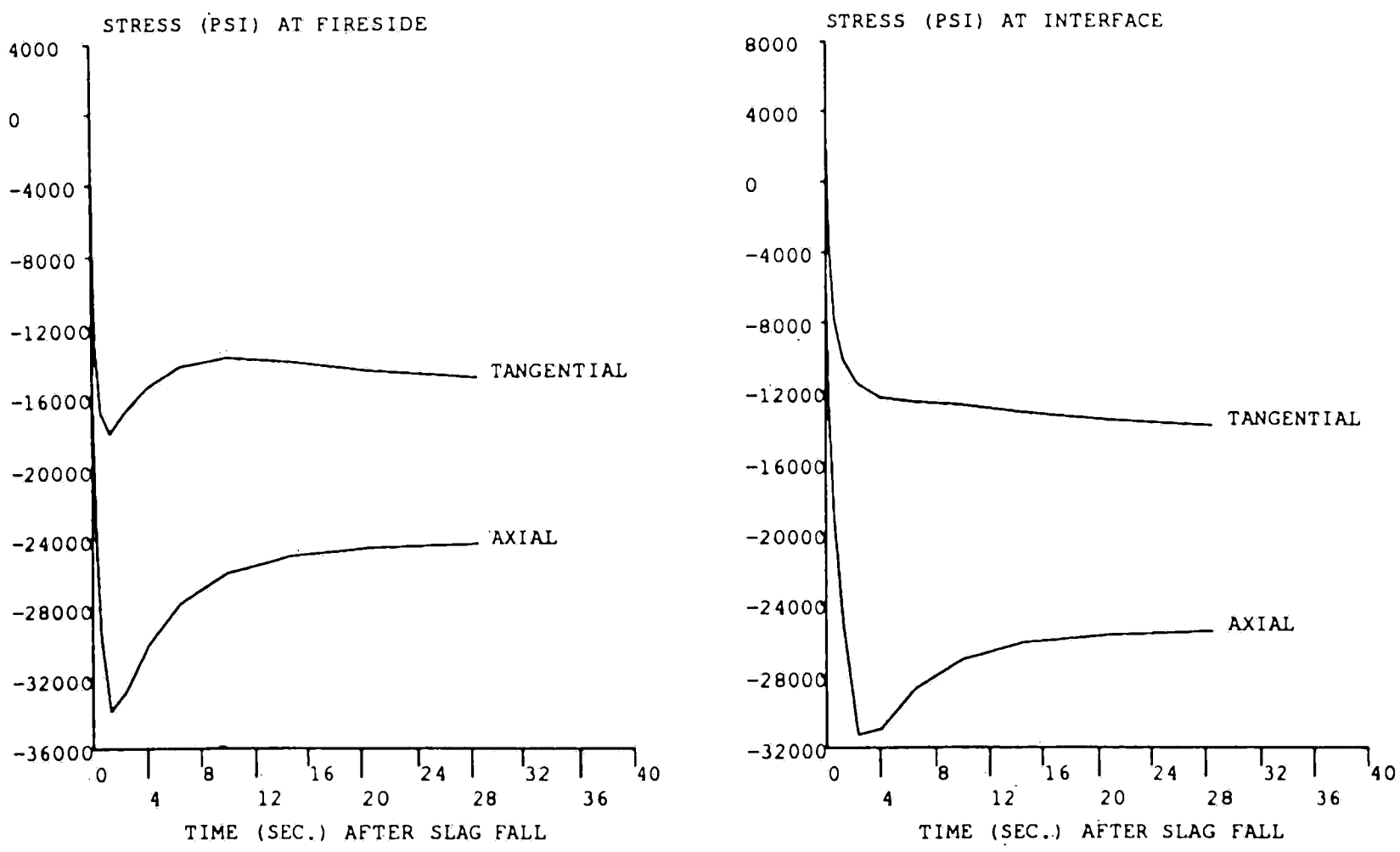

a. Fireside

b. Interface

Figure 6.2: Axial and tangential stresses as functions of time following the slag fall at two locations on path AA' for the waterwall made entirely of T22.

Figure 6.3 shows some stress distributions on path FF′ for the waterwall made entirely of T22. The distributions are shown with slag buildup and at various times after the slag fall. Keep in mind that radial and tangential stress directions are based on a cylindrical coordinate system located at the arc-center of the fillet. Figures 6.3(a) and (b) show a rapid increase, following the slag fall, in compressive stress in the axial and tangential directions near the fireside. However, there is a larger residual tensile stress (about 35,500 psi) in the tangential direction than in the axial direction (20,000 psi). Moreover it appears that the material at the fireside yields in tension when returning the the initial temperatures. Notice also in Figure 6.3(c) that, during the slag fall, the radial stress in the outer region becomes compressive and about half as large as the stresses in the other two directions. When the temperatures return to their initial levels there is a residual tensile radial stress of 10,000 psi. If this had been a case with an actual coating whose material properties matched those of T22, then this radial fatigue cycle could lead to delamination of the coating. Figure 6.3(d) shows the von Mises stress distribution in the fillet region. Notice the development of plastic flow near the fireside following the slag fall as well as a reverse plastic flow after returning to the temperatures prior to the slag fall. It appears that the residual tangential stress would have been much higher were it not for this reverse flow. Such a severe fatigue cycle indicates a tendency to form cracks perpendicular to the tangential direction (vertical).

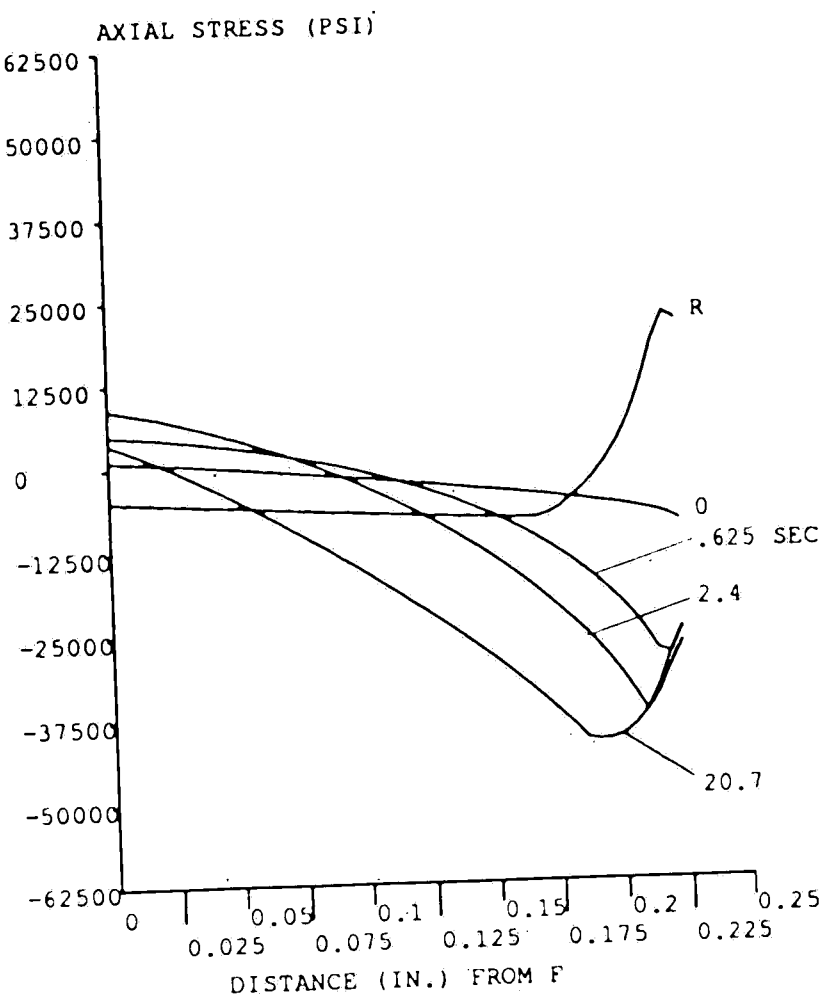

a. Axial stress

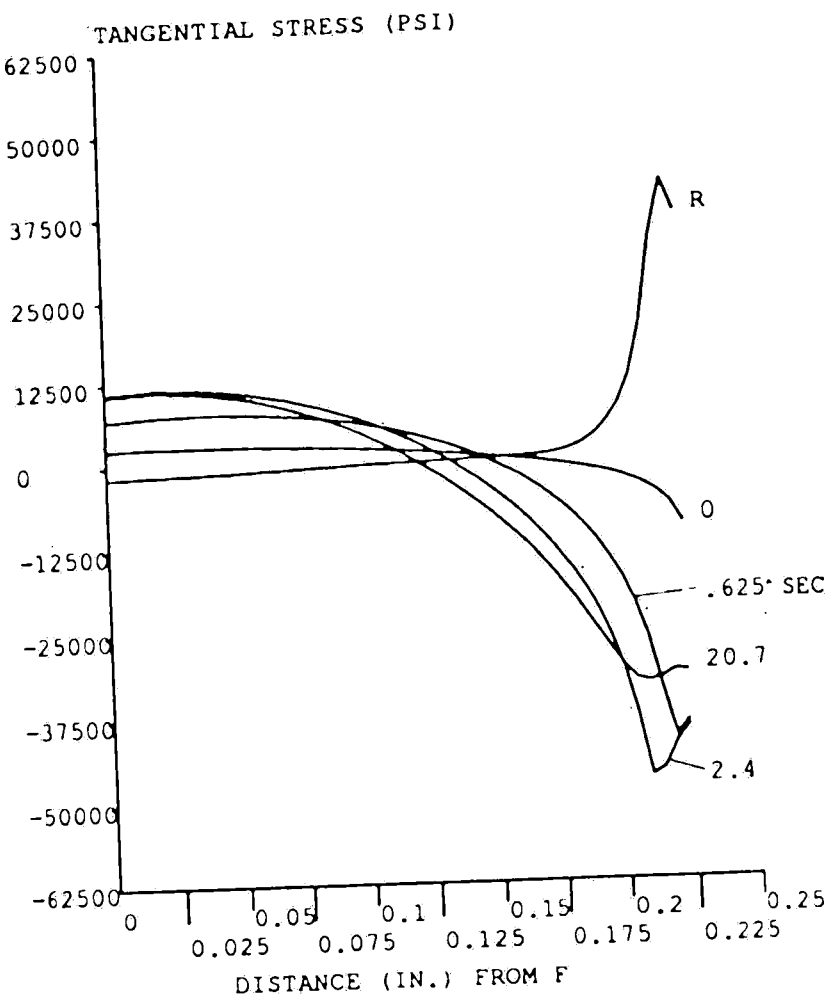

b. Tangential stress

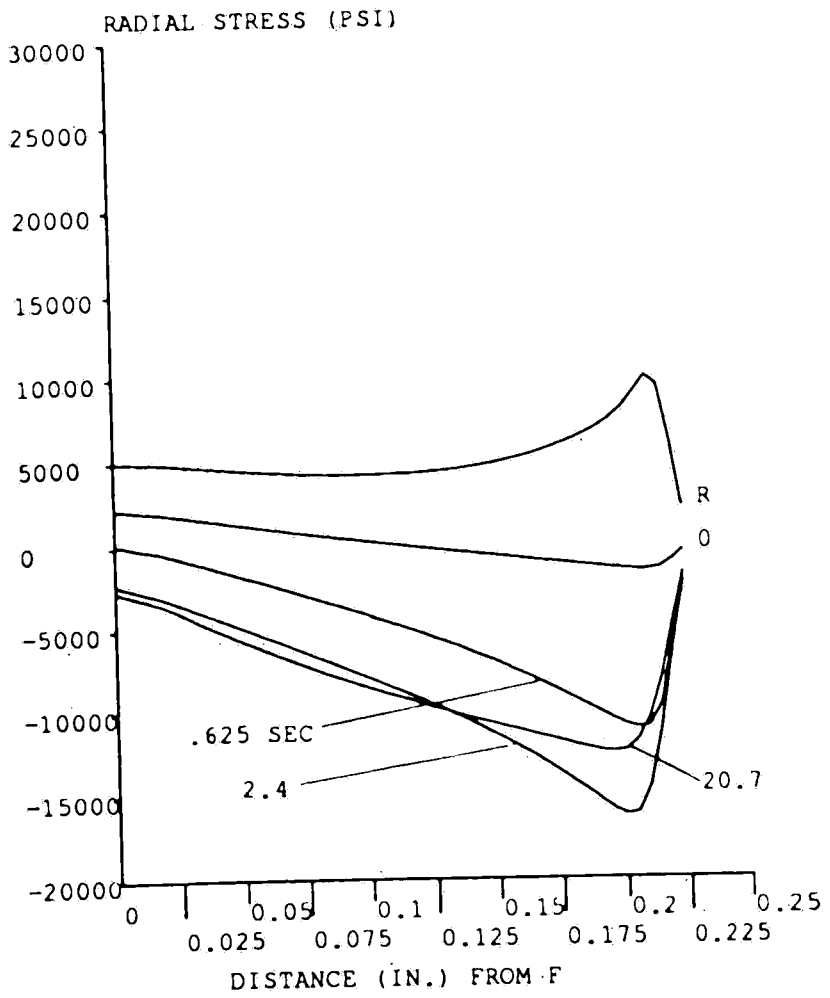

c. Radial stress

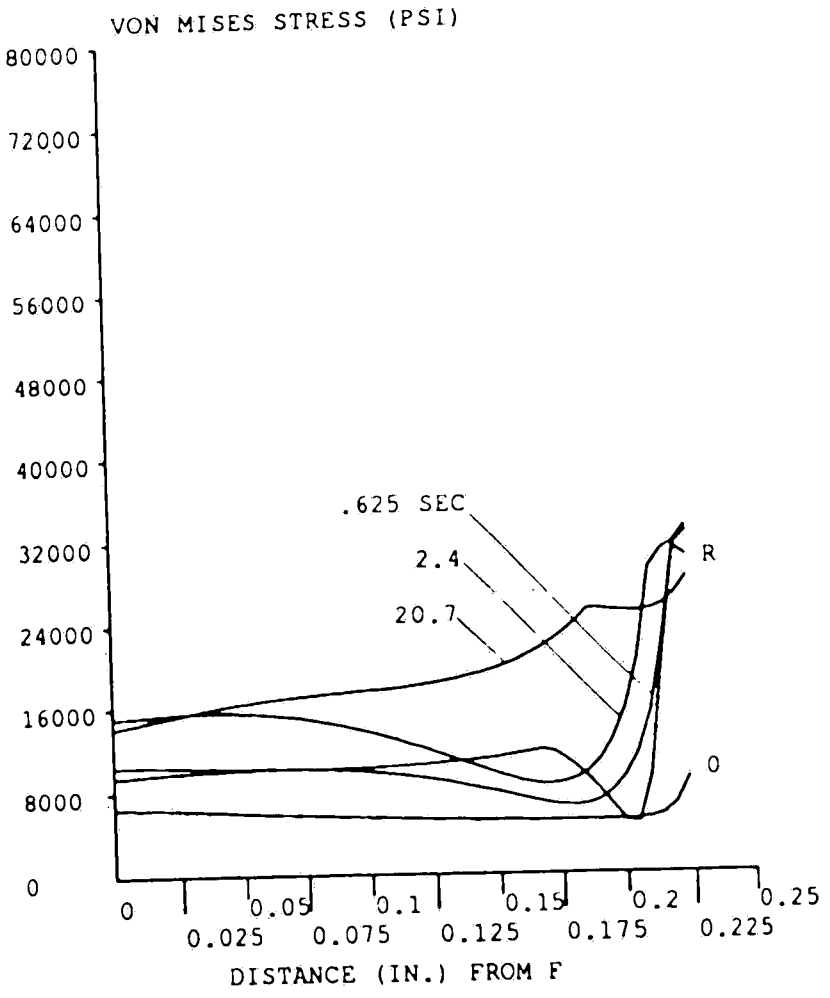

d. Von Mises stress

Figure 6.3: Stress distributions on path FF′ with a slag buildup (0 and R) and at various times after the slag fall, for the waterwall made entirely of T22.

Figure 6.4 shows the time dependence of axial, tangential and radial stresses following the slag fall, at two locations on path FF′, for the waterwall made entirely of T22. Figure 6.4(a) shows how the tangential stress at the fireside becomes more compressive than the axial stress following the slag fall and that yielding begins less than one second after the slag fall. Figure 6.4(b) shows that the radial stress at the interface also becomes more compressive after the slag fall. However, at this location the axial stress has the largest magnitude.

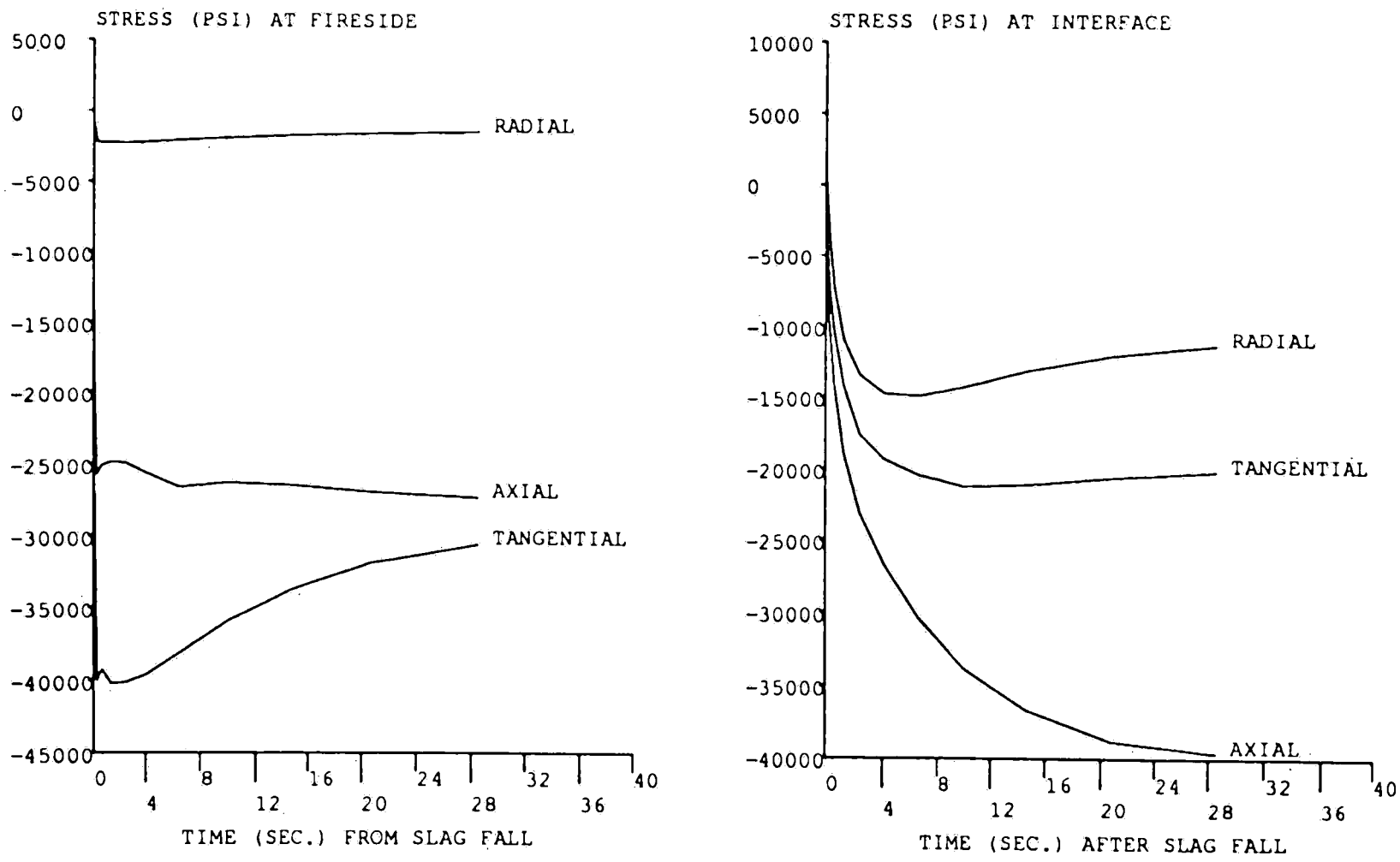

a. Fireside

b. Interface

Figure 6.4: Axial, tangential and radial stresses as functions of time following the slag fall at two locations on path FF′ for the waterwall made entirely of T22.

Case 2: CC50 coating. For a second set of calculations, the combination of a T22 base tube and CC50 coating material is used. Figure 6.5 illustrates the resulting stress distributions on path AA′ with a slag buildup and at several times following the slag fall. Keep in mind that CC50 has a coefficient of thermal expansion about twenty percent less than that of the base T22. Therefore initially, the coating is subjected to tensile stress in both the axial and the tangential directions and the base tube is subjected to compressive axial and tangential stress adjacent to the coating. Because of the relatively large mismatch in coefficient of thermal expansion there is a large difference between the stress levels in the coating and the base. Following the slag fall, the temperatures in the coating and the outer portion of the base increase. Due to the constraint from the cooler inner material, the base material close to the coating yields in compression and the tensile stress in the coating decreases. Upon returning to the initial temperatures, the coating is at slightly reduced tensile stress levels of about 37,000 psi in the axial and 44,000 psi in the tangential directions. The residual tensile stress levels at the apex fireside for the waterwall made entirely of T22 were 21,000 psi in the axial direction and 12,500 psi in the tangential direction. However, the primary reason for the high residual tensile stresses in case 1 was the low yield stress of T22 whereas the main reason for the high residual tensile stresses in case 2 is the large mismatch in coeffecient of thermal expansion and the fact that there was no yielding in the coating. Nevertheless, with this combination of base and coating materials, the coating is always under high tensile stress, whereby it is exposed to a more deleterious fatigue cycle and is more susceptible to intergranular corrosion [1]. Hence, crack initiation on the grain boundaries would be likely.

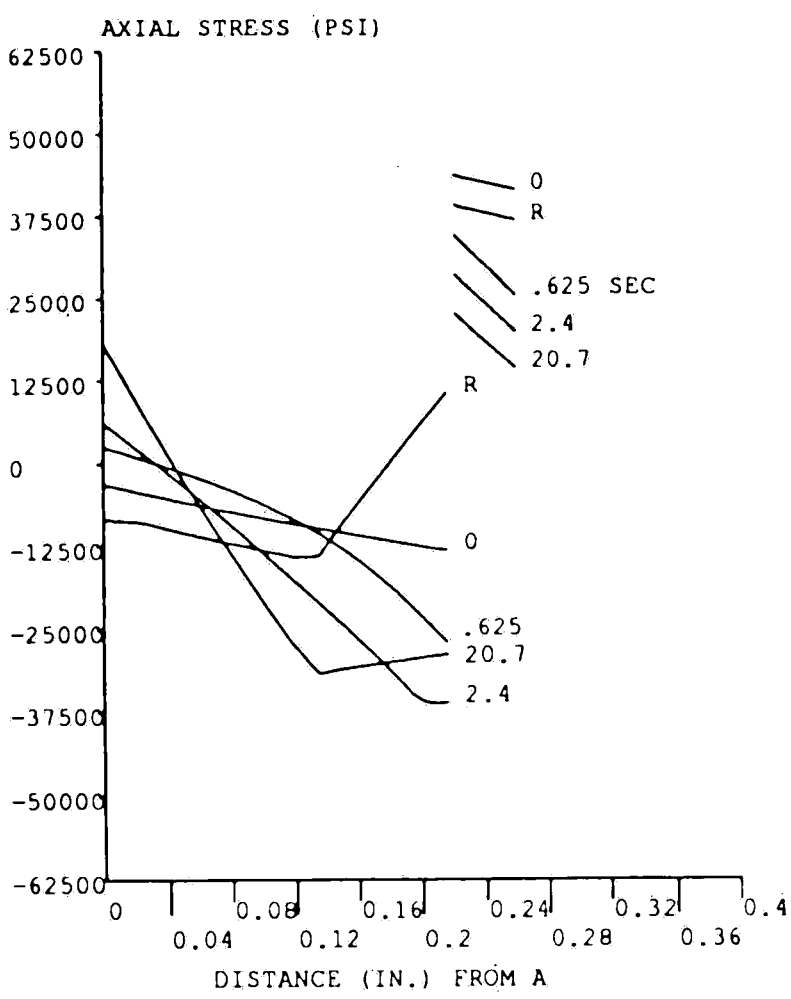

a. Axial stress

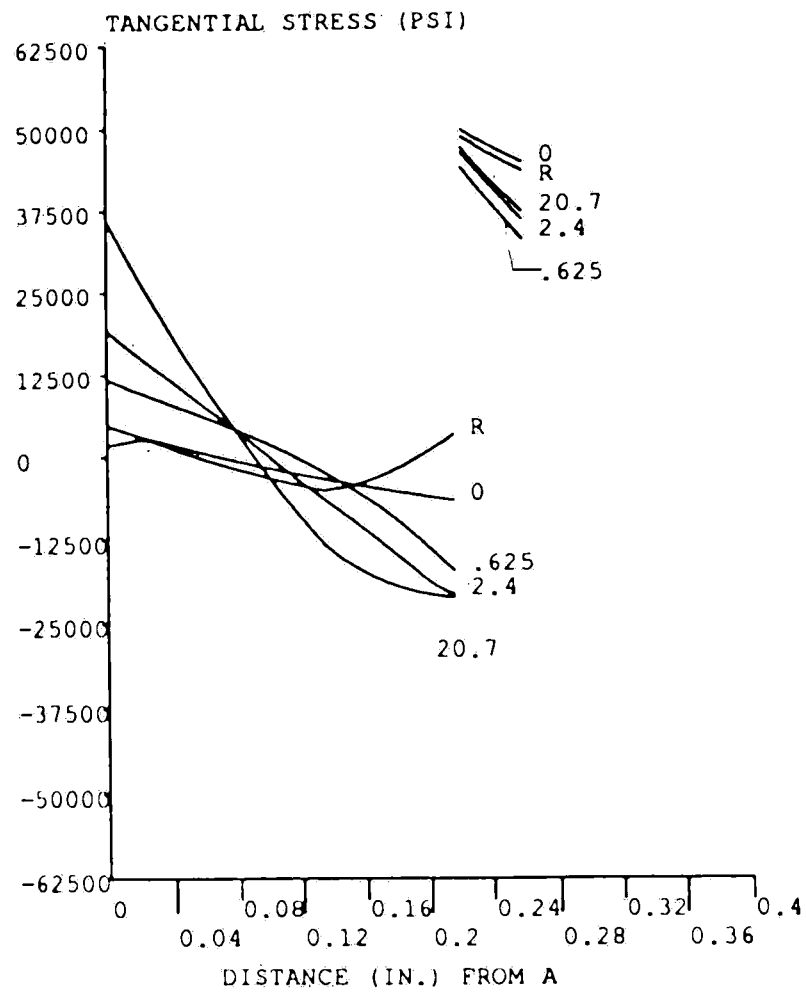

b. Tangential stress

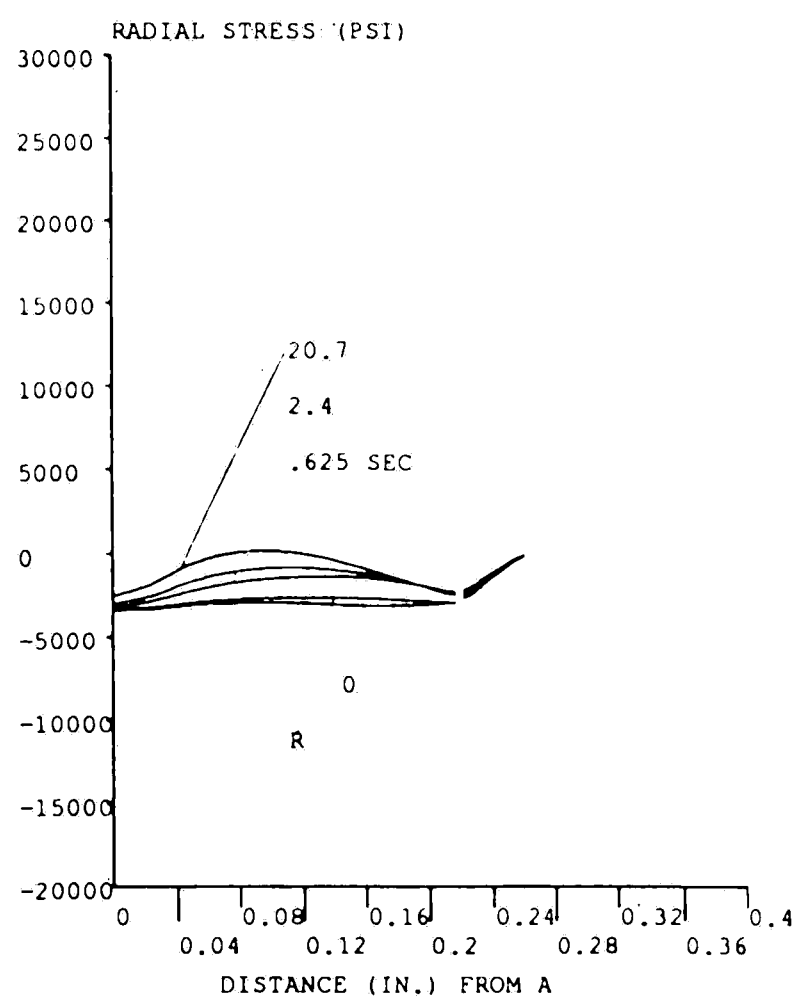

c. Radial stress

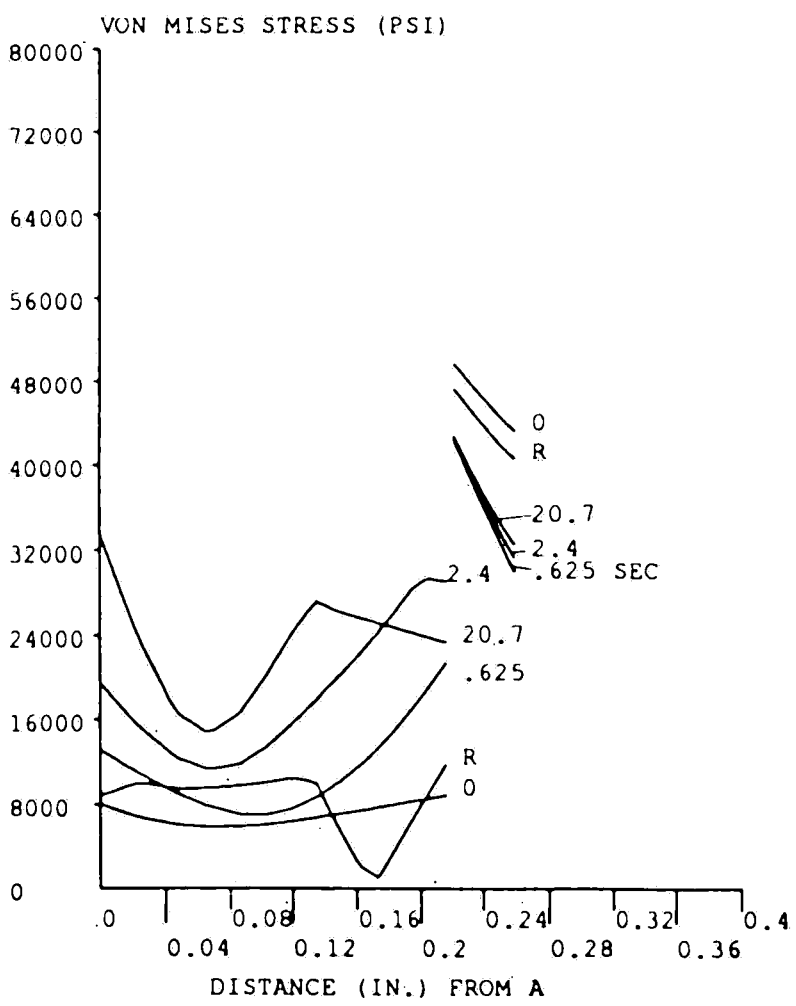

d. Von Mises stress

Figure 6.5: Stress distributions on path AA′ with a slag buildup (0 and R) and at various times after the slag fall, for T22 base and CC50 coating.

Figure 6.6 shows the time dependence, following the slag fall, of the axial and tangential stresses at the apex fireside and interface, for the combination of T22 base and CC50 coating. At the fireside and interface (Figure 6.6(a) and (b)) the tangential stress in the coating is higher than the axial stress. But the axial stress is subject to greater change following the slag fall. This more extreme fatigue cycle in the axial direction would increase the tendency to form circumferential fatigue cracks; however, the steady high tension in the tangential direction could lead to creep damage as well. At the interface the base (Figure 6.6(c)) is subject to rapidly increasing compressive stresses in both the axial and tangential directions. However, less than two seconds after the slag fall, the base material reaches maximum compressive stress levels, due to yielding, with the axial direction subject to greater compressive stress. Subsequently the stress levels are reduced as the material heats up and the yield limit for T22 is reduced.

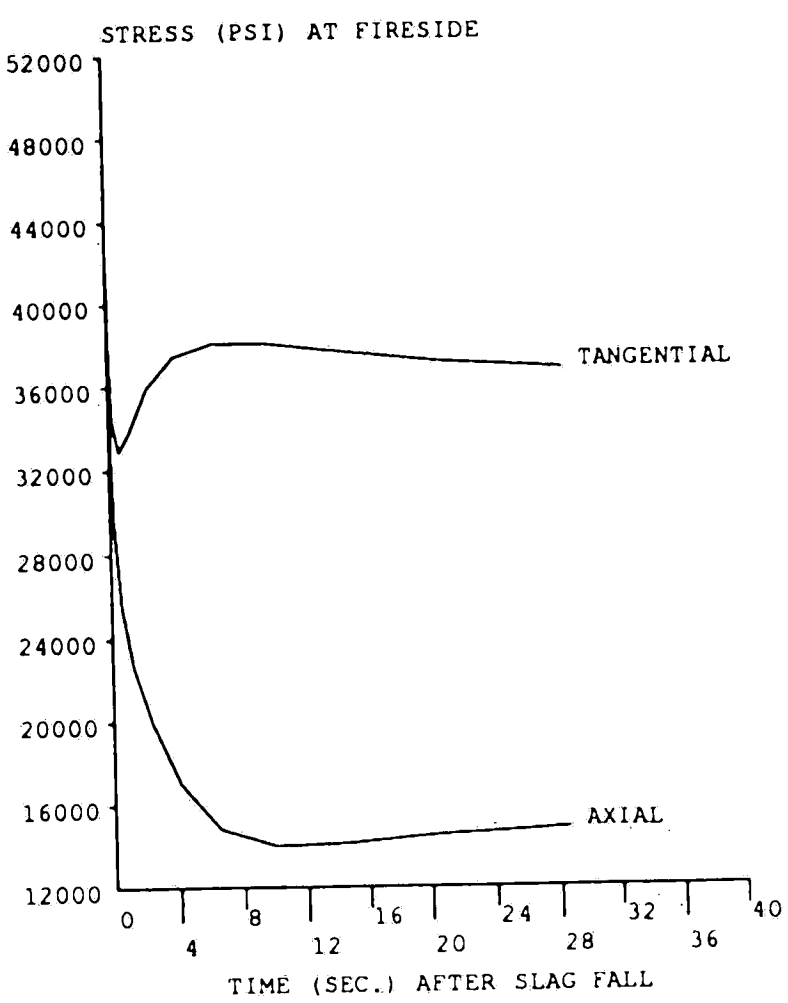

a. Apex fireside

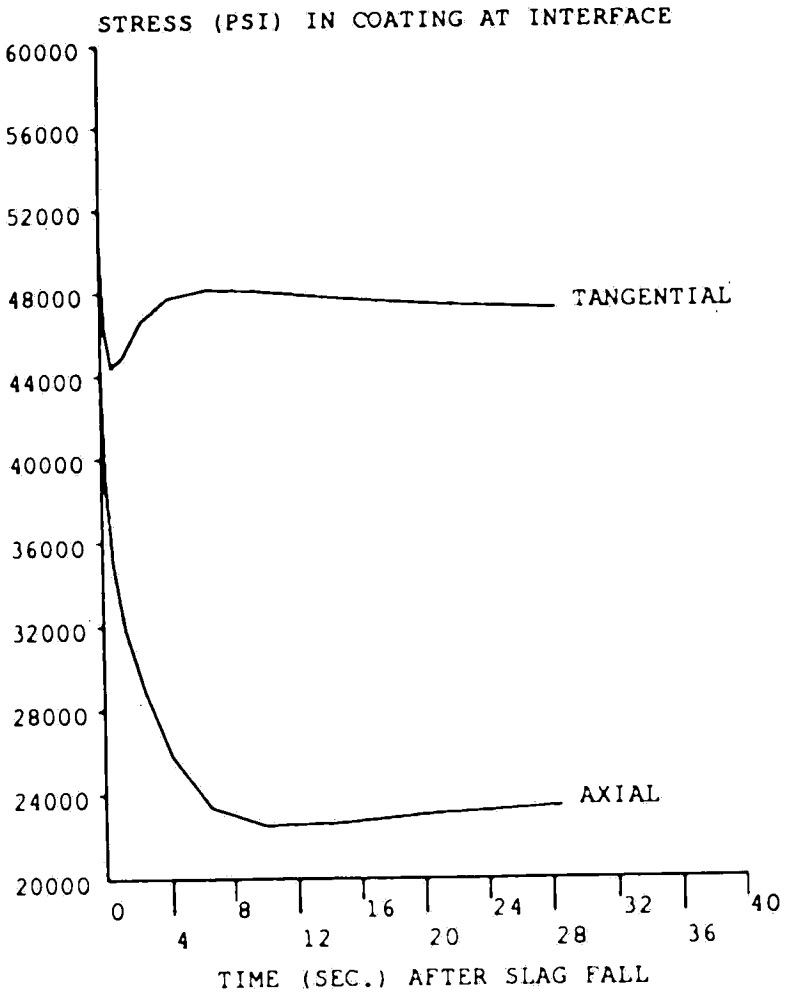

b. Apex interface (coating)

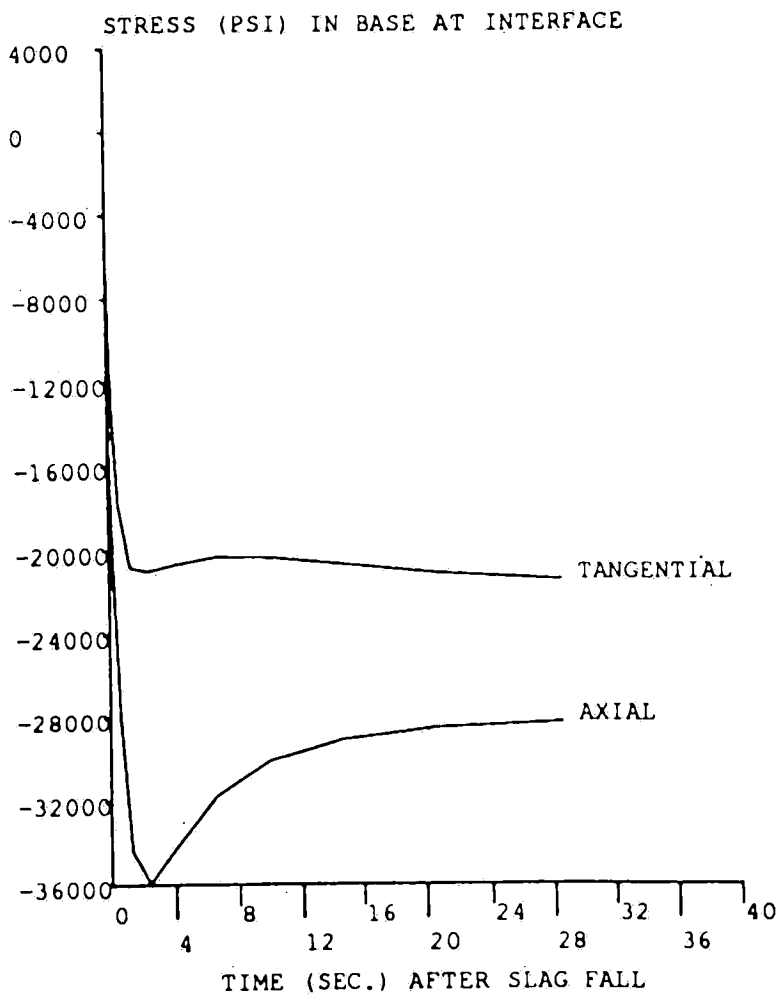

c. Apex interface (base)

Figure 6.6: Axial and tangential stresses as functions of time following the slag fall at two locations on path AA' for T22 base and CC50 coating.

Figure 6.7 shows stress distributions on path FF′, for the combination of T22 base and CC50 coating. The distributions are shown with a slag buildup and at various times following the slag fall. Before the slag fall the base material near the interface has already yielded a small amount as seen by the plastic zone in that region on the plot of von Mises stress (Figure 6.7(d)). The material at the interface is subjected to tensile radial stress which drops from about 25,000 psi to 16,000 psi following the slag fall (Figure 6.7(c)). This tensile radial fatigue cycle at the interface could also lead to eventual debonding of the coating in the fillet region. The coating initially is subjected to large tensile stresses in both the axial and tangential directions. Following the slag fall these stresses decrease to about 20,000 psi at the surface, but they eventually return to their intitial values of 47,000 psi in the axial direction and 80,000 psi in the tangential direction after more slag builds up. For comparison, the control case results in residual tensile stresses at the fillet fireside of about 20,000 psi in the axial direction and 35,500 psi in the tangential direction. This extreme tensile fatigue cycle could lead to vertical and horizontal cracks at the surface of the coating.

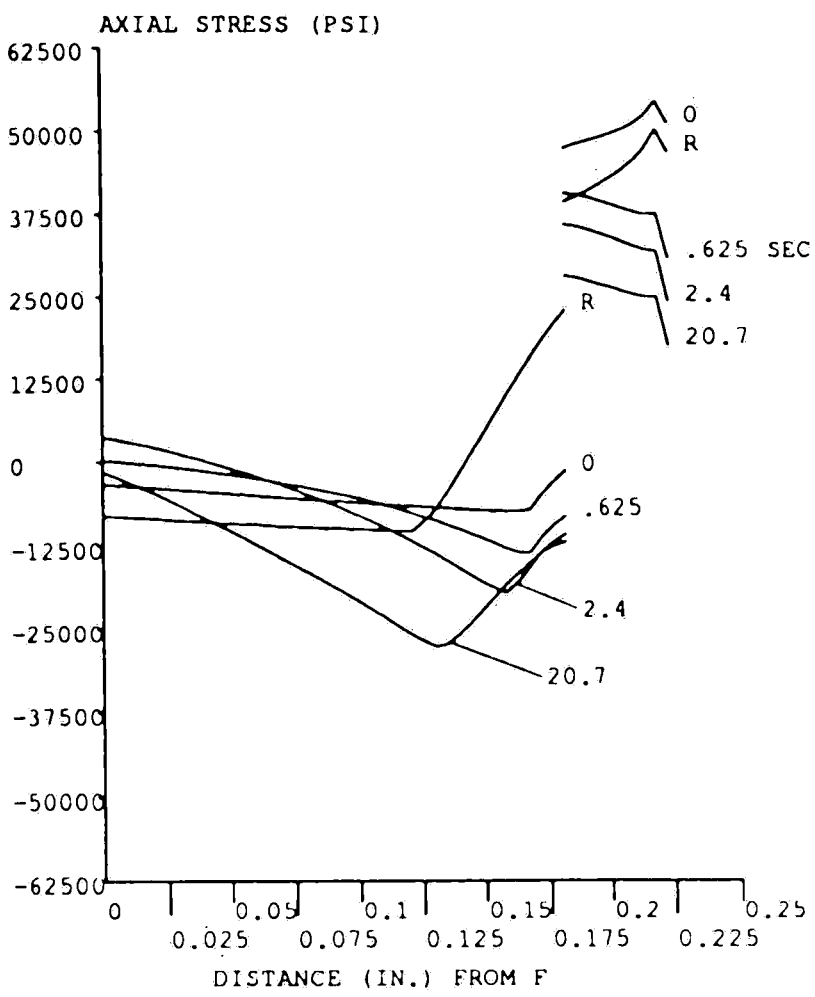

a. Axial stress

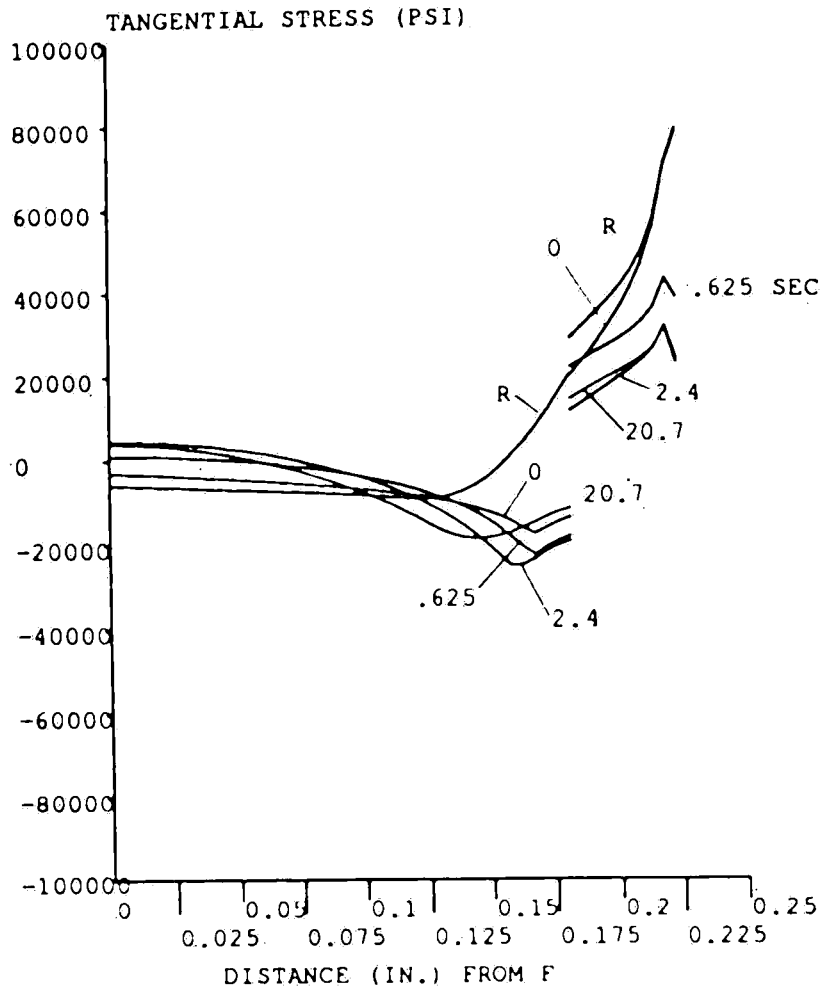

b. Tangential stress

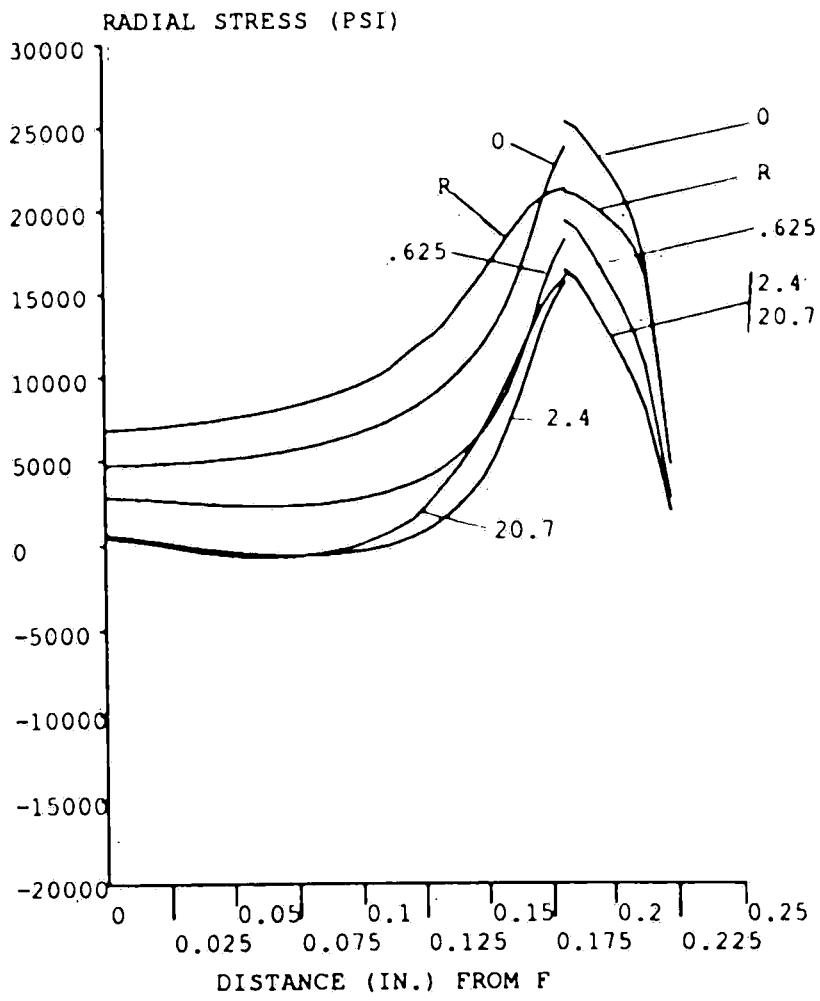

c. Radial stress

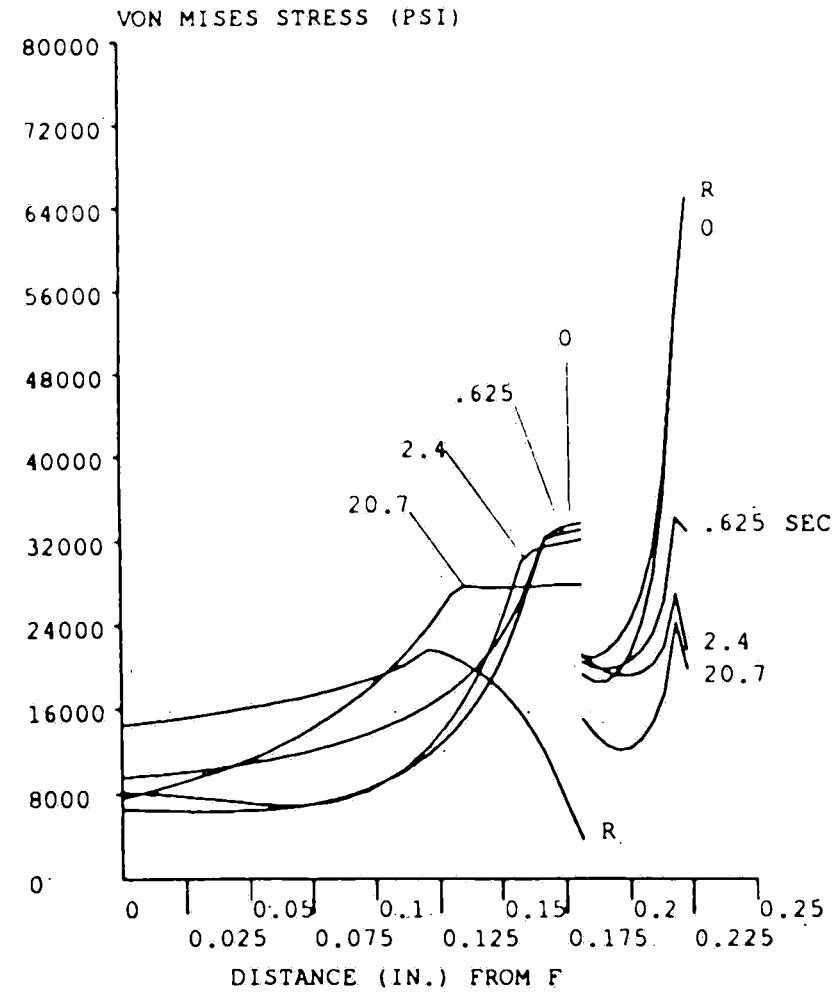

d. Von Mises stress

Figure 6.7: Stress distributions on path FF′ with a slag buildup (0 and R) and at various times after the slag fall, for T22 base and CC50 coating.

Figure 6.8 shows axial, tangential, and radial stress as functions of time following the slag fall at two locations on path FF′, for the combination of T22 base and CC50 coating. Notice in Figure 6.8(a) that the fireside is subjected to nearly equal axial and tangential tensile stresses that decrease following the slag fall. At the interface, the stresses in the coating (Figure 6.8(b)) also decrease following the slag fall, however the axial stress is largest and the tangential stress is smallest. Finally as shown in Figure 6.8(c), the tensile radial stress and the compressive axial and tangential stresses in the base material at the interface decrease following the slag fall but stabilize in less than two seconds to indicate the onset of yielding.

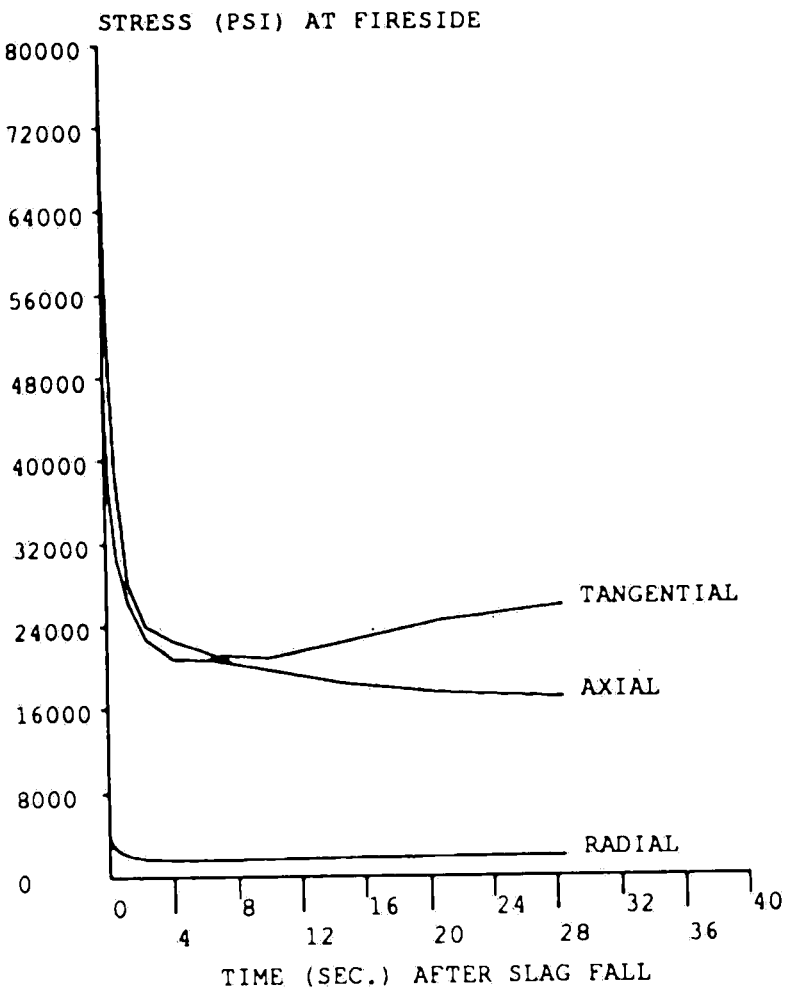

a. Fireside

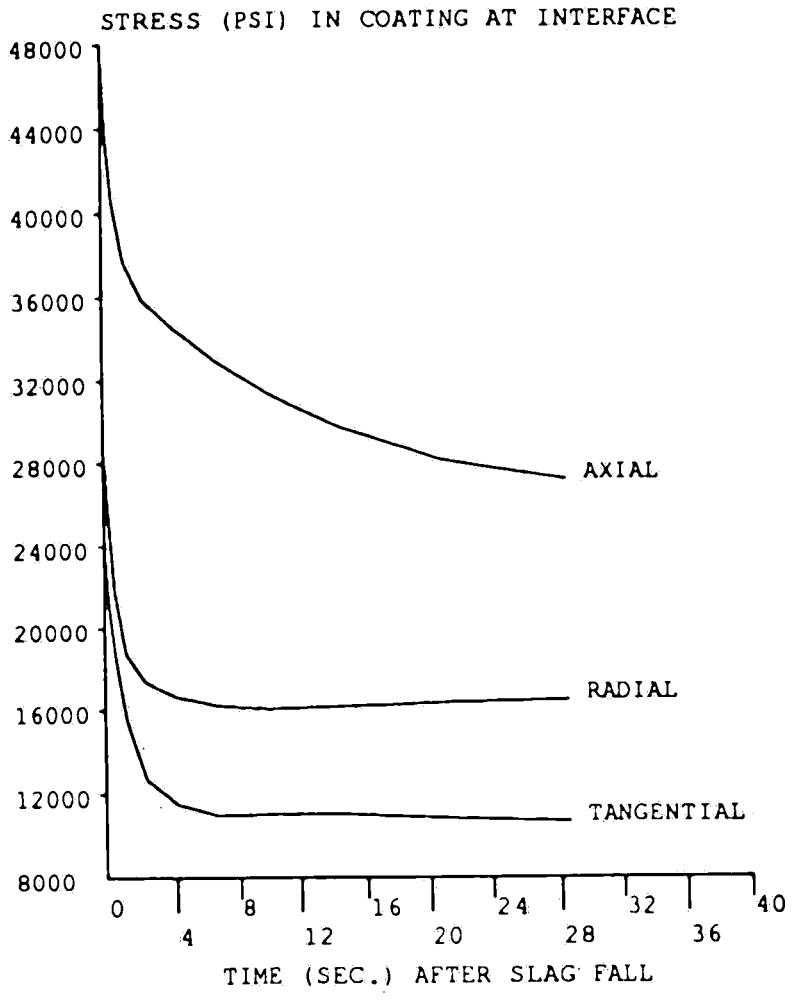

b. Interface (coating)

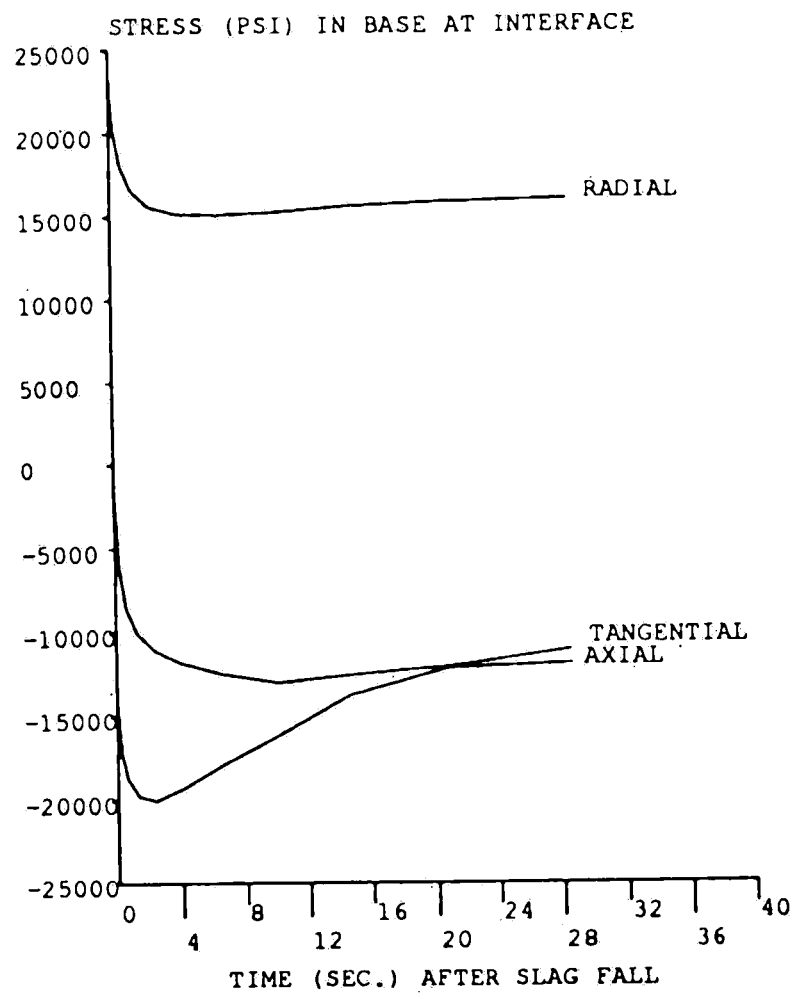

c. Interface (base)

Figure 6.8: Axial, tangential and radial stresses as functions of time following the slag fall at two locations on path FF′ for T22 base and CC50 coating.

Case 3: Modified coating. In the following analysis, a new combination of a T22 base and a coating with α_c five percent less than α_b is used. Figure 6.9 shows the resulting stress distrubutions on path AA′ with a slag buildup and at several times following the slag fall. Because the coefficient of thermal expansion for the coating is now only five percent less than that of the base material (T22), the stress difference at the interface between the coating and base is smaller than for case 2. Initially, the axial stress in the coating is slightly tensile and in the base it varies from tension at the waterside to compression adjacent to the coating. Following the slag fall, the larger temperatures near the fireside drive both the coating and the base into compression. The base yields in compression while the coating, still within its elastic range does not. Upon returning to the initial temperatures, there is an axial residual tensile stress in the base adjacent to the coating and and axial compressive stress in the coating of 1,000 psi at the fireside. However, due to the lack of yielding in the tangential direction, there is a residual tensile stress of 9,000 psi at the fireside in the tangential direction. These are, however, modest values when compared with residual tensile stresses at the fireside of 21,000 psi in the axial direction and 12,500 psi in the tangential direction for the control case. While the compressive yielding of the base has not been eliminated, the corrosion resistant coating undergoes a less severe fatigue cycle and is less susceptible to intergranular corrosion because the residual tensile stresses have been reduced. Hence, the likelyhood of crack initiation is reduced.

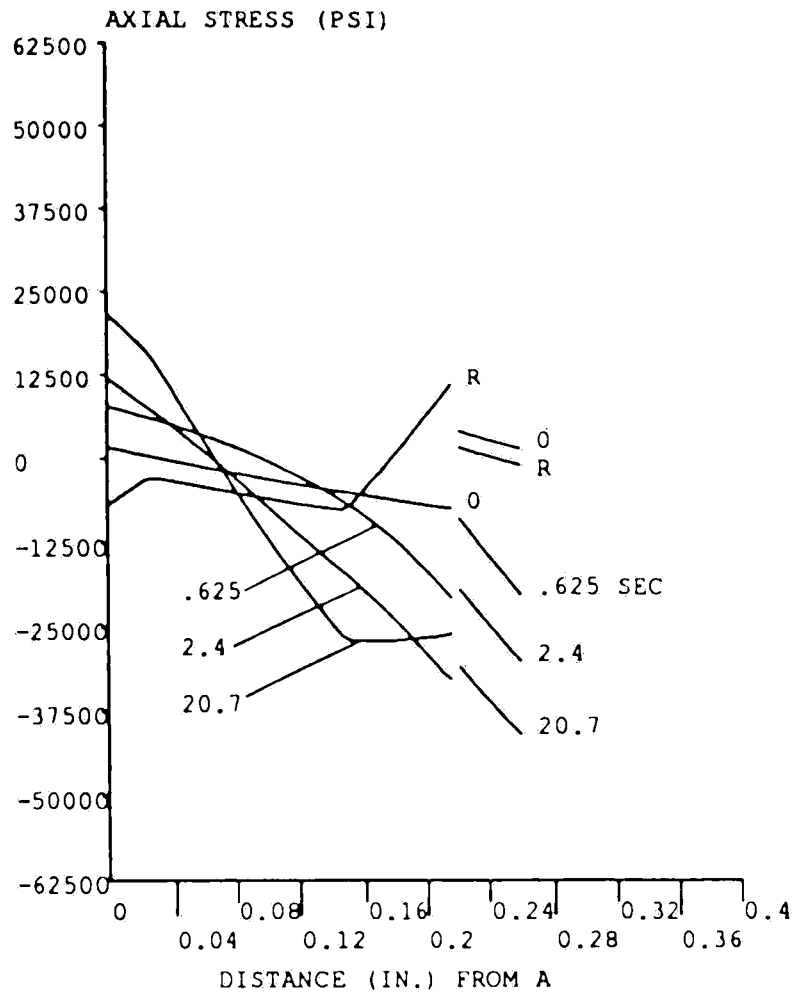

a. Axial stress

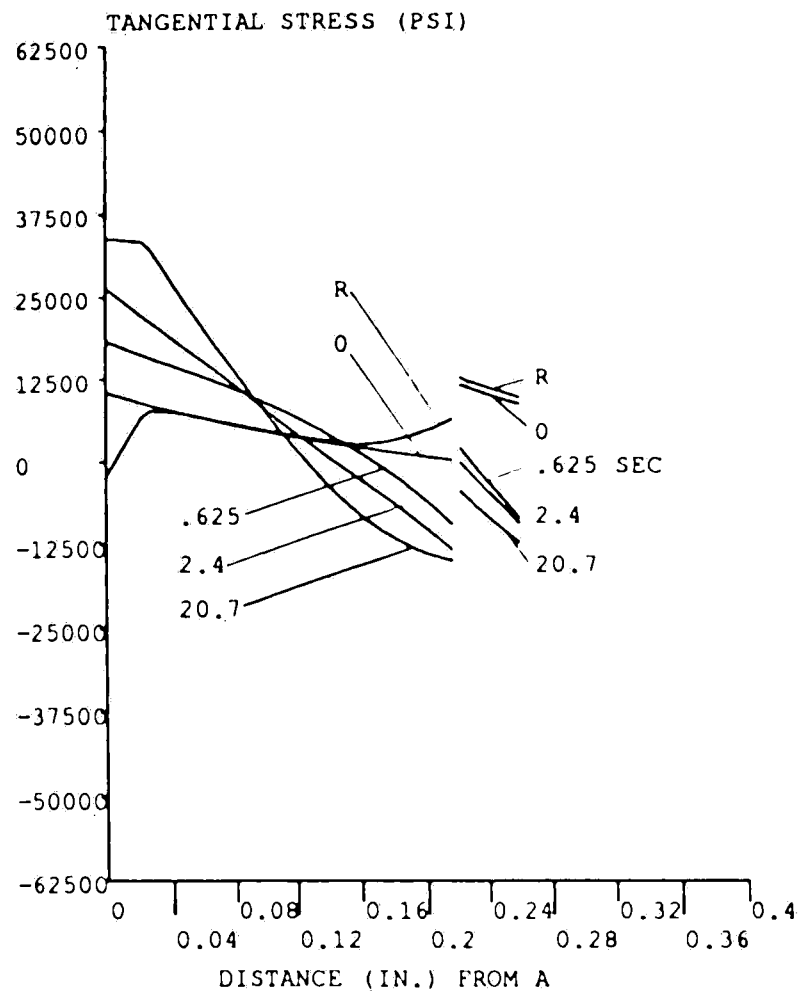

b. Tangential stress

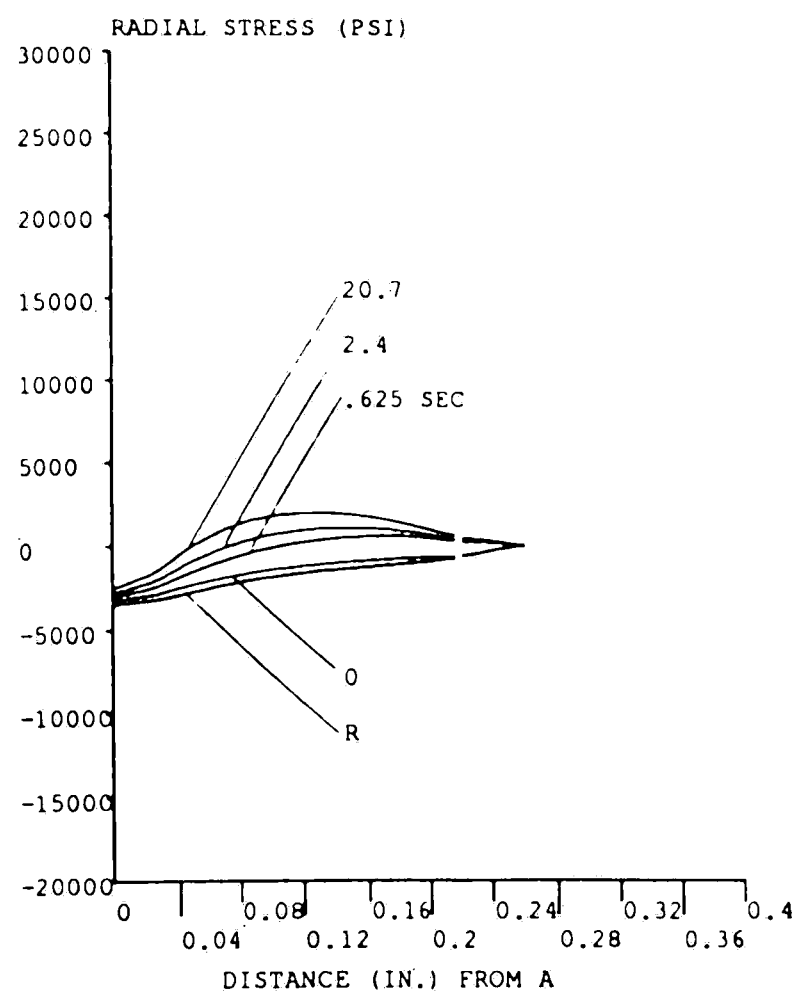

c. Radial stress

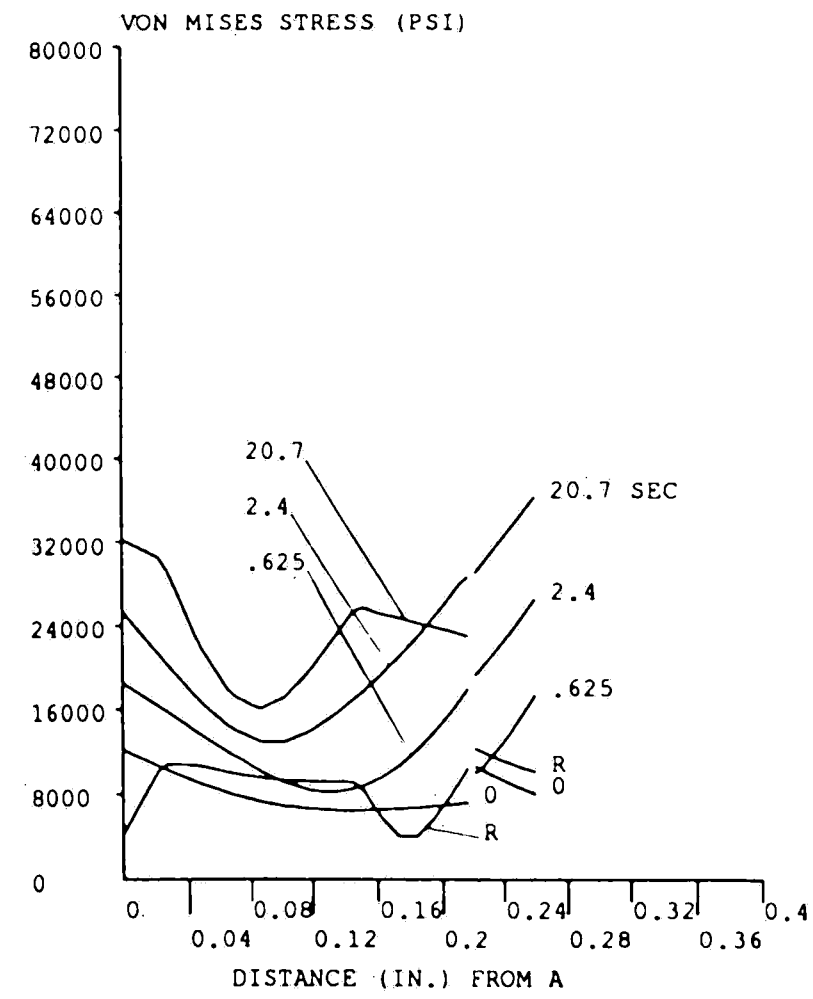

d. Von Mises stress

Figure 6.9: Stress distributions on path AA' with a slag buildup (0 and R) and at various times after the slag fall, for T22 base and coating with $\alpha_c/\alpha_b = .95$.

Figure 6.10 shows the time dependence of the axial and tangential stresses following the slag fall, at two locations on path AA′, for the modified combination of T22 base and coating with α_c only five percent less than α_b. Figures 6.10(a) and (b) show the stresses in the coating at the fireside and at the interface as they become compressive following the slag fall. They do not, however, reach the yield limit of 65 ksi used for this material. Finally Figure 6.10(c) shows how both the axial and tangential stresses in the base material at the interface also become highly compressive following the slag fall. However, less than two seconds after the slag fall the yield limit is reached and the stress levels are reduced as the yield strength for the base material (T22) decreases with increasing temperature.

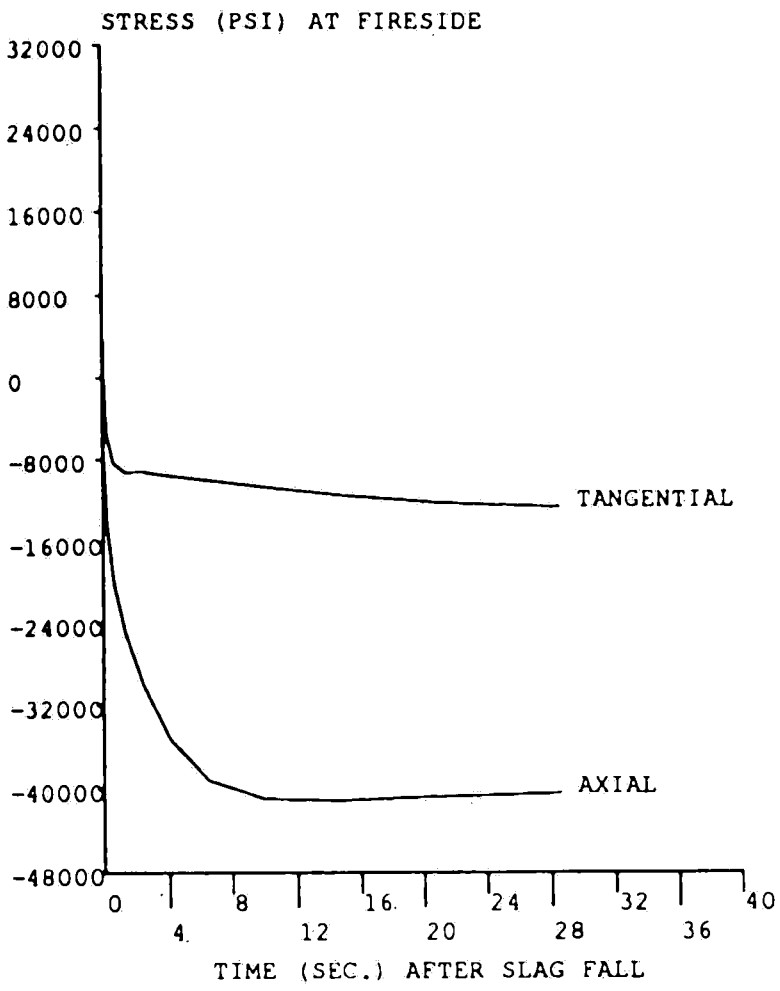

a. Fireside

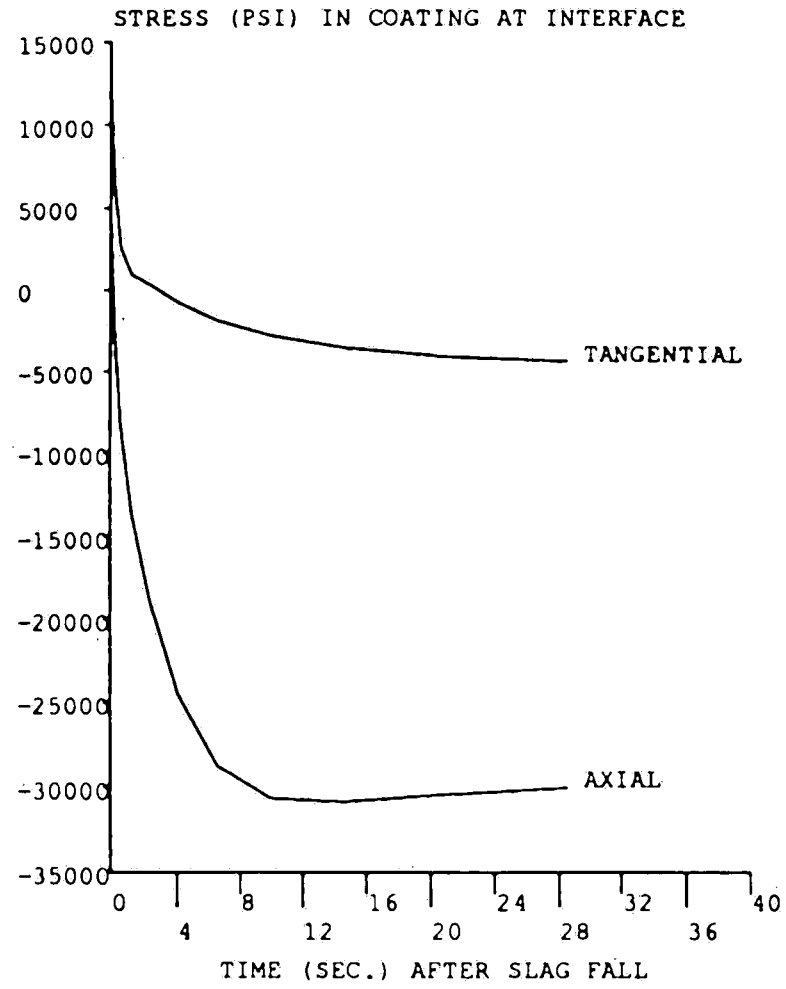

b. Interface (coating)

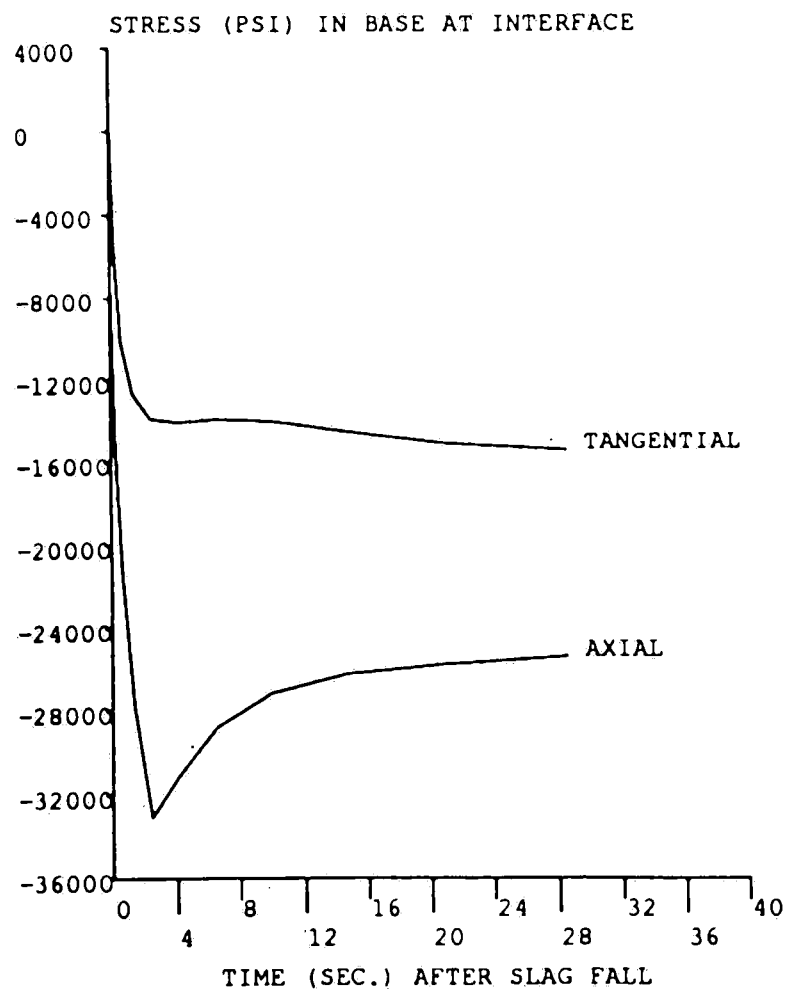

c. Interface (base)

Figure 6.10: Axial and tangential stresses as functions of time following the slag fall, at two locations on path AA', for T22 base and coating with $\alpha_c/\alpha_b = 0.95$

Figure 6.11 shows the resulting stress distributions on path FF′, for the combination of T22 base and a coating with α_c five percent less than α_b. The distributions are shown with a slag buildup and at various times following the slag fall. There is little yielding of either the base or the coating. This can be seen in Figure 6.11 as the axial, tangential, radial and von Mises stress distributions return nearly to their original distributions prior to the slag fall. A slight amount of compressive yielding of the base material adjacent to the interface results in a residual axial stress in the coating that is only 3,500 psi in tension. However, yielding in the coating, primarily in the tangential direction, results in a tensile residual stress of about 17,000 psi in that direction at the fireside. This could make the fillet area more susceptible to axial corrosion/fatigue cracks. However, these results compare favorably with the residual tensile stresses at the fireside of 20,000 psi in the axial direction and 35,500 psi in the tangential direction for the control case. Figure 6.11(d) shows that initially the radial stress at the interface is tensile but following the slag fall becomes compressive and eventually returns to a residual tensile stress level of 5,000 psi as slag builds back up. This is not an improvement over the control case, where the residual radial stress is also 5,000 psi at the interface, but it is better than the tensile residual radial stress of 25,000 psi which drops to 16,000 psi with each subsequent slag fall, as seen in the case with CC50 coating.

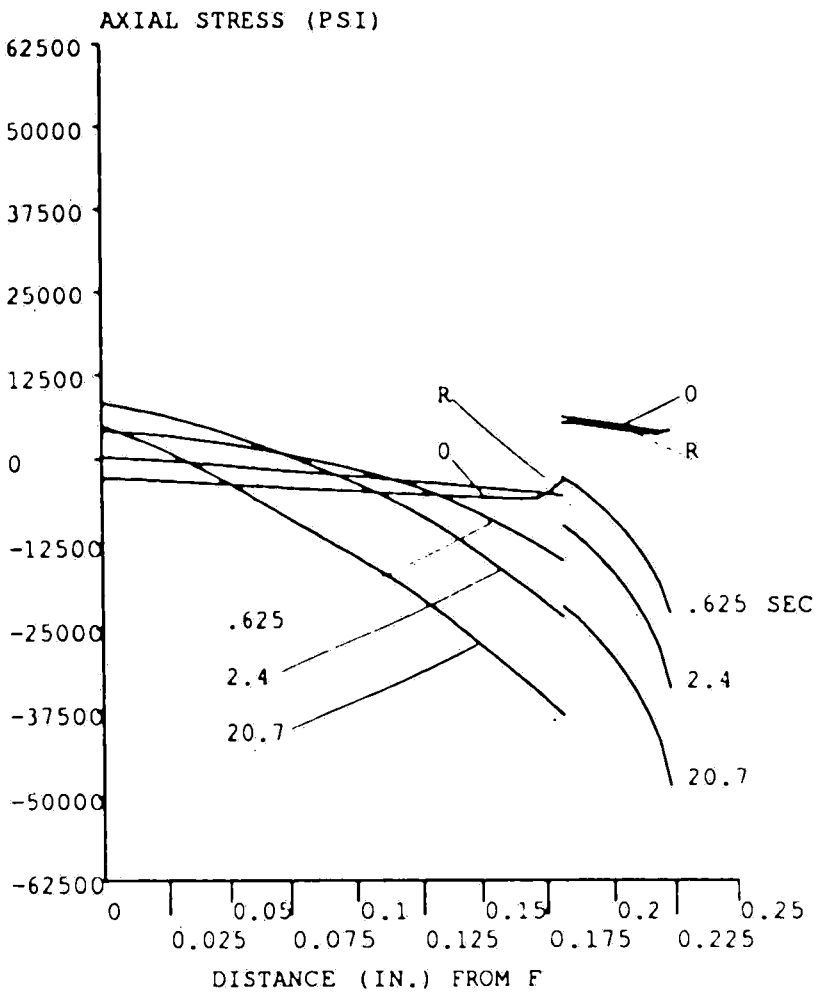

a. Axial stress

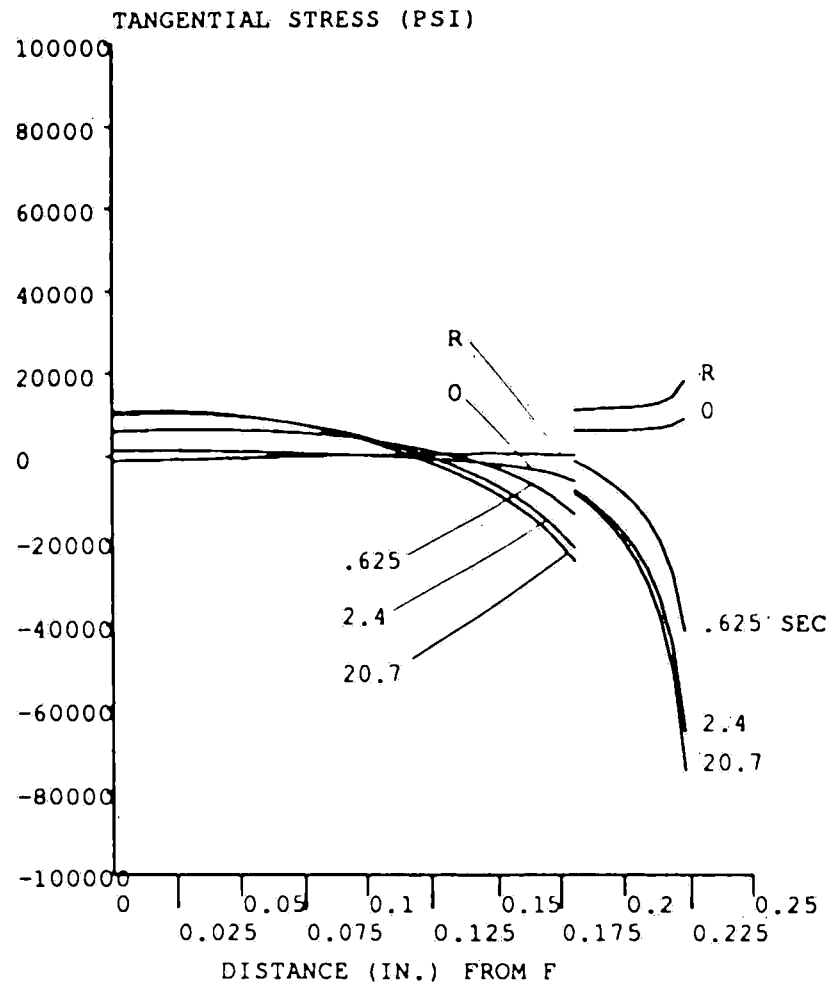

b. Tangential stress

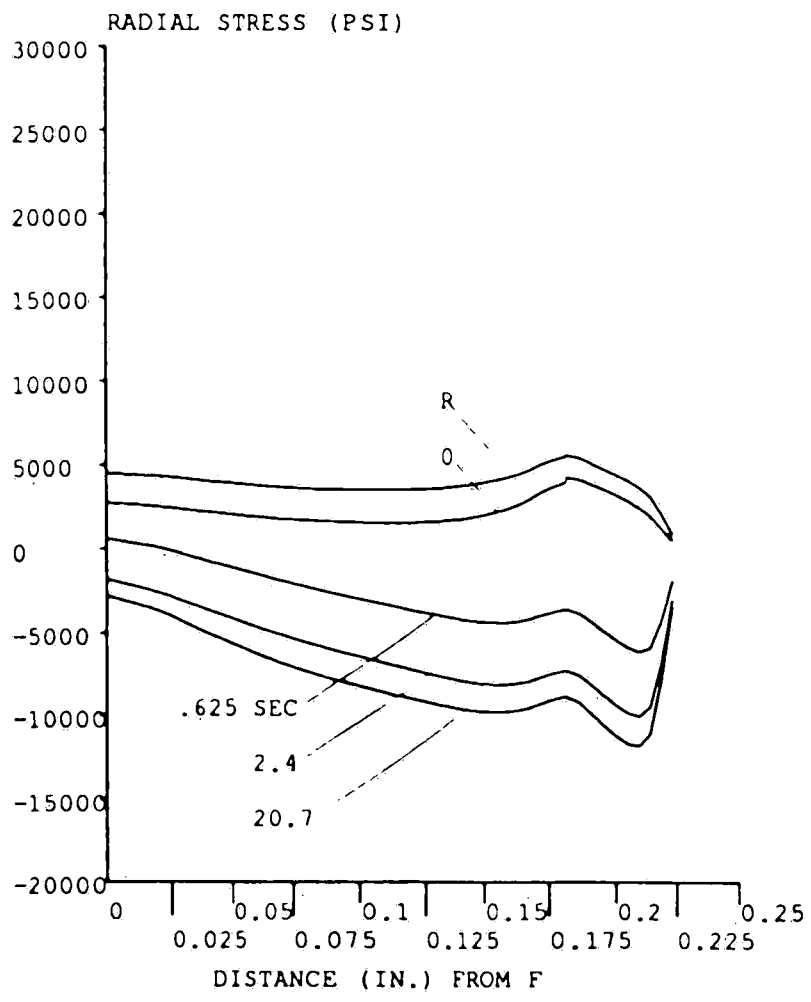

c. Radial stress

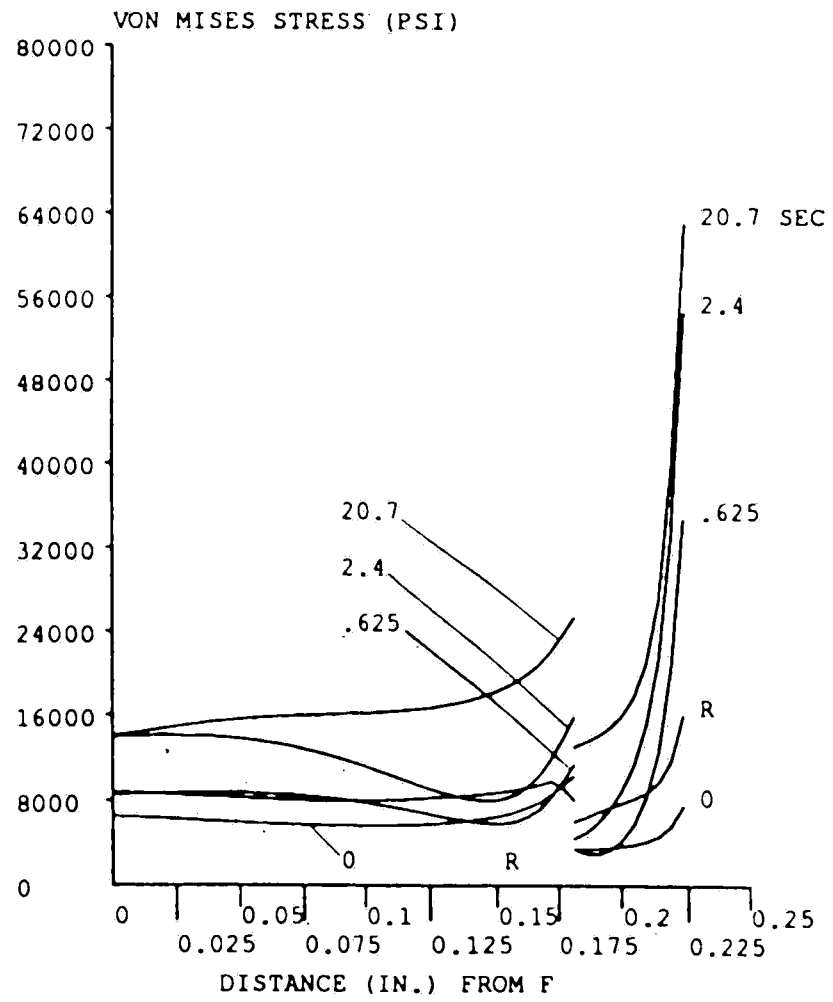

d. Von Mises stress

Figure 6.11: Stress distributions on path FF′ with a slag buildup (0 and R) and at various times after the slag fall, for T22 base and coating with $\alpha_c/\alpha_b = .95$.

Finally Figure 6.12 illustrates the time dependence of axial, tangential and radial stress following the slag fall, at two locations on path FF'. Figures 6.12(a) and (b) show that the tangential and axial stresses in the coating become highly compressive following the slag fall until the coating yields and the stresses remain relatively constant. Figure 6.12(c) shows how the axial stress in the base becomes more compressive than the tangential stress following the slag fall untill the base yields in compression and again the stress levels stabilize. The radial stress at the interface becomes compressive following the slag fall, but then becomes tensile after the slag builds up again (Figure 6.11(c)).

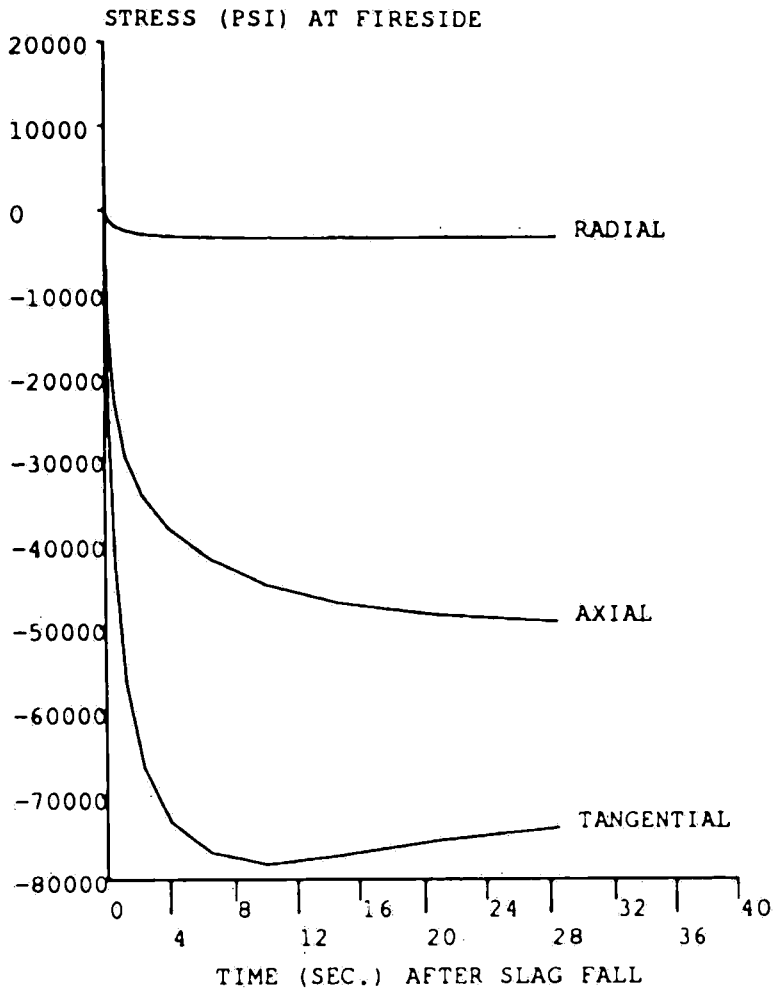

a. Fireside

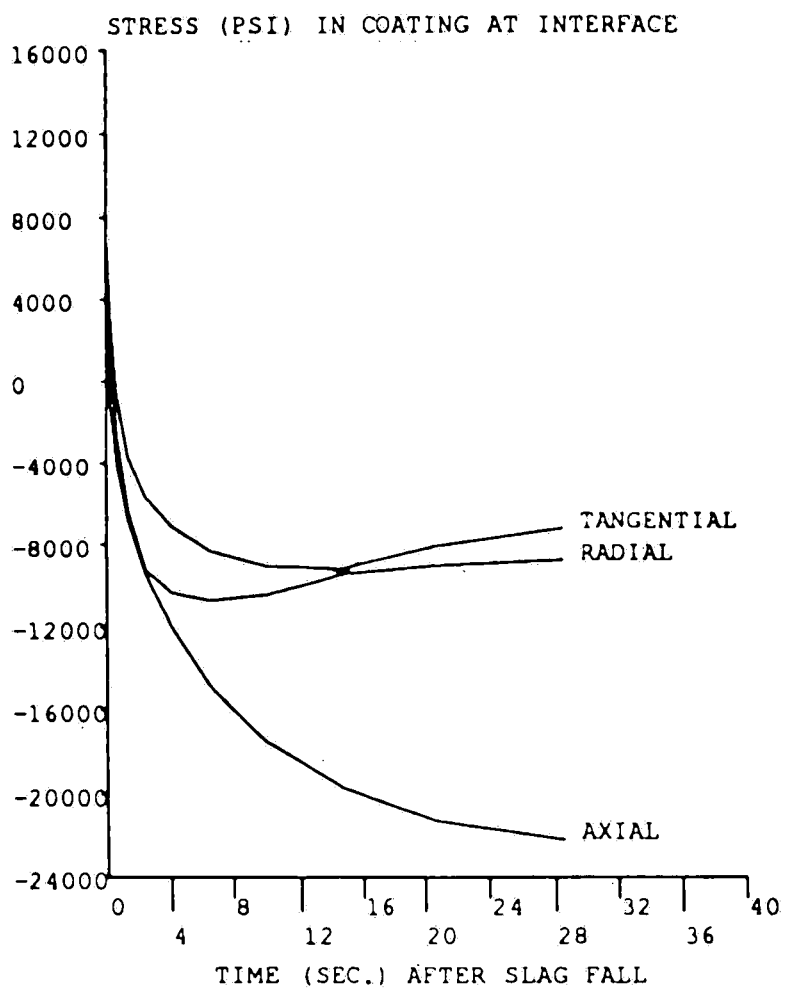

b. Interface (coating)

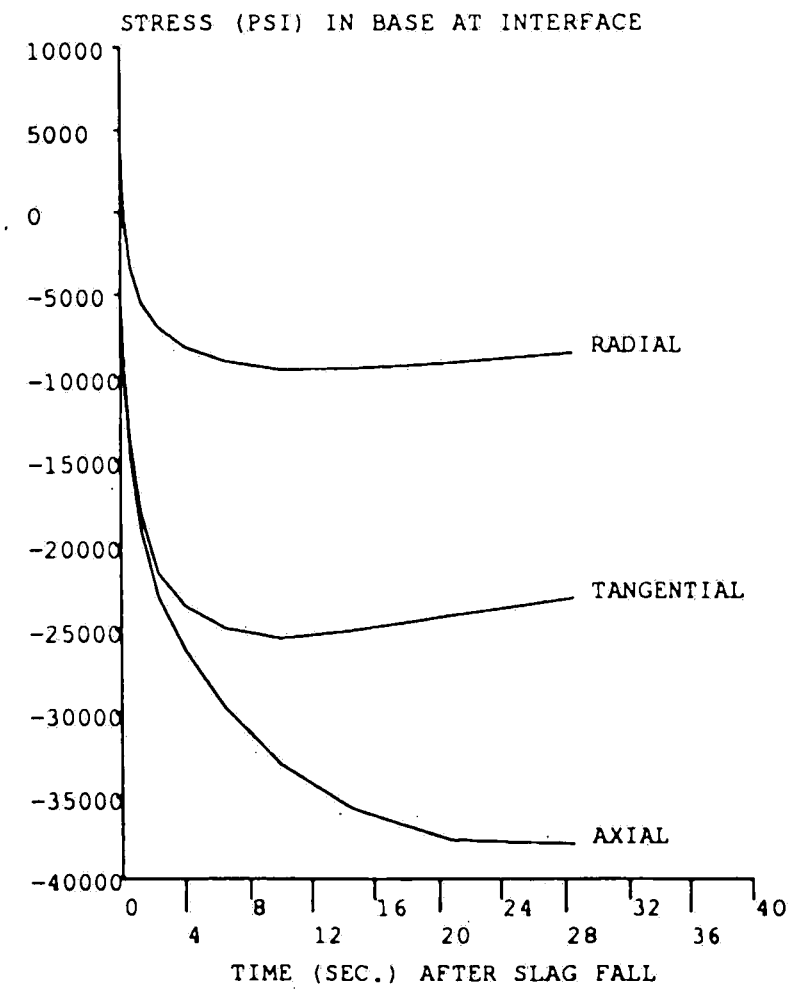

c. Interface (base)

Figure 6.12: Axial, tangential and radial stresses as functions of time following the slag fall at two points on path FF′ for T22 base and coating with $\alpha_c/\alpha_b = 0.95$

7. Conclusions

The analysis shows that some coatings decrease yielding of the material at the waterwall apex following a slag fall and in fact produce substantially lower residual tensile stresses. The calculations show that for a waterwall with a coating whose coefficient of thermal expansion is five percent less than the T22 base and whose yield stress is 100% more, the base material at the apex yields following a slag fall, and the coating does not. There is a subsequent residual tensile stress in the base adjacent to the coating and a net compressive stress in the axial direction of 1,000 psi and a tensile stress of 9,000 psi in the tangential direction at the apex fireside. This would produce a waterwall whose fireside surface is less susceptible to intergranular corrosion and thermal fatigue failure.

However, in the fillet region it is not possible to completely eliminate yielding of the coating. But it does appear that using the coating with α_c/α_b=0.95 results in a residual stress of only 3,500 psi in the axial direction and a residual tensile stress of 17,000 psi in the tangential direction at the fireside. This is certainly better than residual tangential stresses of 80,000 psi for the case of CC50 coating and T22 base and 35,500 psi for the control case with the waterwall made entirely of T22. There may, however, be a system which reduces the stresses at the fillet. It might be possible to increase the coating thickness at the fillet in order to increase the fillet radius and reduce the stress concentration. Furthermore, using a combination of base and coating with α_c/α_b slightly less than 0.95 might result in splitting the residual tensile stresses to achieve approximately 12,000 psi in the axial direction at the apex fireside and 12,000 psi in the tangential direction at the fillet fireside.

The model used to perform the finite element calculations should be used to evaluate other choices of materials for coatings and bases. It should be noted that the coefficient of thermal expansion of INCONEL 625 is about five percent less than that of the base T22 and its yield limit is also about 65,000 psi. Therefore this combination

should produce results similar to those presented in the third case. Furthermore, the use of powderized 400 series stainless steel for a laser clad coating should be investigated because it, too, is already being used in boilers.

Finally, the possibility of a waterside thermal shock might be investigated. The correlation used to determine the convection coefficient on the waterside of the waterwall includes parameters (cooling water temperature, pressure and flow velocity) that, if varied, would produce significantly different convection coefficients. Therefore the forced convection condition would be changed during the thermal analysis and produce a nonsteady temperature distribution at the waterside. The resulting thermal transient either alone or in combination with a slag fall could possibly produce even larger transient thermal stresses than those from a slag fall alone. The waterside stresses would, therefore, have to be examined in greater detail.

References

1. Smith, B. J., The Cause of Circumferential Cracking in Waterwall Boiler Tubes, Bethlehem, Lehigh University, M.S. Thesis, Jan. 1990.

2. Wu, Y. K., Elastic-Plastic Stress Analysis of Waterwall Tubes Subjected to Transient Thermal Loads, Bethlehem, Lehigh University, M.S. Thesis, Jan., 1990.

3. Smith, B. J., Erskine, C. P., Hartranft, R. J., and Marder, A. R., Corrosion-Fatigue Circumferential Cracking in Cr-Mo Low Alloy Boiler Tube Steels: Part 2 - Laboratory Simulation, To be pubished, March, 1991.

4. Energy Research Center, Life Extension of Power PLant Boiler Tubes by Protective Coating, Task A: Literature Review, A report prepared by S. T. Bluni and B. J. Smith, Bethlehem, Energy Research Center of Lehigh University, February, 1990.

5. Smith, B. J., and Marder, A. R., "Characterization of Chromium Diffusion (Chromize) Coatings in a High Temperature Coal Combustion Environment", a paper presented at the Fourth International Conference on Surface Modification Technologies, Paris, France, November 6-9, 1990.

6. Energy Research Center, INCONEL 625 Laser Clad Coating for Boiler Tube Corrosion Protection, A report prepared by B. Elliot and B. J. Smith, Bethlehem, Energy Research Center of Lehigh University, 1990.

7. Roberts, B., and Rice, W. S., Jr., Experiment 641, Welded Furnace Wall Panels, KDL Report 6101, Tennessee, Combustion Engineering, January, 1961.

8. Babcock and Wilcox, Steam, Its Generation and Use, New York, 1978, p. 3.7.

9. Pennsylvania Electic Co., A Study of Waterwall Cracking in Conemaugh Units 1 & 2, A report prepared by MPR Associates Inc., Johnstown, Pennsylvania Electric Co., 1983.

10. G. J. Desalvo, and J. A. Swanson, ANSYS-Engineering Analysis System User's Manual, Swanson Analysis Systems Inc., May 1, 1989.

11. American Society for Metals, Metals Handbook, Ninth Edition, Vol. 1, Properties and Selection / Irons and Steel, 1978.

12. Boyer, H. E., Atlas of Stress-Strain Curves, Ohio, ASM International, 1987, p. 275.

13. United States Steel, Steels for Elevated Temperature Services, Pittsburgh, 1974, p. 42.

14. American Society for Metals, Metals Handbook, Ninth Edition, Vol. 3, Properties and Selection / Stainless Steels, Tool Materials and Special Purpose Metals, 1980, pp. 109-110.

15. Ozisik, M. N., Heat Transfer-A Basic Approach, New York, McGraw-Hill, 1977, p. 7.

16. Keenan, J., Keyes, F. G., Hill, P. G., and Moore, J. G., Steam Tables Thermodynamic Properties of Water Including Vapor, Liquid, and Solid Phases, New York, John Wiley and Sons, Inc., 1978, pp. 113-123.

17. Kakac, S., "The Effect of Temperature-Dependent Fluid Properties on Convective Heat Transfer", in Handbook of Single Phase Convective Heat Transfer, S. Kakac, R. K. Shah, and W. Aung, eds., New York, John Wiley and Sons, 1987, pp. 18.33.

18. Irvine, T. F., and Hartnett, J. P., Steam and Air Tables, Washington D. C., Hemisphere Publishing Corp., 1976, p. 63.

Appendix I: Calculation of waterside convection coefficient

The following are typical values of the waterside convection coefficient as given by equations 3.4 through 3.8. The calculation is for cooling water at a bulk temperature of 370 °C (698 °F) and 25 MPa (3626.0 psia) and various inner wall temperatures of the waterwall tube. The inner diameter of the tube, d, is $2.057(10)^{-2}$ m (0.8100 in.) and the mean flow velocity, u_m, is 2.000 m/s (72.00 in./sec.) The relevent properties for water at supercritical pressure (25 MPa) are as follows,

Temp.	ρ	k	c_p	i	$\mu\cdot(10)^5$	c_p
	ref.[18]	ref.[18]	ref.[16]	ref.[16]	ref.[18]	eq.(3.8)
°C	kg/m^3	W/m·°C	kJ/kg·°C	kJ/kg	kg/m·s	kJ/kg·°C
370.0	507.6	0.3960	11.00	1811	6.300	----
310.0	723.1	0.5610	5.300	1384	9.060	7.117
320.0	703.7	0.5400	5.600	1437	8.700	7.480
330.0	678.4	0.5180	6.000	1496	8.330	7.875
340.0	654.9	0.4970	6.400	1555	7.970	8.533
350.0	624.2	0.4760	7.000	1621	7.600	9.500
360.0	590.0	0.4360	8.000	1696	6.950	11.50
370.0	507.6	0.3960	11.00	1811	6.300	----
380.0	446.4	0.3320	22.00	1926	5.420	11.50
385.0	313.5	0.2880	65.00	2089	4.870	18.53
390.0	242.1	0.2450	34.00	2253	4.310	22.10
395.0	196.9	0.2010	17.00	2416	3.760	24.20
400.0	166.1	0.1570	13.00	2579	3.210	25.60
405.0	156.0	0.1510	11.00	2627	3.190	23.31
410.0	147.1	0.1440	9.200	2676	3.160	21.63
420.0	131.9	0.1310	7.200	2772	3.110	19.22
430.0	123.0	0.1220	6.200	2834	3.090	17.05

Therefore,

the bulk Reynolds number is $Re_b = 3.315(10)^5$, eq.(3.6)

and the bulk Prandtl number is $Pr_b = 1.750$, eq.(3.7)

and,

Temp.	ρ_w/ρ_b	$c_p/c_{p,b}$	Nu_b eq.(3.5)	h_b eq.(3.4)	Temp.	$h_b \cdot (10)^3$
°C				$W/m^2 \cdot °C$	°F	$BTU/in^2 \cdot sec \cdot °F$
310.0	0.8378	0.6470	648.7	12490	590.0	4.242
320.0	0.8649	0.6800	668.1	12860	608.0	4.369
330.0	0.8919	0.7159	688.3	13250	626.0	4.501
340.0	0.9189	0.7758	717.1	13810	644.0	4.690
350.0	0.9459	0.8636	755.1	14540	662.0	4.938
360.0	0.9730	1.045	822.0	15830	680.0	5.376
370.0	1.000	1.000	814.2	15670	698.0	5.325
380.0	1.027	1.045	835.5	16080	716.0	5.464
385.0	1.041	1.685	1015	19540	725.0	6.639
390.0	1.054	2.009	1093	21050	734.0	7.151
395.0	1.068	2.200	1138	21910	743.0	7.444
00.0	1.081	2.327	1169	22500	752.0	7.642
405.0	1.095	2.119	1130	21750	761.0	7.389
410.0	1.108	1.966	1100	21180	770.0	7.196
420.0	1.135	1.747	1057	20350	788.0	6.914
430.0	1.162	1.550	1015	19540	806.0	6.638

The temperatures from column six above (°F) and the corresponding values for the convection coefficient, h_b ($BTU/in^2 \cdot sec \cdot °F$), are entered manually into ANSYS for use during the thermal analysis.

Appendix II: ANSYS Procedure

```
/PREP7
/TITLE,3-D MODEL
KAN,-1

C**********          *Necessary waterwall dimensions
RI=0.405              *Inner radius of tube
TH=0.22               *Tube wall thickness
THM=0.275             *Thickness of membrane
CC=1.835              *Center to center tube spacing
FR=0.05               *Fillet radius
THC=1.0               *Coating thickness (mm)
THC=THC/25.4          *Coating thickness (in.)

                      *Calculated waterwall dimensions
ZD=TH*.25             *Model thickness
RO=RI+TH              *Outer diameter of tube
ROC=RO+THC            *Outer radius of coating
THMC=THM+THC          *Thickness of half membrane with coating
CC=CC/2               *Half tube spacing
THM=THM/2             *Half membrane thickness
```

```
CSYS,1                                                    *Create geometry
K,1,RO,90       $K,2,RI,90      $K,3,RI,0
K,4,RI,-90      $K,5,RO,-90     $K,6,RO,0
CSYS,0
K,7,CC,THM      $K,8,CC,-THM
K,9,0,-THM      $K,10,0,THM
CSYS,1
L,1,2,15,3      $L,2,3,20       $L,3,4,20
L,5,4,10        $L,5,6L,6,1
CSYS,0
L,7,10          $L,8,9
K,11,CC,0       $L,7,11,15,3    $L,11,8,10
LINTER,6,7      $LINTER,8,5
LDELE,12,13     $LDELE,6        $LDELE,14
KDELE,9,10
LFILL,11,7,FR   $LFILL,8,5,FR
L,3,6,8         $L,6,11,16
KDEL,12,13
L,9,3,15,3      $L,10,6,15,3
L,14,6,10       $L,15,3,10
LMOD,11,,,20    $LMOD,6,,,8     $LMOD,7,,,16
LMOD,8,,,16     $LMOD,12,,,8    $LMOD,5,,,20
CSYS,0
K,16,0          $K,17,0,0,ZD    $L,16,17,1
A,1,2,3,9       $A,9,3,6,10     $A,10,6,11,7
A,8,11,6,14     $A,14,6,3,15    $A,15,3,4,5
```

```
CSYS,1
K,18,ROC,90    $K,19,ROC      $L,18,19
CSYS,0
K,20,0,THMC    $K,21,CC,THMC
L,20,21        $LINTER,20,21
LDEL,21,22     $KDEL,19,20
LFILLT,20,23,FR/2              $KDEL,12
CSYS,0
L,18,1,10,2    $L,13,9,10,2
L,19,10,10,2   $L,21,7,10,2
LMOD,20,,,20   $LMOD,21,,,8    $LMOD,23,,,16
A,18,1,9,13    $A,13,9,10,19   $A,19,10,7,21

LOCAL,11,1,.6593,.2020,0              *Coord. sys. for use in fillet area
CSYS,0                                *Switch back to global cartesian

VDRAG,1,2,3,4,5,6,19           $VDRAG,7,8,9,,,,19
ET,1,70        $ELSIZE,,,2
VMESH,1,6      $MAT,2          $VMESH,7,9
MERGE          $LDELE,19       $KDELE,16,17

WSORT,Y                               *Sorts in y direction in ascending order
```

```
C**********                    *Enter material properties

C**********                    *Thermal properties for T22

CP0S=32.86                     *Y-intercept

CP1S=.029                      *Slope

C,1,CP0S,CP1S                  *Specific heat for T22

K0S=5.47E-4    $K1S=-0.110E-6

KXX,1,K0S,K1S                  *Conduction coefficient for T22

DENS,1,7.32E-4                 *Density of T22
```

```
C**********                    *Thermal properties for CC50 STAINLESS

C,2,46.4                       *Specific heat for CC50

K0C=2.59E-4    $K1C=.156E-6

KXX,2,K0C,K1C                  *Conduction coefficient for CC50

DENS,2,7.04E-4                 *Density of CC50
```

```
C**********                    *Create radiation coefficient

Tbr=2500.                      *Bulk temp. for radiation

ST=3.3407e-15                  *Stefan Boltzman constant

aTa=459.67                     *Rankine,= zero degrees faranheit
```

```
C0=Tbr**2      $C01=Tbr*aTa $C01=C01*2.

C02=aTa**2     $C02=C02*2.  $C0=C0+C01

C0=C0+C02      $C03=aTa*2.  $C03=C03+Tbr

C0=C0*C03      $C0=C0*ST    $C1=Tbr*Tbr

C11=Tbr*aTa    $C11=C11*4.  $C12=aTa**2

C12=C12*6.     $C1=C1+C11   $C1=C1+C12
```

```
C1=C1*ST      $C2=aTa*4.    $C2=C2+Tbr
C2=C2*ST      $C3=ST
HF,2,C0,C1,C2,C3                    *radiation coefficient for fireside

C**********                         *Create free convection coefficient
Tab=80                              *Ambient temp for outside back
HF,3,1.7E-6                         *Free convection coefficient

C**********                         *Create temperature dependent forced
C**********                         *convection coeffient for inside
C**********                         *at a pressure of 3626 psi and Tbulk of 700
Tbw=700                             *Bulk temperature of water in tube
C**********                         *Enter temperatures at which coefficient
C**********                         *will be defined
MPTGEN,,8,590,18.
MPTEMP,,725,734,743,752,761,770
MPTEMP,,788,806
C**********                         *Enter coefficients
MPDATA,HF,4,,4.24E-3,4.37E-3,4.50E-3,4.69E-3,4.94E-3,5.38E-3
MPDATA,HF,4,,5.32E-3,5.46E-3,6.64E-3,7.15E-3,7.44E-3,7.64E-3
MPDATA,HF,4,,7.39E-3,7.20E-3,6.91E-3,6.64E-3
```

```
C**********                          *Start specifying thermal loads
t1=0.0                               *Initial time
t2=0.001                             *Time-step parameter

C**********                          *Make initial temp dist
CSYS,1
KPRSEL,X,RI  $LSKP,1       $ARLS,1
ACVSF,ALL,-4,Tbw                     *Apply forced convection to inside
CSYS,0
KPALL        $LSALL        $ARALL
ARSEL,,37    $ARASEL,,41   $ARASEL,,45
ACVSF,ALL,-2,Tbr*.45                 *Apply radiation to outside fireside
ARALL
ARSEL,,29    $ARASEL,,25   $ARASEL,,22
ACVSF,ALL,-3,(Tab+700)/2             *Apply free convection to outside back
ARALL
TIME,t1      $LWRITE
C**********                          *Begin transient phase
ITER,-99,0,99                        *Solutions in 99 or less iterations
KBC,1                                *Change in heat flux is immediate
ARSEL,,37    $ARASEL,,41   $ARASEL,,45
ACVSF,ALL,-2,Tbr                     *Apply radiation to outside fireside
ARALL
```

```
C**********                          *Make load steps
*CREATE,LOAD                         *This is a macro
SET,K,ARG1**4
SET,t3,K*t2     $SET,t4,t3+t1
TIME,t4         $LWRITE
*END
*USE,LOAD,1
RP15,,1
```

```
AFWRITE     $FINI                    *Write file 27 and leave prep7
/INPUT,27   $FINI                    *Solve for temperatures
```

```
C**********                          *Process results of thermal analysis
/POST1
*CREATE,PLOT                         *This is a macro
SET,ARG1     $NALL        $EALL
PLPATH,ARG2,ARG3,TEMP                *Plot temperature distribution
/NOERASE     $*END


FRAME,675,1050
/SHOW,APEXT33,DAT
*USE,PLOT,1,2,2381          $*USE,PLOT,6,2,2381
*USE,PLOT,8,2,2381          $*USE,PLOT,11,2,2381
*USE,PLOT,13,2,2381         $/ERASE

/SHOW,FILLT33,DAT
*USE,PLOT,1,677,2835        $USE,PLOT,6,677,2835
*USE,PLOT,8,677,2835        $USE,PLOT,11,677,2835
*USE,PLOT,13,677,2835       $/ERASE
FINI                                 *Leave Post1

/POST26                              *Make temp. vs. time graphs
TIME,0,50.625 $XVAR,1       $PLTIME,0,30
DISP,2,2381,TEMP,APF        $DISP,3,1,TEMP,API
DISP,4,2385,TEMP,FIF        $DISP,5,699,TEMP,FII
/SHOW,A26T33,DAT,1          $PLVAR,2,3
/SHOW,F26T33,DAT,1          $PLVAR,4,5
FINI                                 *Leave post26 and ANSYS
```

```
C**********                                  *Begin structural analysis

/PREP7        $RESUME

/TITLE,TRANSIENT STRESS DISTRIBUTION AT VARIOUS TIMES

KAN,0                                        *Structural analysis

KEYOPT,1,3,1                                 *Invoke generalized plane strain option

TREF,70                                      *No stress at 70 deg. F.


C**********                                  *Mechanical properties of T22

EX,1,30e6                                    *Constant young's modulus

NUXY,1,.3                                    *Constant poisson's ratio

AL0S=7.33E-6  $AL1S=1.30E-9

ALPX,1,AL0S,AL1S                             *Coefficient of thermal expansion


KNL,1                                        *Non-linear analysis (plasticity)

NL,1,13,10                                   *Bilinear stress-strain curve

NL,1,19,575.,700.,750.,900.,1050.,1100.          *Defining temperatures

NL,1,25,34300.,34000.,32500.,28000.,19000.,16000.    *Yield stresses

NL,1,31,1.15E6,1.11E6,1.10E6,1.00E6,0.65E6,0.48E6    *Tangent Moduli


C**********                                  *Mechanical properties of CC50 STAINLESS

EX,2,29.E6                                   *Young's modulous

NUXY,2,.3                                    *Poisson's ratio

AL0C=5.80E-6 $AL1C=.635E-9

ALPX,2,AL0C,AL1C                             *Coefficient of thermal expansion
```

```
KNL,1                                   *Non-linear analysis
NL,2,13,10                              *Bilinear stress-strain curve
NL,2,19,68.,2000.                       *Temperature range
NL,2,25,65000.,65000.                   *Yield stress
NL,2,31,0.,0.                           *Zero slope after yield

C**********                             *Physical constraints
CPSIZE,100
NRSEL,Z,0       $NRSEL,X,0
D,ALL,UX,0                              *Left edge of pipe half is fixed in x
NRSEL,Y,-RO  $D,ALL,UY,0                *Bottom outside node fixed in y
NALL            $NRSEL,Z,0    $NRSEL,X,CC
CP,1,UX,ALL                             *Rt. side of membrane has uniform disp. in x
NALL

C**********                             *Apply internal pressure to inner radius
CSYS,1          $KPRSEL,X,RI
LSKP,1          $ARLS,1
APSF,ALL,3626
APSF,ALL,3626
ARALL           $LSALL
KPALL           $CSYS,0
```

```
C**********

ITER,-99,0,99                          *Solutions in 99 or less iterations

t1=0.0          $t2=0.001


*CREATE,ACTEM                          *This is a macro to get the temperatures

SET,K,ARG1**4

SET,t3,K*t2     $SET,t4,t3+t1

KTEMP,,,t4                             *Get the temperatures

TIME,T4         $LWRITE                *Nail the time of the load step

*END

*USE,ACTEM,0              $RP16,,1


KTEMP,,,0                              *Get initial temps for residual stresses

TIME,100        $LWRITE


AFWRITE         $FINI                  *Write file 27 and leave prep7

/INPUT,27       $FINI                  *Solve structural problem
```

```
/POST1                                  *Start post processing of structural analysis
C**********                             *Plot axial stress
*CREATE,PLOT                            *This is a macro for plotting
SET,ARG1      $NALL         $EALL
ERSEL,MAT,1                             *Select only base material
PLPATH,ARG2,ARG3,SZ
/NOERASE      EINV                      *Select coating
PLPATH,ARG2,ARG3,SZ       $*END
/RATIO,1,.8                             *X-axis length/Y-axis length = .8
FRAME,-60000,60000        $/SHOW,APEXAX33,DAT
*USE,PLOT,1,2,2381        $*USE,PLOT,6,2,2381
*USE,PLOT,8,2,2381        $*USE,PLOT,13,2,2381
*USE,PLOT,17,2,2381       $/ERASE

$/SHOW,FILLAX33,DAT
*USE,PLOT,1,677,2835      $*USE,PLOT,6,677,2835
*USE,PLOT,8,677,2835      $*USE,PLOT,13,677,2835
*USE,PLOT,17,677,2835     $/ERASE

C**********                             *Plot tangential stress
*CREATE,PLOT
SET,ARG1      $NALL         $EALL
ERSEL,MAT,1
PLPATH,ARG2,ARG3,SY
/NOERASE      $EINV
PLPATH,ARG2,ARG3,SY       $*END
```

```
/SHOW,APEXTA33,DAT      $CSYS,1
*USE,PLOT,1,2,2381      $*USE,PLOT,6,2,2381
*USE,PLOT,8,2,2381      $*USE,PLOT,13,2,2381
*USE,PLOT,17,2,2381     $/ERASE

FRAME,-89000,89000
/SHOW,FILLTA33,DAT      $CSYS,11
*USE,PLOT,1,677,2835    $*USE,PLOT,6,677,2835
*USE,PLOT,8,677,2835    $*USE,PLOT,13,677,2835
*USE,PLOT,17,677,2835   $/ERASE
```

```
C**********                          *Plot radial stress
*CREATE,PLOT
SET,ARG1     $NALL      $EALL
ERSEL,MAT,1
PLPATH,ARG2,ARG3,SX
/NOERASE     $EINV
PLPATH,ARG2,ARG3,SX     $*END
```

```
FRAME,-19000,29000
/SHOW,APEXRA33,DAT      $CSYS,1
*USE,PLOT,1,2,2381      $*USE,PLOT,6,2,2381
*USE,PLOT,8,2,2381      $*USE,PLOT,13,2,2381
*USE,PLOT,17,2,2381     $/ERASE
```

```
/SHOW,FILLRA33,DAT        $CSYS,11
*USE,PLOT,1,677,2835      $*USE,PLOT,6,677,2835
*USE,PLOT,8,677,2835      $*USE,PLOT,13,677,2835
*USE,PLOT,17,677,2835     $/ERASE

C**********                          *Plot von Mises stress
*CREATE,PLOT
SET,ARG1     $NALL        $EALL
ERSEL,MAT,1
PLPATH,ARG2,ARG3,SIGE
/NOERASE     $EINV
PLPATH,ARG2,ARG3,SIGE     $*END
/RATIO,1,.8
FRAME,0,75000
/SHOW,APEXVM33,DAT        $CSYS,0
*USE,PLOT,1,2,2381        $*USE,PLOT,6,2,2381
USE,PLOT,8,2,2381         $*USE,PLOT,13,2,2381
USE,PLOT,17,2,2381        $/ERASE

/SHOW,FILLVM33,DAT
*USE,PLOT,1,677,2835      $*USE,PLOT,6,677,2835
*USE,PLOT,8,677,2835      $*USE,PLOT,13,677,2835
*USE,PLOT,17,677,2835     $/ERASE

FINI                                 *Leave post1
```

```
/POST26                                    *Plot stresses vs. time
TIME,0,100      $XVAR,1      $PLTIME,0,30

ESTR,2,1101,13,AFT                         *Apex, fireside, tangential
ESTR,3,1101,15,AFA                         *Apex, fireside, axial
ESTR,4,1281,19,AICT                        *Apex, interface, in coating, tangential
ESTR,5,1281,21,AICA                        *Apex, interface, in coatint, axial
ESTR,6,1,13,AIBT                           *Apex, interface, in base, tangential
ESTR,7,1,15,AIBA                           *Apex, interface, in base, axial
/SHOW,APF33,DAT,1      $PLVAR,2,3
/SHOW,APIC33,DAT,1     $PLVAR,4,5
/SHOW,APIB33,DAT,1     $PLVAR,6,7

ESTR,2,1305,61,FF1                         *Fillet, fireside, sig1
STR,3,1305,62,FF2                          *Fillet, fireside, sig2
ESTR,4,1305,63,FF3                         *Fillet, fireside, sig3
ESTR,5,1377,66,FIC1                        *Fillet, interface, in coating, sig1
ESTR,6,1377,67,FIC2                        *Fillet, interface, in coating, sig2
ESTR,7,1377,68,FIC3                        *Fillet, interface, in coating, sig3
ESTR,8,305,61,FIB1                         *Fillet, interface, in base, sig1
ESTR,9,305,62,FIB2                         *Fillet, interface, in base, sig2
ESTR,10,305,63,FIB3                        *Fillet, interface, in base, sig3
/SHOW,FIF33,DAT,1      $PLVAR,2,3,4
/SHOW,FIIC33,DAT,1     $PLVAR,5,6,7
/SHOW,FIIB33,DAT,1     $PLVAR,8,9,10
FINI           $/EOF                       *Leave post26 and exit ANSYS
```

Vita

The author was born to Edward and Ann B. Erskine on November 20, 1966 in Manhasset, New York. He completed his primary and secondary education in the Ridgefield Connecticut public school system in June 1984. The following fall he started undergraduate courses at Lehigh University. His Junior year was spent at the University of Manchester Institute of Science and Technology in England. He received a Bachelor of Science in Mechanical Engineering from Lehigh in June 1988.

The following summer was spent at Lehigh researching the possibility of using ultra-low frequency sound to revive an infant suffering from sleep apnea. He then worked at AT&T Bell Laboratories designing mechanical components for communications equipment.

In August, 1989 he returned to Lehigh for graduate study. His research was sponsored by a consortium of six electric utility companies. He expects to graduate from Lehigh in June 1991 with a Master of Science degree in Mechanical Engineering.